REPUBLIQUE ALGERIENNE DEMOCRATIQUE ET POPULAIRE
Ministère de l'Enseignement Supérieur et de la Recherche Scientifique
Ecole Nationale Polytechnique

Department of Electronics
Laboratory: Signal and Communications

Doctoral thesis
in electronics

REGION-BASED ACTIVE CONTOURS MODELS FOR IMAGE SEGMENTATION

Proposed by:

BIRANE Abdelkader

Supervised by: Ms. L. Hamami Professor (ENP)

Presented and publicly supported on 04/07/2021

BOARD OF EXAMINERS :

President	:	GUERTI Mhania	Prof.	ENP
Supervisor	:	HAMAMI MITICHE Latifa	Prof.	ENP
Member	:	ADNANE Mourad	Prof.	ENP
Member	:	BENBLIDIA Nadjia	Prof.	USDB
Member	:	ACHELI Dalila	Prof.	UMBB
Member	:	SMARA Youcef	Prof.	USTHB
Invited	:	BENALIA Nourelhouda	MCB	ENP

ENP 2021

REPUBLIQUE ALGERIENNE DEMOCRATIQUE ET POPULAIRE
Ministère de l'Enseignement Supérieur et de la Recherche Scientifique
Ecole Nationale Polytechnique

Department of Electronics
Laboratory: Signal and Communications

Doctoral thesis
in electronics

REGION-BASED ACTIVE CONTOURS MODELS FOR IMAGE SEGMENTATION

Proposed by:

BIRANE Abdelkader

Supervised by: Ms. L. Hamami Professor (ENP)

Presented and publicly supported on 04/07/2021

BOARD OF EXAMINERS :

President	:	GUERTI Mhania	Prof.	ENP
Supervisor	:	HAMAMI MITICHE Latifa	Prof.	ENP
Member	:	ADNANE Mourad	Prof.	ENP
Member	:	BENBLIDIA Nadjia	Prof.	USDB
Member	:	ACHELI Dalila	Prof.	UMBB
Member	:	SMARA Youcef	Prof.	USTHB
Invited	:	BENALIA Nourelhouda	MCB	ENP

ENP 2021

REPUBLIQUE ALGERIENNE DEMOCRATIQUE ET POPULAIRE
Ministère de l'Enseignement Supérieur et de la Recherche Scientifique
Ecole Nationale Polytechnique

Département d'électroniques

Laboratoire : Signal et Communications

Thèse de doctorat
en électronique

SEGMENTATION D'IMAGE PAR LES MODÈLES DE CONTOURS ACTIFS BASÉS-RÉGION

Présenté par :

BIRANE Abdelkader

Sous la direction de Mme L. Hamami   Professeur (ENP)

Présenté et soutenue publiquement le 04/07/2021

Composition du Jury :

Président	:	GUERTI Mhania	Professeur	ENP
Rapporteur	:	Latifa HAMAMI MITICHE	Professeur	ENP
Examinateur	:	ADNANE Mourad	Professeur	ENP
Examinateur	:	BENBLIDIA Nadjia	Professeur	USDB
Examinateur	:	ACHELI Dalila	Professeur	UMBB
Examinateur	:	SMARA Youcef	Professeur	USTHB
Invité	:	BENALIA Nourelhouda	MCB	ENP

ENP 2021

For my family

ACKNOWLEDGEMENT

ABSTRACT

ملخص

في هذه الدراسة، اقترحنا ثلاثة نماذج لتقنية الحواف النشطة لتجزئة الصور الطبية. هدفنا الرئيس هو تطوير تقنيات جديدة قوية وفعالة لتجزئة الصور يمكن أن تساعد في التغلب على المشكلات التالية: وجود عدم تجانس شدة في الصور، ووجود أنواع مختلفة من التشويش، وحساسية تقنيات التجزئة لتهيئة الحواف الابتدائية، والتكلفة الحسابية العالية لخوارزميات تجزئة الصور.

الكلمات الدالة

الحواف النشطة، مجموع المستويات، التقسيم، عدم تجانس الشدة، التشويش، تكلفة الحساب.

Résumé

Dans cette étude, nous avons proposé trois modèles de contours actifs pour la segmentation de images médicales. Notre principal objectif est le développement de nouvelles techniques de segmentation d'images robustes et efficaces qui pourraient aider à surmonter les problèmes suivants : la présence d'inhomogénéités d'intensité dans les images, la présence de différents types de bruits, la sensibilité des techniques de segmentations à l'initialisation des contours, et le coût de calcul élevé des algorithmes de segmentations de images.

Mots clés

Contour Actif, Level set, Segmentation, Inhomogénéités d'intensité, bruits, Coût de calcul.

Abstract

In this study, we proposed three active contour models for the segmentation of medical images. Our main objective is the development of new robust and efficient image segmentation techniques that could help overcome the following problems: the presence of intensity inhomogeneities in images, the presence of different types of noise, the sensitivity of the segmentation techniques to initialization of contours, and the high computational cost of image segmentation algorithms.

Keywords

Active Contour, Level set, Segmentation, Intensity inhomogeneities, Noises, Calculation cost.

TABLE OF CONTENTS

CHAPTER I
INTRODUCTION

CHAPTER II
IMAGE SEGMENTATION

CHAPTER III
ACTIVE CONTOUR MODELS

CHAPTER IV

AN EFFICIENT LEVEL SET METHOD BASED ON GLOBAL STATISTICAL INFORMATION FOR IMAGE SEGMENTATION

CHAPTER V

A ROBUST REGION-BASED ACTIVE CONTOUR MODEL BASED ON LOCAL AVERAGE INTENSITY FOR IMAGE SEGMENTATION

CHAPTER VI

A FAST LEVEL SET IMAGE SEGMENTATION DRIVEN BY A NEW REGION DESCRIPTOR

CHAPTER VII

LIST OF TABLES

LIST OF FIGURES

COMMON ACRONYMS

MRI   Magnetic Resonance Imaging

GAC   Geodesic Active Contour Model

CV   Chan And Vese Model.

SDF   Signed Distance Function

DRLSE   Distance Regularized Level Set Evolution.

LBF   Local Binary Fitting Model

LGD   Local Gaussian Distribution Fitting Model

LCV   Local Chan–Vese Model

SBGFRLS   Selective Binary And Gaussian Filtering Regularized Level Set Model.

L0MOS   L0 Regularized Mumford-Shah Model.

L0RDLSM   L0-Regularized Discrete Variational Level Set Method.

JS   Jaccard Similarity Coefficient.

DSC   Dice Similarity Coefficient.

CHAPTER I

INTRODUCTION

"Those who wish to succeed must ask the right preliminary questions."
Aristotle (384 B.C. to 322 B.C.)

In this introduction, we present in a global way the field of computer vision and image processing, in particular, the specific topics of segmentation. This introduction will help the reader understand the aims and contributions of this thesis, which are described in general terms at the end of this introduction. Finally, the organization of the thesis is presented giving the reader a context of understanding and navigation in the work carried out.

1.1 Computer vision and image processing

Digital image processing is a field that continues to grow, with new applications being developed at an ever increasing pace. It is a fascinating and exciting area to be involved in today with application areas ranging from the entertainment industry to the space program [4].

Digital image processing, also referred to as computer imaging, can be defined as the acquisition and processing of visual information by computer. The importance of digital image processing is derived from the fact that our primary sense is our visual sense. Our vision system allows us to gather information without the need for physical interaction; it enables us to analyze all types of information directly from pictures or video. It provides us with the ability to navigate about our environment, and the human visual system is the most sophisticated, advanced neural system in the human body. Most of the scientific discoveries and advancements have relied on the visual system for their development—from the discovery of fire to the design of a cell phone [4].

The information that can be conveyed in images has been known throughout the centuries to be extraordinary—one picture is worth a thousand words. Fortunately, this is the case, because the computer representation of an image requires the equivalent of many thousands of words of data, and without a corresponding amount of information, the medium would be prohibitively inefficient. The massive amount of data required

for images is a primary reason for the development of many subareas within the field of computer imaging, such as image segmentation and image compression. Another important aspect of computer imaging involves the ultimate "receiver" of the visual information in some cases the human visual system, in others the computer itself [4].

This distinction allows us to separate digital image processing into two primary application areas: computer vision applications, and human vision applications, with image analysis being a key component in the development and deployment of both (Figure1.1).
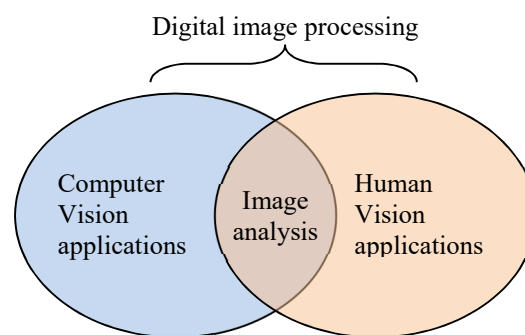
Figure 1.1: Digital image processing can be separated into computer vision and human vision applications, with image analysis being part of both [4].

In computer vision applications the processed (output) images are for use on a computer, while in human vision applications the output images are for human consumption. The human visual system and the computer as a vision system have varying limitations and strengths, and the computer imaging specialist needs to be aware of the functionality of these two very different systems. The human vision system is limited to visible wavelengths of light, which covers only a small portion of the electromagnetic spectrum. The computer is capable of dealing with almost the entire electromagnetic spectrum, ranging from gamma rays to radio waves, and can process other imaging modalities such as ultrasound and magnetic resonance imaging.

Historically, the field of digital image processing grew from electrical engineering as an extension of the signal processing branch, while the computer science discipline was largely responsible for developments in computer vision applications [4].

Image analysis involves the examination of the image data to facilitate solving an imaging problem. Image analysis methods comprise the major components of a computer vision system, where the system is to analyze images and have a computer act on the results.

In one sense a computer vision application is simply a deployed image analysis system. In the development of a human vision image processing application, many images must be examined and tested so image analysis is necessary during the development of the system [4].

Although there is no clear distinction between image processing, image analysis, and computer vision, usually they are considered as hierarchies in the processing continuum. The low-level processing, which involves primitive operations such as noise filtering, contrast enhancement, and image sharpening, is considered as image processing. Note both its inputs and outputs are images. The mid-level processing, which involves segmentation and pattern classification, is considered as image analysis or image understanding [14]. Note its input generally are images, but its outputs are attributes extracted from those images, e.g. edges, contours, and the identity of individual objects, called class. The high-level processing, which involves 'making sense' of an ensemble of recognized objects and performing the cognitive functions at the far end of the processing continuum, is considered as computer vision [14]. We discuss the technologies used in the image analysis and propose novel segmentation methods through this document [13].

A. Main areas in image processing system

Image processing covers four main areas: image formation, analysis, visualization, and management. The algorithms of image enhancement can be assigned as pre and post in all areas [5, 6].

B. Fundamental Steps in Image Processing

In general, digital image processing covers four major areas (Figure 1.2) [5, 6]:

1. **Image formation** includes all the steps from capturing the image to forming a digital image matrix.
2. **Image enhancement** includes all the techniques used to produce a processed image that is suitable for a given application.

3. **Image analysis** includes all the steps of processing, which are used for quantitative measurements as well as abstract interpretations of biomedical images. These steps require a priori knowledge on the nature and content of the images, which must be integrated into the algorithms on a high level of abstraction. Thus, the process of image analysis is very specific, and developed algorithms can be transferred rarely directly into other application domains.

4. **Image visualization** refers to all types of manipulation of this matrix, resulting in an optimized output of the image.

5. **Image management** sums up all techniques that provide the efficient storage, communication, transmission, archiving, and access (retrieval) of image data. Thus, the methods of telemedicine are also a part of the image management.
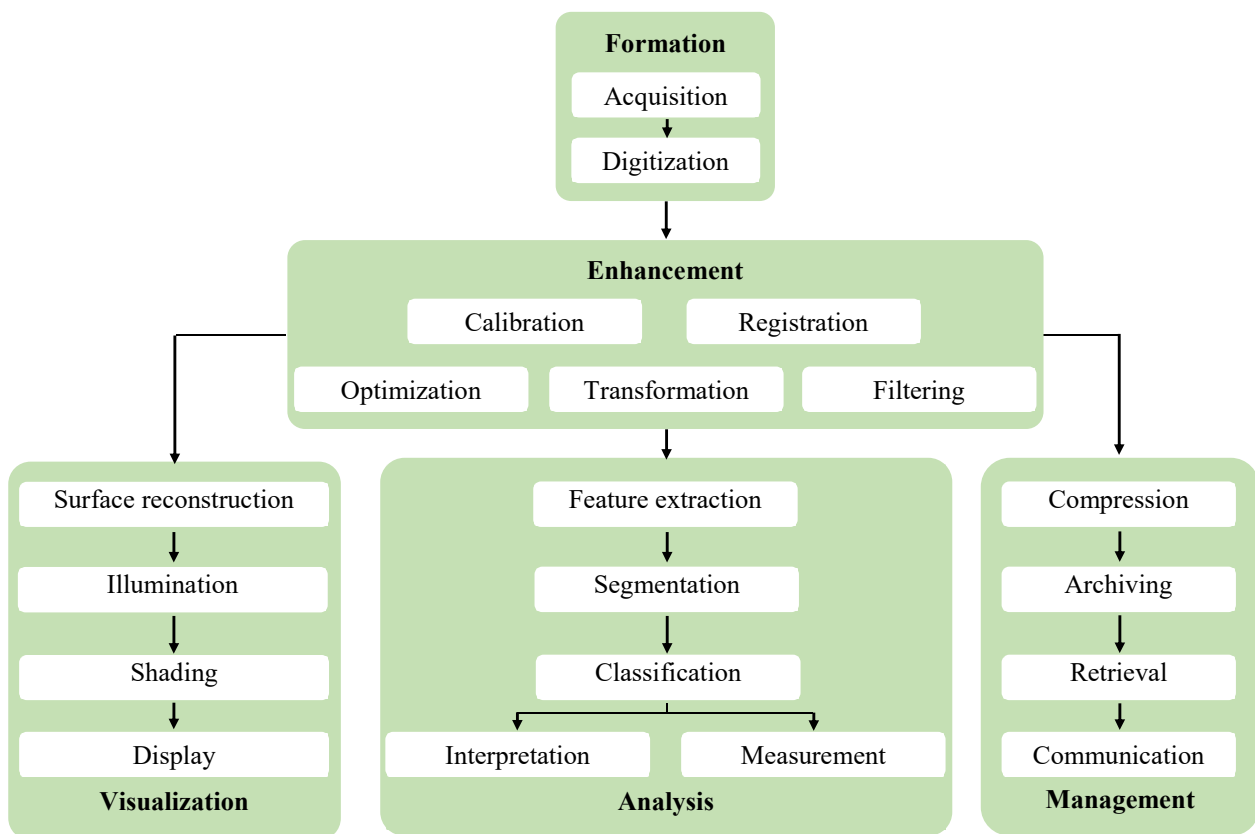
Figure 1.2: Modules of image processing.

1.1.1 Image Segmentation and Active Contours

Image segmentation is one of the most important tasks in image processing which is useful in a wide variety of fields. In the last few decades a wide variety of techniques have been developed to generate automatic image segmentations. Among these

techniques we find the active contours method proposed in 1988 by Kass et al. [26]. The active contours methods evolve a curve to minimize energy functional to find object boundaries. These methods can be broadly classified as edge-based or region based depending on whether the energy functional are defined over edge or region statistics of the image. More recently, some curve evolution techniques that can find global optima have been developed [99].

1.1.2 Medical Image Processing

The commonly used term medical image processing means the provision of digital image processing for medicine. By the increasing use of direct digital imaging systems for medical diagnostics, medical image processing is becoming more and more important in health care. Hence, medical image processing is becoming an inherent part of medical technology.

The pragmatic issues of image generation, processing, presentation, and archiving stood in the focus of research in medical image processing. Today, the automatic interpretation of medical images is a major goal, therefor segmentation, classification, and measurements of medical images is being continuously improved and validated more accurately. Hence, the segmentation is one of the most important steps in the analysis of the medical image data and it helps in diagnosis, surgery planning, surgery simulation... etc. so we focused this work on image segmentation and the processing steps associated with it [14].

Histogram Thresholding

Graph based method

Canny method.

Deformable method.
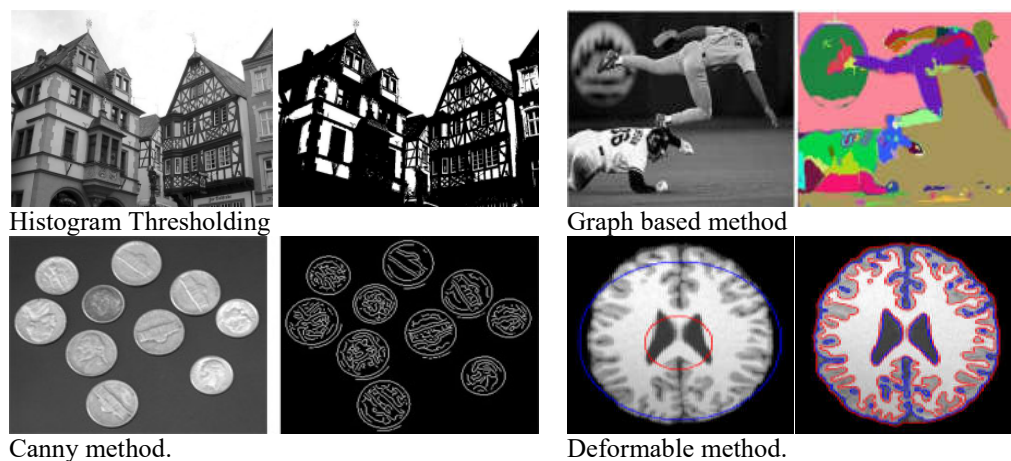
Figure 1.3: Example of image segmentation methods

1.1.3 Main Challenges in Medical Image Segmentation

Over the last decades, image segmentation algorithms have seen considerable progress in dealing with complex and specific medical image analysis tasks, making medical decisions easily and serving as a diagnostic tool. with sufficient performance in terms of accuracy, reliability and speed.

However, there are still challenges to be overcome to ensure an accurate and efficient segmentation. The main challenges are:

1. Sensitivity to the artifacts produced by the image acquisition process:
   - Presence of noise, low contrast, blur and weak boundaries.
   - Presence of image intensity inhomogeneity.
   - The spatial distribution of image data and the overlap between important and non-important features or between multiple objects.
2. Limitations of Methodology and algorithmic:
   - Develop efficient segmentation techniques that can be adapted to a large number of tasks.
   - Elimination of sensitivity to the initialization
   - Minimization of computational time.
   - A suitable Data sets for specific tasks.
   - Efficient methods for ground truth generation for validation.
   - Elaboration or choosing the accurate evaluation metrics for the quantitative evaluation of segmentation results.

These challenges are very important for any image segmentation method - especially in medical imaging - to get more accurate, reliable and faster results for specific tasks.

1.2 Motivations

In this study we focused on the analysis of the medical image segmentation using active contour methods. Achieving accurate and topologically-correct segmentations of medical structures is a crucial step for many post-processing tasks in medical imaging. We aimed at developing new robust and efficient medical image segmentation techniques that may help a clinician in better understanding, diagnosing and treating patients. While existing methods can be effective, they have a number of limitations

like presence of intensity inhomogeneities, noise and the high computational cost... etc. Therefore, this work is motivated by these limitations.

Those limitations led us to consider the following questions on how we can achieve accurate segmentation for medical images:

1. How can we overcome the problem of the presence of intensity inhomogeneities in medical images to achieve efficient segmentation results?
2. How can we segment accurately, blurred images or in the presence of different kinds of noises?
3. Can we develop a segmentation technique less sensitivity to the initialization?
4. Can we reduce the high computational cost and segment our images in a few iterations?

1.3 Contributions

The main contributions of this work are covered in Chapters 3, 4 and 5 of this thesis. Each of these chapters also reviews related work and reports experimental results to demonstrate the applicability of the proposed approaches.

1. Birane Abdelkader, Hamami Latifa, "A Fast level set Image Segmentation driven by a new region descriptor." IET Image Processing, V15, Issue3, Pages 615-623, (2021), doi.org/10.1049/ipr2.12036.
2. Birane Abdelkader, Hamami Latifa, "An efficient level set method based on global statistical information for image segmentation", International Journal of Computers and Applications, (2019), DOI: 10.1080/1206212X.2019.1690797.
3. Birane Abdelkader, Hamami Latifa, "Legendre polynomials Active contour method for image segmentation", International Journal of Systems Applications, Engineering & Development, Volume 12, (2018).
4. Abdelkader, Birane and Hamami Latifa. "Efficient Region Active Contours for Images Segmentation.", Recent Advances in Circuits, Systems, Signal Processing and Communications, (2013). Proceedings of the 8th WSEAS International Conference on Circuits, Systems, Signal and Telecommunications (CSST '14), Tenerife, Spain.

1.4 Organization of this Thesis

This thesis is organized in two parts. The first part consists of the necessary background to understand the contributions of our work. It corresponds to Chapter 1 and 2.

The second part, consisting of Chapters 3, 4 and 5, presents our contributions.

Chapter 1: In this chapter, we present a general overview of the fundamentals of image segmentation such as its definition, its usefulness, and the three levels of research in image segmentation, then we discuss the different segmentation approaches and we summarize the most popular image segmentation techniques. Obviously, we mention the most used datasets for a good evaluation of segmentation quality as well as the main quantitative evaluation metrics, we end with the major applications of image segmentation and future trends.

Chapter 2: This chapter introduces a brief classification of the main active contours presenting the two categories of active contours: the parametric/explicit active contour and the geometric/implicit active contour known as the level set method. we focus more on the level sets method, presenting its different categories of applications: edge-based models, region-based models, and local-region-based models, then some implementation techniques and drawbacks and advantages of the level sets method which is useful to introduce our first three image segmentation models in Chapters 3, 4 and 5.

Chapter 3: In this chapter, we propose an efficient level set method based on global statistical information for image segmentation, where we can benefit from the advantages of the C–V and GAC models.

Chapter 4: In this chapter, we propose a robust region-based active contour model based on local average intensity for image segmentation in presence of intensity inhomogenities. The main idea behind the proposed model is to create an energy functional-driven by the difference between the local average intensity inside and outside the contour. The energy functional is incorporated into a level set functional to achieve its minimization.

Chapter 5: In this chapter, we propose a fast level set image segmentation driven by a new region descriptor. We formulate this model using Legendre polynomials for region intensity approximation which demonstrates excellent robustness and accuracy in

image segmentation, especially images that have an inhomogeneous distribution of intensity and images with the presence of a lot of noise.

Conclusion: In this section, we give a summary of the presented work, draw a conclusion from the thesis as well as illustrating our contribution and improvements, and discussing possible directions for future research.

CHAPTER II

IMAGE SEGMENTATION

"The whole is more than the sum of its parts."
Aristotle (384 B.C. to 322 B.C.)

2.1. Introduction

This chapter is devoted to image segmentation which is an interesting technique that plays a very important role in computer vision and image processing in particular in medical image processing. In this chapter, we present a general overview of the fundamentals of image segmentation such as its definition, its usefulness, and the three levels of research in image segmentation, then we discuss the different segmentation approaches and we summarize the most popular image segmentation techniques. Obviously, we mention the most used datasets for a good evaluation of segmentation quality as well as the main quantitative evaluation metrics, we end with the major applications of image segmentation and future trends.

2.2. Image Segmentation

Segmentation is an important tool in image processing, pattern recognition, scene analysis and computer vision; it has been useful in many applications. The principal goal of the segmentation is to partition an image into meaningful regions (subsets) that are homogeneous with respect to one or more characteristics or features [1], most frequently to distinguish objects or regions of interest (*foreground*) from everything else (*background*) [2].

Image segmentation have been useful in many applications like feature extraction, image measurements, image display, border detection, functional mapping, automated classification of regions, image registration, and atlas-matching, …, etc. In medical imaging, segmentation is important to classify image pixels into anatomical regions, such as bones, muscles, and blood vessels, while in others into pathological regions, such as cancer, tissue deformities, and multiple sclerosis lesions.

A wide variety of segmentation techniques have been proposed. However, there is no one standard segmentation technique that can produce satisfactory results for all imaging applications. The definition of the goal of segmentation varies according to the goal of the study and the type of image data. Different assumptions about the nature of the analyzed images lead to the use of different algorithms [1].

Figure 2.1: Examples of semantic image segmentation. [3]

Aerial images can be used to segment different types of land.
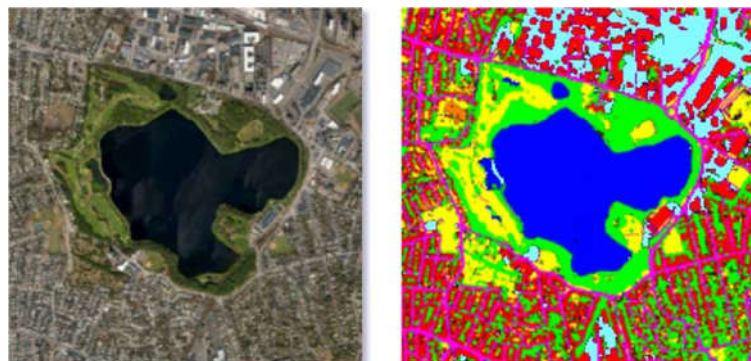
Figure 2.2: Segmentation of a satellite image [4]

Autonomous vehicles such as self-driving cars and drones can benefit from automated segmentation. For example, self-driving cars can detect drivable regions.

Figure 2.3: Segmentation of a road scene [5]

24

Medical image segmentation mainly deals with the segmentation of various images involved in the medical field, such as common nuclear magnetic resonance (MRI) scan images. Its main task is to segment regions of interest from these medical images, such as specific organ parts, objects of interest ... etc.
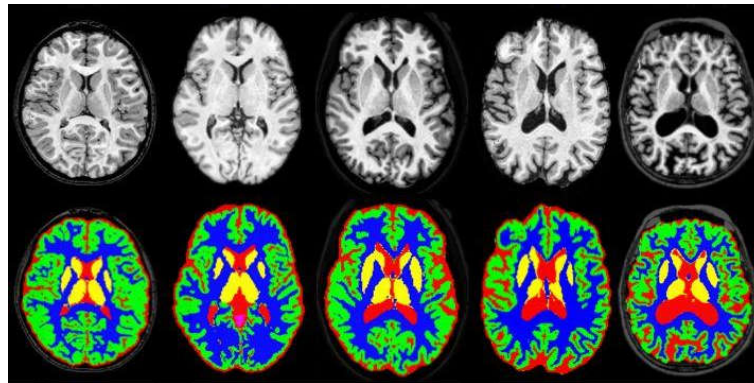
Figure 2.4: Example of brain region segmentation in medical images.

2.2.1 Image Segmentation Fundamentals.

Image segmentation, as a basic operation in computer vision, refers to the process to divide a natural image into some non-overlapped meaningful regions. However, what makes region meaningful can be ambiguous. Sometimes, region can also be part of other regions [7]. So the first challenge in image segmentation is defining which regions (objects) are "meaningful." This task is dependent on the particular application at hand. For instance, in Figure 2.5. the meaningful object can be the sky, the trees, the elephant or the grass depending on the goal of the segmentation and its application. Generally, in the segmentation process, the goal will be to identify the boundary of an object of interest given some initial inputs, which are provided by the user or generated automatically. The second major challenge concerns the fact that the object of interest may have a complex appearance that makes it difficult to distinguish from other surrounding objects or the image background. These two challenges: Segmenting the correct object and segmenting an object correctly are the basis for the majority of on-going research in the field of image segmentation [8].
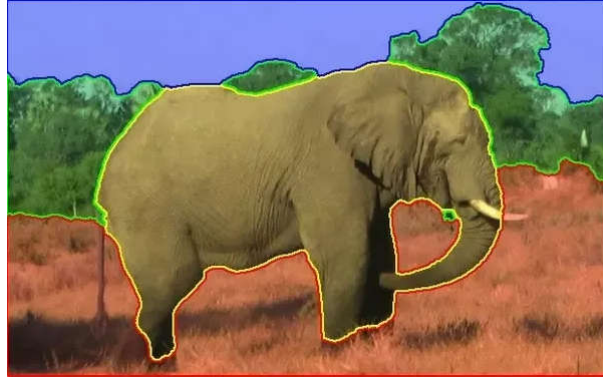
Figure 2.5: Example of an image segmentation

In this sense, what makes a good segmentation needs to be properly defined. In fact, ideally good image segmentation must achieve the following properties (Haralick, 1985) [9]:

- Regions of image segmentation should be uniform and homogeneous with respect to some characteristic such as gray tone or texture.
- Region interiors should be simple and without many small holes.
- Adjacent regions of segmentation should have significantly different values with respect to the characteristic on which they are uniform.
- Boundaries of each segment should be simple, not ragged, and must be spatially accurate.

Achieving all these desired properties is difficult because strictly uniform and homogeneous regions are typically full of small holes and have ragged boundaries.

Insisting that adjacent regions have large differences in values can cause regions to merge and boundaries to be lost.

More specifically, image segmentation can be formally defined as:

Definition 1.1

Let I be an input image defined on continuous domain Ω as a brightness function I: $\Omega \rightarrow \Re$. Image segmentation refers to the process of partitioning Ω into disjoint subsets $\{ \Omega \}_{i=1}^{N}$, i = 1, … ,N, which satisfy [9] :

$$\bigcup_{i=1}^{N} \Omega_i = \Omega;$$

$\Omega_i \cap \Omega_j = \emptyset, \ \forall i \neq j;$

26

$$P(\Omega_i) = \text{true}, \qquad \forall i;$$

$$P\left(\Omega_i \bigcap \Omega_j\right) = false, \qquad \forall i \neq j;$$

P is a logical predicate defined on subsets Ω_i of Ω as follows:

$$P(\Omega_i) = \begin{cases} true \; if \; there \; exists \; a \; constant \; a \; such \; that \; |I(x,y) - a| \leq e \\ \qquad\qquad for \; all \; points \; (x,y) \in \Omega_i, \\ false \; otherwise, \end{cases}$$

where e is a prescribed error tolerance.

There may exist a number of possible partitions, but the selection of an appropriate set of regions depends on the choice of the property *P* association in the region [10].

Three levels image segmentation

The research for image segmentation is carried on at three levels [11, 25]:

1. The first, and also the most basic, is the level of algorithm development,
2. The second, at the middle, is the level of algorithm evaluation,
3. The third, at the top, is the systematic study of evaluation methods.

2.3. Segmentation Approaches

Segmentation techniques can be divided into classes in many ways, depending on classification scheme [1, 12]:

- Manual, semiautomatic, and automatic.
- Pixel-based (local methods) and region-based (global methods).
- Manual delineation, low-level segmentation (thresholding, region growing, etc.), and model-based segmentation (multispectral or feature map techniques, dynamic programming, contour following, etc.).
- Classical (thresholding, edge-based, and region-based techniques), statistical, fuzzy, and neural network techniques.

The most commonly used segmentation techniques can be classified into two broad categories:

1. Edge-based segmentation techniques that look for edges between regions with different characteristics.

2. Region-based segmentation techniques that look for the regions satisfying a given homogeneity criterion.

In addition, there are hybrid segmentation techniques, which result from the combination of single techniques.

2.3.1. Edge-based Segmentation.

The strategy of edge-based segmentation algorithms is to find object boundaries and segment regions enclosed by the boundaries. It is more likely edge detection or boundary detection rather than the literal meaning of image segmentation. An edge can be defined as the boundary between two regions with relatively distinct properties. These algorithms usually operate on edge magnitude and/or phase images produced by an edge operator suited to the expected characteristics of the image. For example, most gradient operators such as Prewitt, Kirsch, or Roberts operators are based on the existence of an ideal step edge. Other edge-based segmentation techniques are graph searching and contour following [1].

Basically, the idea underlying most edge-detection techniques is the computation of a local derivative operator [13].

The gradient vector of an image $I(x, y)$, given by:

$$\nabla I = \begin{bmatrix} \dfrac{\partial I}{\partial x} \\ \dfrac{\partial I}{\partial y} \end{bmatrix} : \ \Omega \rightarrow \Re^2$$

is obtained by the partial derivatives $\partial I/\partial x$ and $\partial I/\partial y$ at every pixel location. The local derivative operation can be done by convolving an image with kernels shown in Figure1.6.

-1
0
1

a

-1	0	1

b
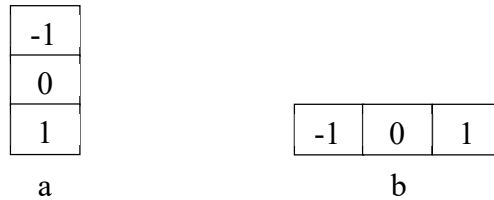
Figure 2.6: Examples of gradient kernels along: (a) vertical direction, (b) horizontal direction

we can calculate the magnitude of the gradient as:

28

$$|\nabla I| = \sqrt{G_x{}^2 + G_y{}^2} = \sqrt{(\partial I/\partial x)^2 + (\partial I/\partial y)^2} : \Omega \to \Re$$

and the direction of the gradient as:

$$D = tan^{-1}\left(\frac{G_y}{G_x}\right)$$

where G_x and G_y are gradients in directions x and y, respectively.

The Laplacian of an image function $I(x, y)$ is the sum of the second-order derivatives, defined as :

$$\nabla^2 I = \frac{\partial^2 I}{\partial x^2} + \frac{\partial^2 I}{\partial y^2} : \Omega \to \Re.$$

The general use of the Laplacian is in finding the location of edges using its zero-crossings [14].

All edge detection methods that are based on a gradient or Laplacian are very sensitive to noise. In some applications, noise effects can be reduced by smoothing the image before applying an edge operation. Marr and Hildreth [15] proposed smoothing the image with a Gaussian filter before application of the Laplacian (this operation is called Laplacian of Gaussian, LoG) [1].
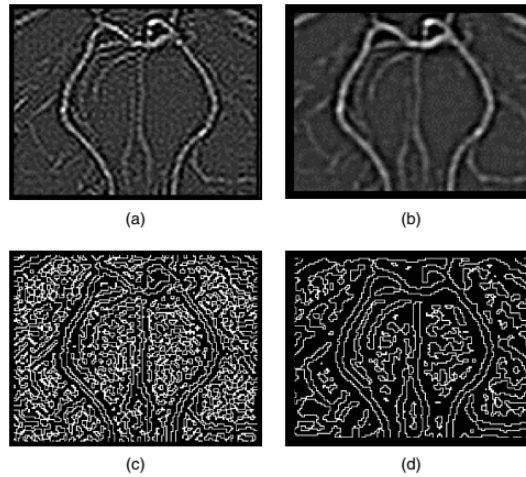
Figure 2.7: Results of Laplacian and Laplacian of Gaussian applied to an Original angiography image showing blood vessels, (a) 3 × 3 Laplacian image, (b) result of a 7 × 7 Gaussian smoothing followed by a 7 × 7 Laplacian, (c) zero-crossings of the Laplacian image (a), (d) zero crossings of the LoG image (b) [1].

- Edge-based techniques are computationally fast and do not require a priori information about image content.

- Edge detection by gradient operations generally work well only in the images with sharp intensity transitions and relatively low noise.

- Due to its sensitivity to noise, some smoothing operation is generally required as preprocessing, and the smoothing effect consequently blurs the edge information.

- The common problem of edge-based segmentation is that often the edges do not enclose the object completely. To form closed boundaries surrounding regions, a post-processing step of linking or grouping edges that correspond to a single boundary is required. The simplest approach to edge linking involves examining pixels in a small neighborhood of the edge pixel (3×3, 5×5, etc.) and linking pixels with similar edge magnitude and/or edge direction. In general, edge linking is computationally expensive and not very reliable [1].

2.3.2 Region-based Segmentation.

Region based segmentation are based on partitioning an image into regions that are similar according to set of predefined criteria. Thresholding, region growing and region splitting and merging are examples of methods in this category [14].

- Thresholding is a common region segmentation method. In this technique a threshold is selected, and an image is divided into groups of pixels having values less than the threshold and groups of pixels with values greater or equal to the threshold. There are several thresholding methods: global methods based on gray-level histograms, global methods based on local properties, local threshold selection, and dynamic thresholding.
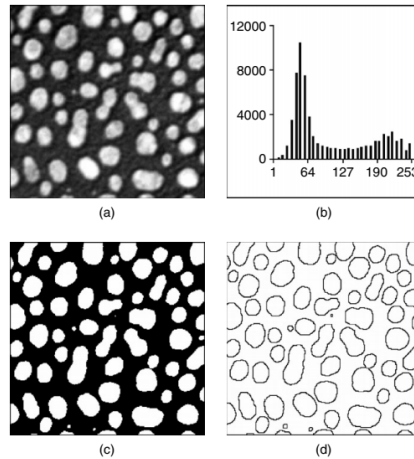
Figure 2.8: An example of global thresholding. (a) Original image, (b) histogram of image (a), (c) result of thresholding with T = 127, (d) outlines of the white cells after applying a 3 × 3 Laplacian to theimage shown in (c) [1].

- Clustering algorithms achieve region segmentation by partitioning the image into sets or clusters of pixels that have strong similarity in the feature space. The basic operation is to examine each pixel and assign it to the cluster that best represents the value of its characteristic vector of features of interest.
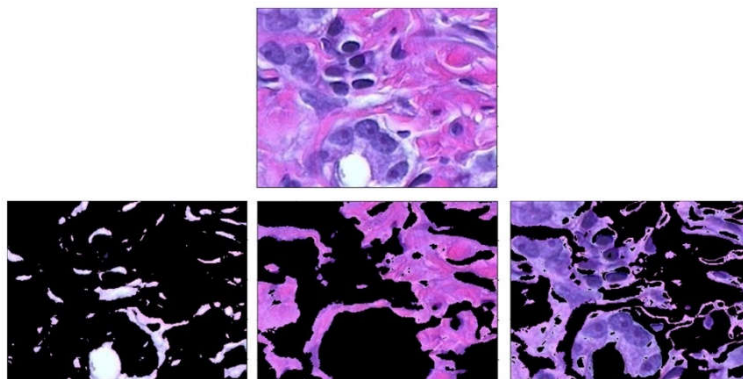
Figure 2.9: Using clustering to distinguish between tissue types (bottom) in an image of body tissue (top) stained with hematoxylin and eosin (H&E). (https://fr.mathworks.com/discovery/image-segmentation.html)

- Region growing is another class of region segmentation algorithms that assign adjacent pixels or regions to the same segment if their image values are close enough, according to some preselected criterion of closeness [1].

Region-based approaches are generally less sensitive to noise, and usually produce more reasonable segmentation results as they rely on global properties rather than local properties, but their implementation complexity and computational cost can be often quite large [13].

31

2.3.4 Hybrid Segmentation Procedures.

Both the edge-based approaches and region-based approaches have their own strengths and weaknesses. edge-based methods are more sensitive to noise than region-based methods. On the other hand, region-based methods are computationally expensive and are often complicated in their implementation. The premise of hybrid approaches is to exploit the strength of each method hopefully to cover the weakness of the other method.

2.3.5 Popular Image Segmentation Techniques.

The definition of the goal of segmentation varies according to the goal of the study and the type of image data. Different assumptions about the nature of the analyzed images lead to the use of different algorithms [1].

aiming to provide a big picture of the different types of image segmentation techniques. We use a classification tree as shown in Figure 2.10 to classify the most well-known image segmentation techniques based on their technical and mathematical foundations [16].
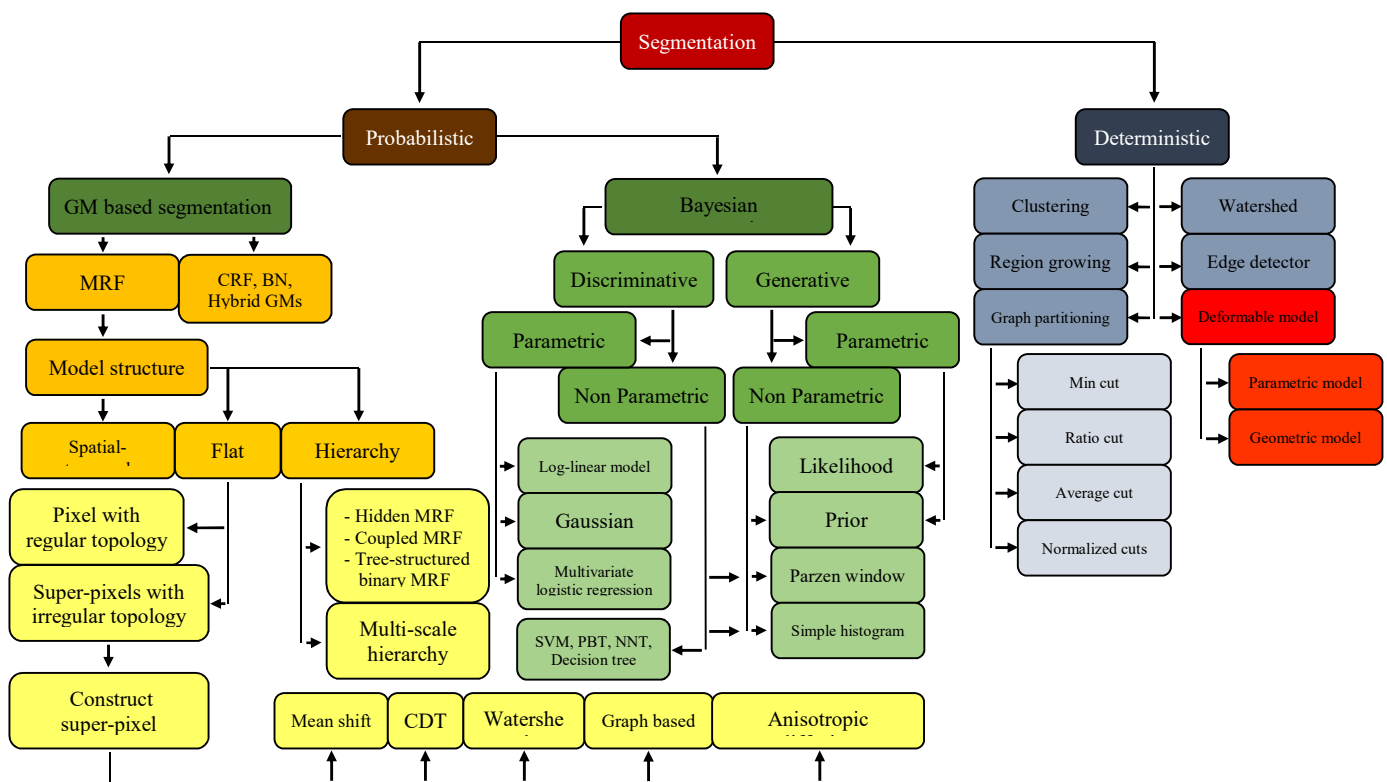
Figure 2.10: Classification tree of popular image segmentation techniques.

2.6 Datasets and evaluation of segmentation quality

To inspire new methods and objectively evaluate their performance for certain applications, different datasets and evaluation metrics have been proposed.

2.6.1 Datasets

Below we summarize the most influential datasets which are widely used in the existing segmentation literature ranging from unsupervised image segmentation to fully-supervised scene understanding:

A. Berkeley segmentation dataset and benchmark (BSDS) [17] is one of the earliest and largest datasets for contour detection and single image object-agnostic segmentation with human annotation [7]. The public benchmark [18] has two versions where each image size is 481 × 321:

The first one called as BSDS300, which includes 300 images and its corresponding ground truth data (each image has at least 4 human annotations), is divided into training set which contains 200 images and test set including 100 images.
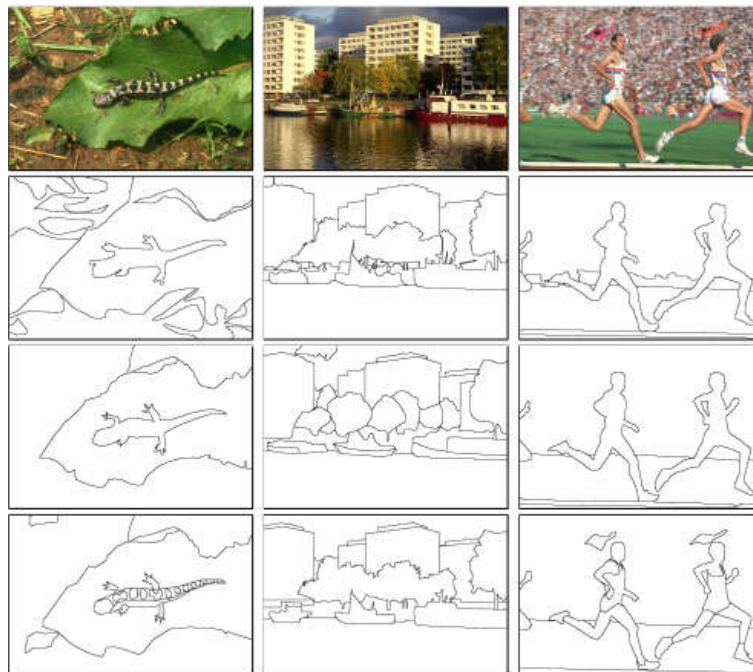
Figure 2.11: BSDS300: Top to Bottom**:** Image and ground-truth segment boundaries hand drawn by three different human subjects. [18]

The last one is the BSDS500, an extended version of the BSDS300 that includes 200 fresh test images.

Figure 2.12 presents some examples from the BSDS. Note that each image has multiple ground truths annotated by different human observers [19].
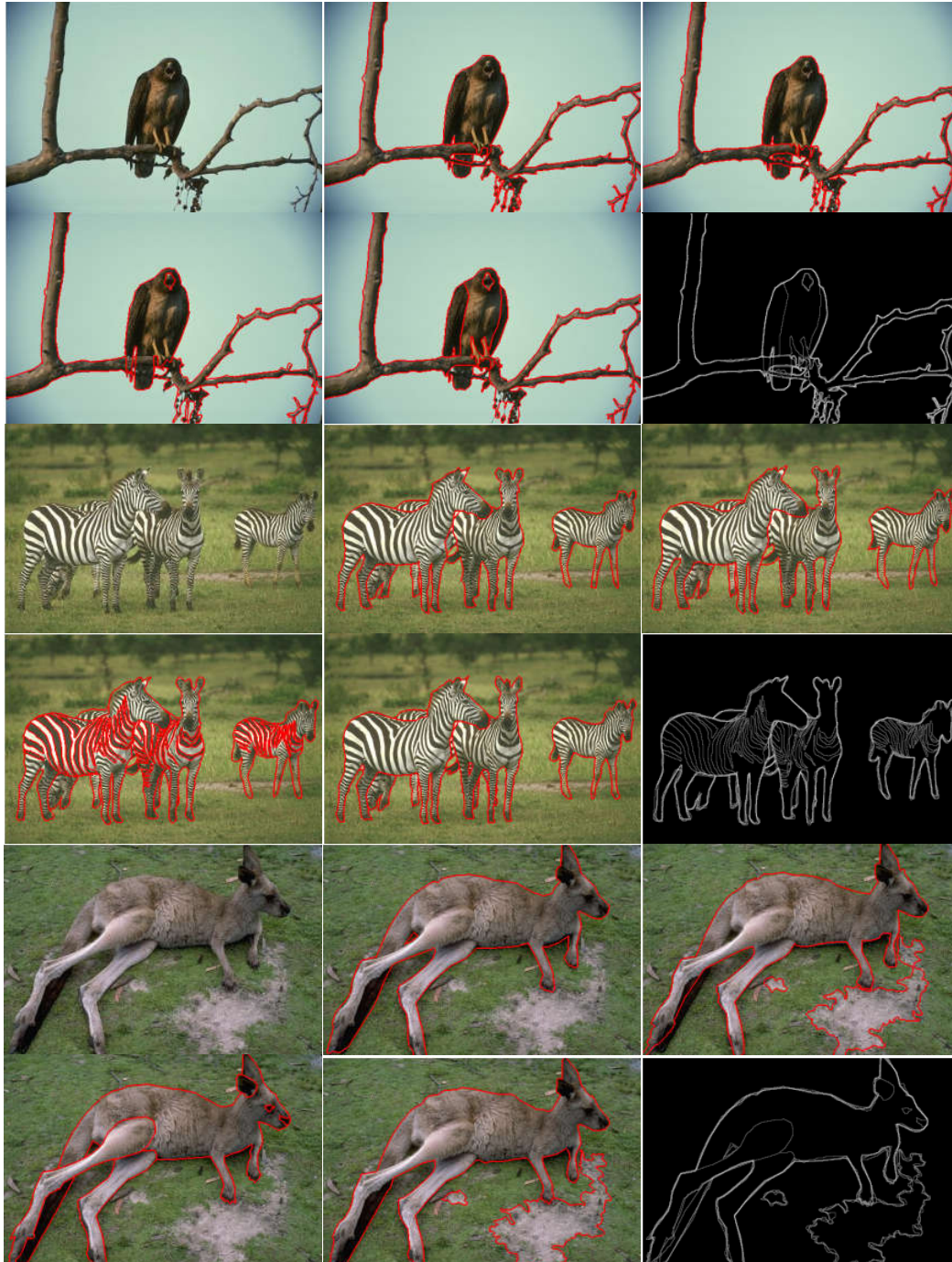
Figure 2.12: Berkeley Segmentation Dataset [19]**.**

B. Microsoft Research Cambridge (MSRC) dataset [20] was first introduced in the context of supervised class segmentation. Soon, this dataset has been widely used to

evaluate scene labeling including both image segmentation and multi-class object recognition. The MSRC dataset contains two versions [19]:

The MSRCV0 has 21-classes (3,457 images), and the MSRCV2 is composed of 591 photographs (all images are approximately 320 × 240 pixels) of the following 21 object classes: building, grass, tree, cow, sheep, sky, airplane, water, face, car, bike, flower, sign, bird, book, chair, road, cat, dog, body, boat [20].

Figure 2.13: A selection of images in the 21-class database and their corresponding ground-truth annotations [20].

The MSRCV2 has been used as the standard benchmark for evaluating image segmentation as well as co-segmentation and object discovery, since it has the largest number of categories, and provides clean ground-truth labeling for all objects.

Figure 2.14 presents some examples from the MSRCV2, where each color corresponds to a class [19].
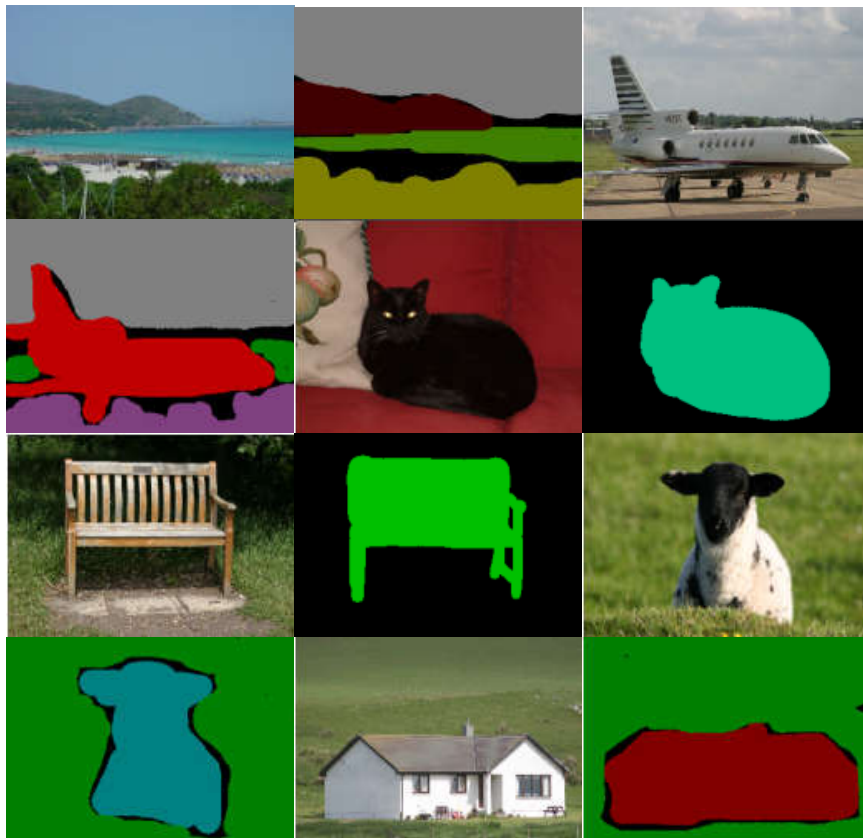
Figure 2.14: MSRCV2 object category image database [19].

2.6.2 Evaluation metrics

Generally, researchers tend to evaluate image segmentation algorithms quantitatively using different evaluation metrics to fully present their performance. This domain has attracted great interest, and many different evaluation metrics have been developed. Zhang et al. [21] presented a good survey on this topic.

The metrics for evaluation of segmentation algorithms are mainly classified into two types supervised and unsupervised. The supervised evaluation metrics need a reference image for analyzing the efficiency of the segmentation algorithm. The reference image is also called ground truth image or gold standard image.

The ground truth image is generated by an expert physician (radiologist) by carefully tracing the region of interest in the medical image [22]. The reference image will be compared with the segmentation algorithm output to determine the efficiency. The degree of similarity between the ground truth image and the segmentation algorithm output determines the quality of the segmented image.

In some cases, it is not possible to create a reference image and in that case, the unsupervised evaluation metrics are used [23].

Figure 2.15 represents success and error rates with respect to ground truth image.
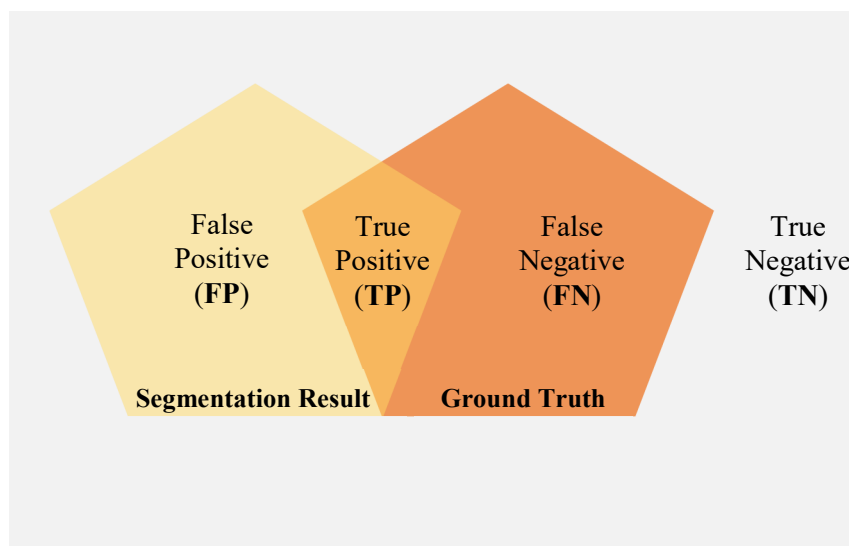
Figure 2.15: Success and error rates in segmentation evaluation.

Some of the widely used segmentation metrics based on the segmented and ground truth image are depicted in Table 1.1.

Table 1.1 Metrics for the evaluation of segmentation algorithms [23].

Success and Error rates		Similarity and Distance measures	
Sensitivity	$\dfrac{|TP|}{|TP|+|FN|}$	Dice coefficient (DC)	$\dfrac{2|TP|}{2|TP|+|FN|+|FP|}$
Specificity	$\dfrac{|TN|}{|TN|+|FP|}$	Jaccard coefficient (JC)	$\dfrac{|TP|}{|TP|+|FN|+|FP|}$
Precision	$\dfrac{|TP|}{|TP|+|FP|}$	Overlap ratio (OR)	$\dfrac{DC}{2-DC}$
TP rate	$\dfrac{|TP|}{|TP|+|FP|}$	Volume similarity (VS)	$\left(\dfrac{V_s-V_g}{V_g}\right)\times 100$
TN rate	$\dfrac{|TN|}{|TN|+|FN|}$	Variation of information (VI)	$VI(S,G)=H(S)+H(G)+I(S,G)$
FP rate	$\dfrac{|FP|}{|FP|+|TN|}$	Williams index	$W_g=\dfrac{(n-1)\sum_i^n D_{pg}}{2\sum_{i=2}^n\sum_{j=1}^{i=1} D_{pq}}$
FN rate	$\dfrac{|FN|}{|FN|+|TP|}$	Hausdorff distance	$H=max(H_{SG},H_{GS})$
Classification error rate	$\dfrac{|FP|+|FN|}{|FP|+|TP|+|FN|+|TN|}$	Rand index (RI)	$\dfrac{|TP|+|TN|}{|FP|+|TP|+|FN|+|TN|}$
		Adjusted rand index	$\dfrac{RI-R_{exp}}{1-R_{exp}}$
Likelihood ratio positive	$\dfrac{sensitivity}{1-specificity|}$	Hamming distance	$D_H(S\Rightarrow R)=\sum_{r_i\in RS_k\neq S_j}\sum_{S_k\cap r_i\neq 0}|r_i\cap S_k|$
		Region-based hamming distance	$p=1-\dfrac{D_H(S\Rightarrow R)+D_H(R\Rightarrow S)}{2\times|S|}$
Likelihood ratio negative	$\dfrac{1-sensitivity}{specificity|}$	Mean absolute difference	$MAD_J=\dfrac{1}{K}\sum_{i=1}^K d(b_i,T)$
Accuracy	$\dfrac{|TP|+|TN|}{|FP|+|TP|+|FN|+|TN|}$	Maximum difference	$MAXD_J=max_{i\in[1,K]}\{d(b_1,T)\}$

2.7. Major applications of image segmentation

Some of the current major application areas of segmentation are [24]:

1. **Medical image interpretation:** Medical imaging is becoming a major component of patients care and medical research. It is presently used to diagnose various clinical conditions such as diseases. It is also the focus of extensive research for the critical impact it can have on health care in general. Segmentation is essential in medical image interpretation. For instance, segmentation serves functional neuroimaging to map brain functions in PET (positron emission tomography) or MRI (magnetic resonance imaging) scans. Neuroimaging is an important research tool in fields such as cognitive neuroscience and cognitive psychology, to investigate the relationship between cognition and neural structure and activity. Segmentation of CT and MRI images, or of other scans, such as ultrasound and thermal, are also used to diagnose diseases, as in mammography's images of the lungs, or cardiac images.

2. **Remote Sensing:** Agricultural remote sensing, which originated in the 1950s, is a long-standing application. Today, most agricultural producers use remote sensing for a variety of purposes. For instance, remote sensing can inform them on crop disease, insect infestation, weed proliferation, and weather damage, as well provide them with crop inventory, water resources mapping, grazing land repartition and status, and soil composition. This information, most of which is attainable through image segmentation, affords producers precise farming management and monitoring capabilities.

3. Remote sensing is also a vital tool to study ecological systems, of interest to scientists and practitioners from various disciplines such as geology, forestry, agronomy, hydrology, and environmental management. The purpose is to evaluate and monitor ecological resources. Image segmentation assists in determining the geographical repartition of the ecological units to study.

4. **Robotics:** Robotics applications of computer vision are long standing and numerous. Image segmentation is of fundamental importance in the field because it can assist a visually guided mobile robot to navigate autonomously and react to the presence of objects in its visual field. A variety of images can

be used for this purpose, such as color, range, optical flow, and images from multiple viewpoints, such as stereo.

5. **Visual field monitoring:** Security is of great current concern in a wide range of practical domains. Applications include monitoring traffic, securing sensitive sites of human activity such as airports, and protecting private property. Functions of a visual surveillance system include change detection, event recognition, and tracking targets such as airborne devices and people.

2.8. Future trends

The subject of image and video segmentation covers a very large area, and further developments could move in many directions; a few of them are indicated as follows [25]:

1. **Mathematical models and theories:** It is said there is yet no general theory for image and video segmentation. However, this does not prevent the introduction of various mathematical theories into the research of image and video segmentation. Many novel models have also been created over the years which have had certain success. To further push the research on image and video segmentation, and to drive the research beyond being ad hoc process, more mathematical models and theories would be required and used in the future.

2. **High level study:** As discussed in the beginning of this chapter, the research on image and video segmentation is currently conducted in three levels : the development of segmentation algorithms, the evaluation of segmentation quality and performance as well as the systematic study of evaluation methods. With a large number of segmentation algorithms being developed, the performance evaluation of these algorithms has attracted more research efforts. The results obtained from high-level study could greatly help the development of new segmentation algorithms and/or the effective utilization of the existing segmentation algorithms.

3. **Incorporating human factors:** Image (and video) segmentation is a critical step of image analysis occupying the middle layer of image engineering, which means it is influenced not only from data but also from human factors. It seems that the assistance of humans, knowledgeable in the application domain, will remain essential in any practical image segmentation method. Incorporating

high-level human knowledge algorithmically into the computer remains a challenge.

4. **Application-oriented segmentation:** Image and video segmentation have been proved necessary in many applications. Though the general process of segmentation is well defined in all applications, the particular requirements for segmentation can be different, and this difference leads to a variety of application-oriented segmentation. For example, in target detection, capturing a recognizable target, instead of segmenting it precisely, would be more significant. Another example is that the extraction of meaningful regions, instead of precisely segmenting objects, has proved to be effective in content-based visual information retrieval tasks.

2.9 Conclusion

Image segmentation plays a crucial role in the extraction of useful information and attributes from images for all imaging applications. It is one of the important steps leading to image understanding, analysis, and interpretation. Image segmentation is not only important for feature extraction and visualization but also for image measurements, 3D visualization, registration, computer-aided diagnosis, and compression, to name just a few. This chapter provided a brief introduction to the fundamental concepts of segmentation and commonly used methods. As new and more sophisticated techniques are being developed, there is a need for objective evaluation and quantitative testing procedures. It is in this context that an overview of the main evaluation metrics and famous dataset were presented in this chapter. Major applications of image segmentation and future trends were mentioned briefly in this chapter.

CHAPTER III

ACTIVE CONTOUR MODELS

"If I have seen further it is by standing on the shoulders of Giants."

Issac Newton (1642 - 1727)

3.1 Introduction

This chapter briefly introduces the most common categories of active contour models used for image segmentation. We start with a brief classification of the main active contours. Next, we present the two categories of active contours: the parametric/explicit active contour and the geometric/implicit active contour known as the level set method. we focus more on the level sets method, presenting its different categories of applications: edge-based models, region-based models, and local-region-based models, then some implementation techniques and drawbacks and advantages of the level sets method.

3.2 Deformable models

During the last two decades the deformable models has become quite popular for a variety of applications, particularly image segmentation and motion tracking. This methodology is based upon the utilization of curves or surfaces, defined within the image domain, that are deformed under the influence of "internal" and "external" forces. There are basically two main types of deformable models:

Parametric/explicit and geometric/implicit. The former represents curves and surfaces explicitly in their parametric forms during deformation, allowing direct interaction with the model and leading to a compact representation for fast real-time implementation.

Alternatively, the latter can handle topological changes naturally because these models are based on the theory of curve evolution, and they represent curves and surfaces implicitly as a level set of a higher-dimensional scalar function. Figure 3.1 shows a brief classification of the main existing deformable models.
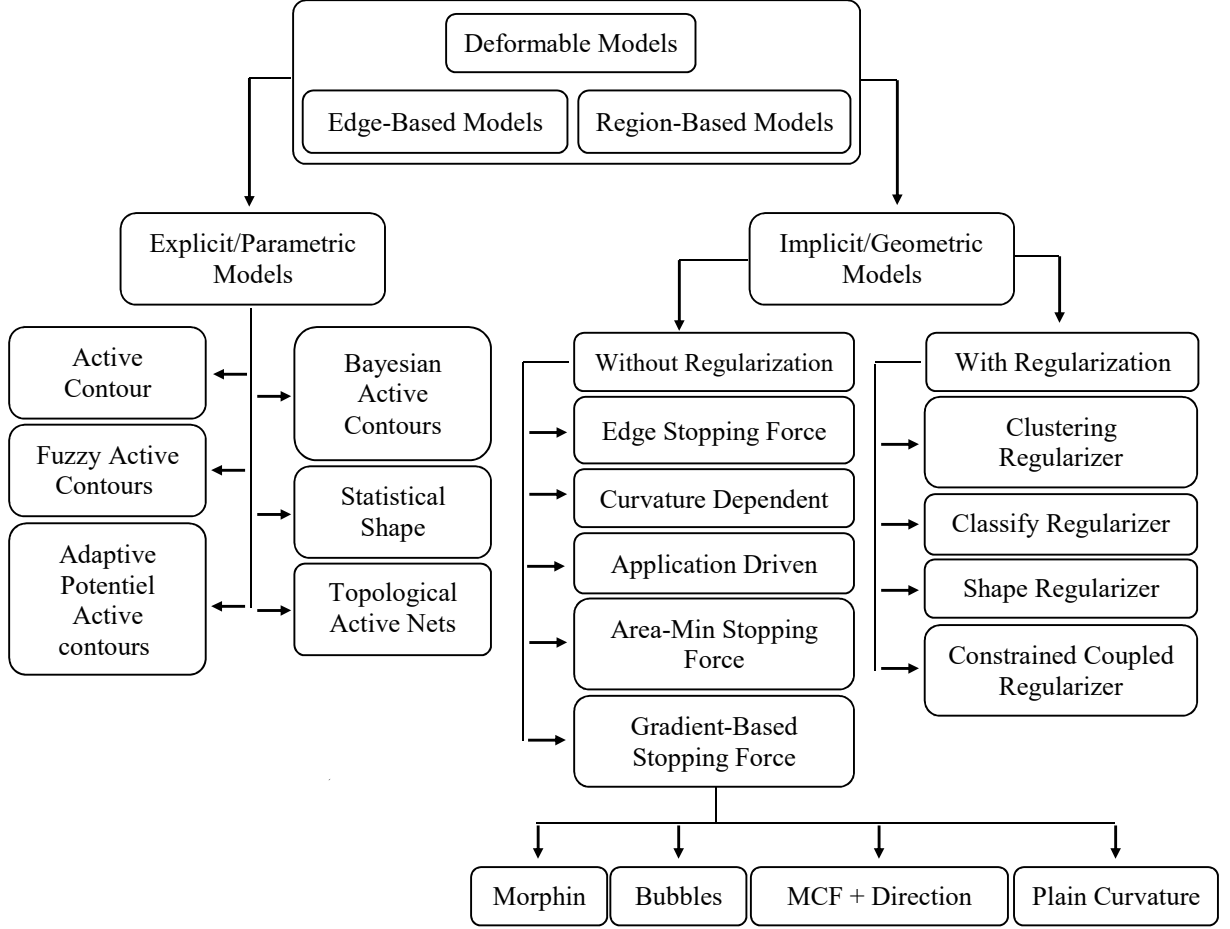
Figure 3.1: Classification of the main existing deformable models.

3.2.1 Parametric models

3.2. 1. 1 The Kass-Witkin-Terzopoulos Snakes model

The first model of active contour was proposed by Kass et al. [26] and named snakes due to the appearance of curve evolution. It uses a parametric representation of the curve:

$$C(s) = \big(X(s)\big) \colon s \in [0,1] \to \Omega, \tag{3.1}$$

where $X \in R^2$ is the coordinate of the contour C, and s is the normalized arc length. The snake model deforms this continuous and elastic curve to fit the nearest salient image characteristics. For any observed image $I \colon \Omega \to R$, the evolution of C is given by the minimization of the following energy function :

$$E_{snake}(C) = E_{internal} + E_{external}$$

$$E_{\text{snake}}(C) = \int_0^1 \frac{1}{2}\left(\alpha(s)\left|\frac{\partial C(s)}{\partial s}\right|^2 + \beta(s)\left|\frac{\partial^2 C(s)}{\partial s^2}\right|^2\right) - \left|\nabla I(C(s))\right|^2 ds, \qquad (3.2)$$

where $\frac{\partial C(s)}{\partial s}$ and $\frac{\partial^2 C(s)}{\partial s^2}$ denote the derivatives with respect to the curve parameter, $\alpha(s)$ and $\beta(s)$ are non-negative parameters, and ∇ represents the spatial gradient operator. The first two terms here correspond to the internal energy in Eq. (2.1), which constraints the geometry of C. More specifically, the first-order differential measures the rate of changes in the length of C ; the second-order one is a rigidity term that makes the snake maintain its original smoothness and shape. Their importance are adjusted by the weights

$\alpha(s)$ and $\beta(s)$ respectively. In the absence of other constraints, the internal energy of snakes simply makes **C** collapse to a point. The external energy term of the snake model is an edge term. It is used to control external attraction forces which drive **C** towards desired edges.
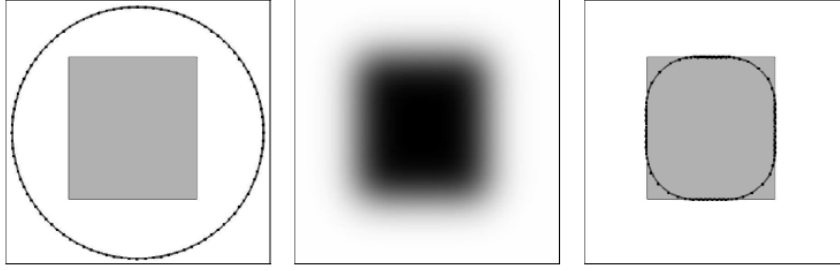
Figure 3.2: Segmentation example using snake model [27]. From left to right: input image with the initial contour, Gaussian-smoothed input image, the final segmentation.

The segmentation problem now turns to find a parametric curve that minimizes both internal and external energies defined in Eq. (3.2), which can be solved by the Euler-Lagrange equation as follows :

$$\frac{dE_{\text{snake}}}{dC} = -\frac{\partial}{\partial s}\left(\alpha(s)\frac{\partial C(s)}{\partial s}\right) + \frac{\partial^2}{\partial s^2}\left(\beta(s)\frac{\partial^2 C(s)}{\partial s^2}\right) - \nabla\left|\nabla I(C(s))\right|^2 = 0. \qquad (3,3)$$

This partial differential equation (PDE) expresses the balance of internal forces (first two terms) and external forces (last term), when the contour rests at equilibrium. Under these two forces, C can be attracted to the boundary of the targeted object. For simplicity, $\alpha(s)$ and $\beta(s)$ are usually assumed to be constants. Suppose an artificial time t and a initial contour C_0, the motion function to minimize the snake energy Eq. (3.2) by iterative gradient descent is given by :

$$\frac{\partial C(s,t)}{\partial t} = -\frac{dE_{snake}}{dC}$$

$$= \alpha \frac{\partial^2 C(s)}{\partial s^2} - \beta(s) \frac{\partial^4 C(s)}{\partial s^4} + \nabla \left| \nabla I\big(C(s)\big) \right|^2. \qquad (3,4)$$

$$C(s,0) = C_0$$

The snake model can guarantee a smooth and continuous segmentation contour, but there still exits several limitations. The initial contour C_0 should be located in the vicinity of the real boundary ; otherwise, snakes may converge to a wrong result. Indeed, the external energy term in Eq. (3.4) is basically an edge detector, therefore its value is relatively large around the image boundaries and smaller in uniform regions. As illustrated in Figure 3.2, the input image is a uniform grey square on a uniform white background. In order to create a sufficiently large basin of attraction, the input image is first Gaussian smoothed as shown in the middle of Figure 3.2. Due to this procedure, the edge gradient is noticeable at a larger range. However, this smoothing process will lead to an over smoothed biased segmentation, for instance without sharp corners and fine details, as illustrated on the example given in the right of Figure 3.2.

3.2. 1. 2 Balloon force

Several methods have been proposed to improve the performance of the snake model. One popular and simple solution consists on the addition of a new internal energy term to Eq. (2.2), in order to make the model behave like an inflatable balloon [28]:

$$E_{Ballons}(C) = \gamma \int_{\Omega_i} dx , \qquad (3,5)$$

where Ω_i represents the region inside of the closed curve C. The balloon force either shrinks ($\gamma > 0$) or expands ($\gamma < 0$) the contour C constantly. Therefore, we need to know in advance whether the initial contour is located inside or outside of the object of interest.

Moreover, the magnitude of γ can lead to a biased segmentation, which, in practice, can be minimized by decreasing the magnitude of γ during the curve evolution [29].

3.2. 1. 3 Gradient Vector Flow Model (GVF)

However, the traditional snake model is limited in practical applications. The main reasons are due to its small capture range and poor performing in the aspect of converging into concavities. To address these problems, Xu and Prince [30] proposed

GVF field as a new external force field. GVF field uses $v(x,y) = [u(x,y), v(x,y)]$ to replace $E_{external}$.

$v(x,y)$ is obtained by minimizing the following energy function:

$$E = \iint \mu |\nabla v|^2 + |\nabla f|^2 |v - \nabla f| dx dy \qquad (3.6)$$

where f represents the edge map of image I. ∇f denotes gradient field of μ is a parameter controlling the smoothness of GVF field. μ is larger if noise level is higher, and it can be set based on the noise level of an image.

Although GVF snake model solves the problem that the curve cannot converge into indentations, it still performs badly in converging into long and thin indentations. To settle this problem, Xu [31] and co-workers added two weighting coefficients into the iterative equation of GVF external force field in 1998. Thereby a new external force field called GGVF field was obtained and GGVF snake model was put forward. Compared with GVF snake model, GGVF snake model has been improved in the performance of converging into indentation and noise robustness. Energy function of GGVF snake model is defined as:

$$E = \iint g(|\nabla f|)|\nabla v|^2 + h(|\nabla f|)|v - \nabla f| dx dy \qquad (3.7)$$

Including:

$$g(|\nabla f|) = e^{-\frac{|\nabla f|}{k}} \qquad (3.8)$$

$$h(|\nabla f|) = 1 - g(\nabla f) \qquad (3.9)$$

The first item on the right side of (5) is smoothing item, which can produce a vector field. The second item is data item, which can drive vector field v to close to the gradient ∇f of edge image. Parameter k determines the weighting value to balance smoothing term and data term. The value of k is related to noise strength of an image. The higher the noise level is; the larger value of k is [32].

The classic snakes provide an accurate location of the edges only if the initial contour is given sufficiently near the edges because they make use of only the local information along the contour. Estimating a proper position of initial contours without prior knowledge is a difficult problem. Also, classic snakes cannot detect more than one boundary simultaneously because the snakes maintain the same topology during the

evolution stage. That is, snakes cannot split to multiple boundaries or merge from multiple initial contours. Level set theory has given a solution for this problem [13].

3.3.2 Geometric models (Level Set method)

The level-set framework has been first proposed in Physics by Osher and Sethian [33] to solve the problem of front propagation. The medialization of the contour using this type of representation has then been proposed by Malladi et al. [37], though the contour evolution was not due to a variational formulation. This variational formulation has been introduced by Caselles et al. [34] and almost simultaneously by Yezzi et al. [41] These research efforts find their origin in the difficulty to handle topologically complex shapes (e.g. object having a hole or multiple non convex components) with the parametric formulation of the active contour's evolution. On the contrary, the contour's representation using level-set allows to easily deal with those kind of shapes as well as with splitting and merging of the contour due to its implicit formulation. Moreover, this removes the problem of contour self-intersections and the need for control point resampling mechanisms. Another advantage of this representation lies in the fact that it allows to discretize the evolution equation on a regular grid.

The level set method [34] is based upon representing an interface as the zero level set of some higher dimensional function ϕ. Typically, the level set function ϕ. is the signed distance function to the interface γ, where $\phi > 0$ on one side of the interface and $\phi < 0$ on the other side. A diagram relating the level set function to the interface is shown in Figure 3.3.
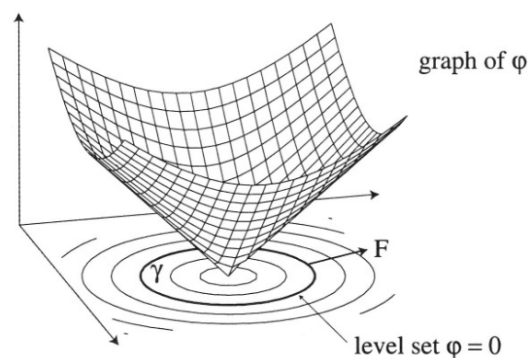
Figure 3.3: Level set function for a circle

At all times, the interface is given by the equation $\phi(x, y, t) = 0$. In order to move the interface, we need to describe the evolution equation of the whole function ϕ.

Let $X(t) = (x(t), y(t))$ be a point on the interface. We are given that $\frac{d}{dt}X(t) = Fn$ for some normal speed function F. Since $X(t)$ is on the interface at all times, then it must be that $\phi(x(t), t) \equiv 0$ for all t. If we differentiate with respect to t, we get:

$$\phi_t + \nabla\phi . \frac{d}{dt}X(t) = 0 \tag{3.10}$$

$$\phi_t + \nabla\phi . Fn = 0 \tag{3.11}$$

Now, the normal to the interface is the normal to the zero level set, and hence we have:

$$n = \frac{\nabla\phi}{\|\nabla\phi\|}$$

Using this, (3.11) becomes:

$$\phi_t + F . \|\nabla\phi\| = 0 \tag{3.12}$$

This is the basic evolution equation for the level set method.

3.3.2.1 Geometric Edge-based Active Contours

Using Osher and Sethian's [33] approach, Caselles et al. [34], Chopp et al. [35] and Rouy et al. [36] proposed the geodesic active contours model followed by the geometric active contours of Malladi et al. [37]. In contrast to Kass et al. [26], the corresponding flows are independent of the parameterization of the curve and depend only on geometrical quantities like curvature k. The model proposed by Caselles and Malladi was based on the following equation: if $\phi(x, t)$ was a 2-D scalar function that embedded the zero level curve, then the geometric active contour was given by solving [38]:

$$\frac{\partial\phi}{\partial t} = c(x)(k + V_0)|\nabla\phi|, \tag{3.13}$$

$$c(x): stopping\ terme\ type\ 1$$

where k was the level set curvature, V_0 was the constant and was the stopping term (type-1) based on the image gradient and was given as:

$$c(x) = \frac{1}{1 + |\nabla[G_\sigma(x) * I(x)]|}. \tag{3.14}$$

Note that Equation 3.13 is the same as Equation 5 from Malladi et al. [39]. Rewriting Equation 5 from Malladi et al. [39], the stopping force becomes:

47

$$c(x) = e^{\alpha|\nabla[G_\sigma(x)*I(x)]|} \tag{3.15}$$

where α was the gradient constant and $|\nabla[G_\sigma(x)*I(x)]|$ was the absolute of the gradient of the convoluted image. This convolved image was computed by convolving the original image by the Gaussian function with a known standard deviation σ. Taking the constant α as unity and using the exponential series, one can obtain Equation 3.13 from Equation 3.15.

This model has the following weaknesses:

- The stopping term was not robust and hence could not stop the bleeding or leaking of the boundaries.
- The pulling back feature was not strong. This meant that if the front propagated and crossed the goal boundary, then it could not come back.

Kichenassamy et al. [40] and Yezzi et al. [41] tried to solve the above problems by introducing an extra stopping term (type-2), also called the pullback term.

This was expressed mathematically as [38]:

$$\frac{\partial \phi}{\partial t} = c(x)(k + V_0)|\nabla\phi| + (\nabla_c.\nabla\phi) \tag{3.16}$$

$$(\nabla_c.\nabla\phi): stopping\ terme\ type\ 2$$

Note that $(\nabla_c.\nabla\phi)$ denoted the projection of an attractive force vector on the normal to the surface. This force was realized as the gradient of a potential field c . This potential field c for the 2-D and 3-D case was given as: $c(x, y) = -\nabla|G_\sigma(x)*I(x, y)|$ and $c(x, y, z) = -\nabla|G_\sigma(x)*I(x, y, z)|$ respectively. Note that Equation 3.16 is similar to Equation 7 given by Malladi et al. in [39]. Malladi et al. calls the equation as an additional constraint on the surface motion ϕ_t.

Rewriting Equation 7 of Malladi et al. [39] becomes:

$$\phi_t + c(x)(\epsilon k + V_0)|\nabla\phi| + \beta(\nabla_c.\nabla\phi) = 0, \tag{3.17}$$

Where β was the edge strength constant, V_0 was a constant (1 as used by Malladi et al.), k was the curvature dependent speed, ϵ was the constant term controlling the curvature dependent speed and $(\nabla_c.\nabla\phi)$ was the same as defined above.

This model is still suffered from boundary leaking for complex structures.

Siddiqi et al. [42], [43] then changed Kichenassamy et al. [40] and Yezzi et al. 's [41] model by adding an extra term to it [39]:

$$\phi_t + c(x)(k + V_0)|\nabla\phi| + (\nabla_c.\nabla\phi) + \frac{V_0}{2}x.\nabla_c.|\nabla\phi|, \qquad (3.18)$$

$$\frac{V_0}{2}x.\nabla_c.|\nabla\phi|: stopping\ terme\ type\ 3$$

Where $\frac{V_0}{2}x.\nabla_c.|\nabla\phi|$ was the area minimizing term and was mathematically equal to the product of the divergence of the stopping term times the gradient of the flow. This term provided an additional attraction force when the front was in the vicinity of an edge.

The major advantage of this technique include [38]:

- It performed better compared to the first and second implicit models.

The major weaknesses include:

- The system was not very robust at handling the convolutedness of medical shapes.
- The system did not take advantage of the regional neighborhood for the propagation or evolution of level sets.

3.3.2.2 Region-based Active Contours.

Generally, region-based approaches use the image function u_0, not its gradient, to segment the image into homogeneous, connected regions. Most region-based active contour models consist of two parts: the regularity part, which determines the smooth shape of contours, and the energy minimization part, which searches for uniformity of a desired feature within a subset. A nice characteristic of region-based active contours is that the initial contours can be located anywhere in the image as region-based segmentation relies on the global energy minimization rather than local energy minimization. Therefore, less prior knowledge is required than edge-based active contours.

Before considering region-based approaches which segment the image in partitions or regions, we first revisit the Mumford-Shah model.

A. Mumford-Shah energy model

The original Mumford-Shah method [44] for optimal approximation of images aims at finding a set of curves $C = C_1 \cup \dots \cup C_N$ and a smooth function $u : \Omega \rightarrow R$ with possible discontinuities across $\boldsymbol{C}$ approximating the original image u_0. The general form for the Mumford–Shah energy functional can be written as:

$$E_{MS}(u, C) = \int_{\Omega} |u_0(x, y) - u(x, y)|^2 dxdy$$

$$+ \mu \int_{\Omega \backslash C} |\nabla u(x, y)|^2 dxdy + v. \, lengh(C). \tag{3.19}$$

where μ and v are positive constants, Ω denotes the image domain, the segmenting curve $C \subset \Omega$.

The first term in (1) requests that u is a good approximation of u_0, the second term does not allow u to change much in $\Omega \backslash C$, and the third term penalizes the length of the curves.

Tsai et al. (2001) and Chan and Vese (2001) apply the model of Mumford and Shah (1989) for image segmentation and for image denoising by a piecewise smooth or constant function.

B. Chan-Vese model

Piecewise-constant active contour model

Using the Mumford-Shah segmentation model [44] Chan and Vese proposed [45] piecewise-constant active contour model. Piecewise-constant active contour model moves deformable contours minimizing an energy function instead of searching edges. A constant approximates the statistical information of image intensity within a subset, and a set of constants, i.e. a piecewise-constant, approximate the statistics of image intensity along the entire domain of an image. The energy function measures the difference between the piecewise-constant and the actual image intensity at every image pixel. The level set evolution equation is given by:

$$\frac{\partial \phi(x, y)}{\partial t} = \delta_\epsilon(\phi(x, y))[v\kappa(\phi(x, y))$$

$$- \{(I(x, y) - \mu_1)^2 - (I(x, y) - \mu_0)^2\}], \tag{3.20}$$

where μ_0 and μ_1 respectively denote the mean of the image intensity outside and inside of the contours. The final partitioned image can be represented as a set of piecewise-constants, where each subset is represented as a constant. This method has shown the fastest convergence speed among region-based active contours due to the simple representation [13].

(a) Iteration 0

(b) Iteration 40

(c) Iteration 90

(d) Iteration 150
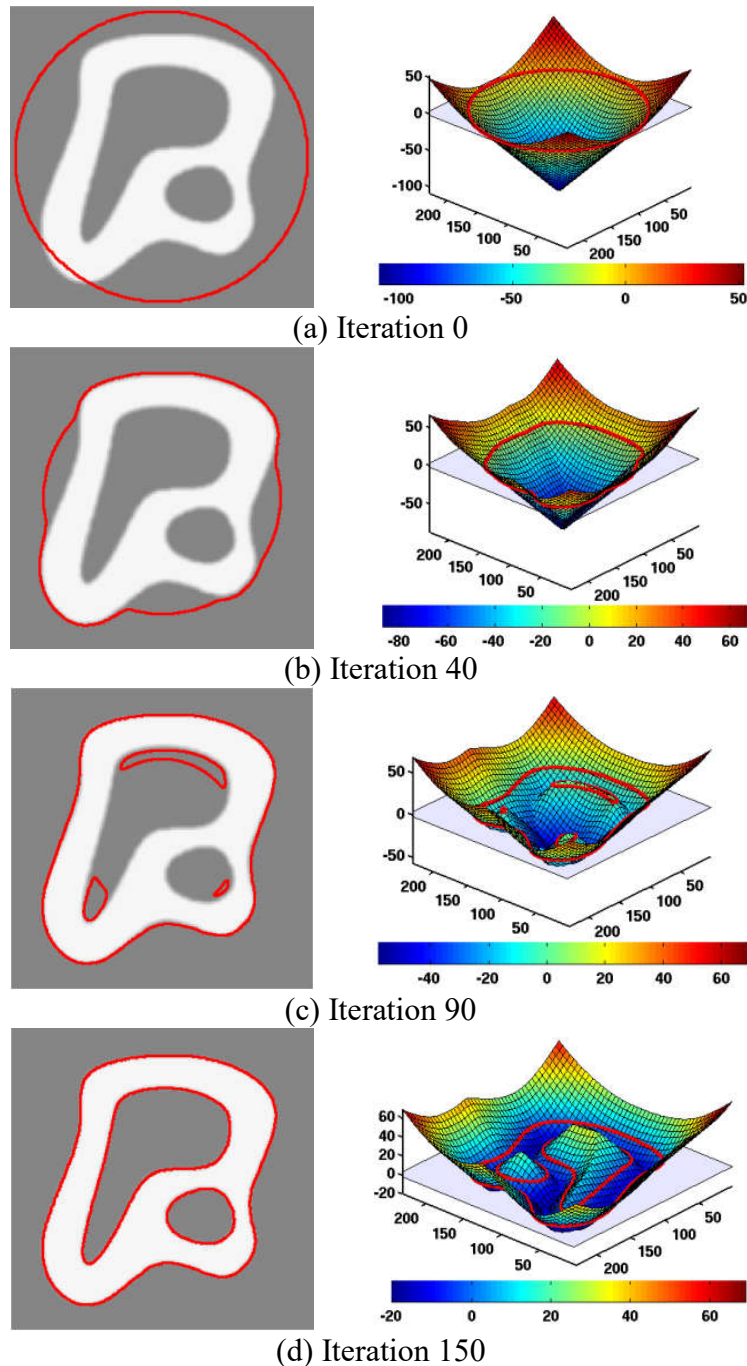
Figure 3.4: Evolution of the level set function using Chan and Vese method.

The zero-level is shown in red [48].

51

Piecewise-smooth active contour model.

an extension of piecewise-constant model using a set of smoothed partial images, was also proposed by Chan and Vese [46, 47]. The same segmentation principles used for piecewise-constant model partitions an image, but a smoothed partial images instead of constants represent each subset. The level set evolution equation is given by:

$$\frac{\partial \phi(x,y)}{\partial t} = \delta_\epsilon(\phi(x,y)) \Big[\nu \kappa(\phi(x,y))$$
$$- \Big\{ \big(I(x,y) - \mu_1(x,y)\big)^2 - \big(I(x,y) - \mu_0(x,y)\big)^2 \Big\}$$
$$- \omega(|\nabla \mu_1(x,y)|^2 - |\nabla \mu_0(x,y)|^2) \Big], \tag{3.21}$$

where $\mu_0(x,y)$ and $\mu_1(x,y)$ respectively denote the smoothed images within the outside and inside of contours.

In [49], Chan and Vese proposed multi-phase active contour model which increases the number of subsets that active contours can find simultaneously.

Multiple active contours evolve independently based on the piecewise-constant model shown in equation 3.20 or the piecewise-smooth model shown in equation 3.21, and multiple subsets are defined by a group of disjoint combination of the level set functions. For example, **N** level set functions define maximum 2**N** subsets of the entire region [13].

Due to the global energy minimization, region-based active contours generally do not have any restriction on the placement of initial contours. That is, region-based active contour can detect interior boundaries regardless of the position of initial contours. The use of pre-defined initial contours provides a method of autonomous segmentation. Also, they are less sensitive to local minima or noise than edge-based active contours. However, due to the assumption of uniform image intensity, most methods are applicable only to images where each subset is representable by a simple expression, e.g. single Gaussian distribution or a constant. If a subset, i.e. class, consists of multiple distinctive sub-classes, these methods would produce over-segmented or under-segmented results [13].

3.3.2.3 Local region based model

Lankton and Tannenbaum, proposed a localizing region-based active contour model in [50]. This formulation handles local statistics and is therefore well suited for

segmenting objects whose boundaries are discontinuous and heterogeneous, where standard region-based methods that use global statistics fail. Moreover, the level set updates on a narrow band around the zero-level set, so the localization framework is a very effective local segmentation method [52].

Let $\Omega \in R^2$ be the image domain, $I : \Omega \to R$, be a given gray level image and C denote a closed curve represented as the zero level set of a signed distance function (SDF) $\phi = \{x \mid \phi(x) = 0\}$. The evolution equation can be formulated as follows:

$$\frac{\partial \phi}{\partial t}(x) = \delta\phi(x) \int_{\Omega_y} B(x,y) . \nabla_{\phi(y)} F(I(y), \phi(y)) dy \tag{3.23}$$

where $\delta\phi$ is the derivative of the Heaviside function, $\nabla_{\phi(y)} F(I(y), \phi(y))$ is a generic region-based energy measure, and the characteristic function $B(x,y)$ marked the local regions in terms of a radius parameter r can be described as follows:

$$B(x,y) = \begin{cases} 1, & \|x - y\| < r, \\ 0 & otherwise. \end{cases}$$

It is noteworthy that almost all the region-based segmentation energies can be put in to this framework. Considering the region-based energy measure proposed by Chan and Vese [46], (3.23) can be reformulated as:

$$\frac{\partial \phi}{\partial t}(x) = \delta\phi(x) \int_{\Omega_y} B(x,y) \delta\phi(y) ((I(y) - u_x)^2 - (I(y) - v_x)^2) dy. \tag{3.24}$$

According to the literature [51], the gradient descent equation given above and the following one have the same stationary solutions:

$$\frac{\partial \phi}{\partial t}(x) = \delta\phi(x) \int_{\Omega_y} B(x,y) ((I(y) - u_x)^2 - (I(y) - v_x)^2) dy. \tag{3.25}$$

Here, $u_x \; and \; v_x$ represent separately the intensity means in the interior and exterior of the contour localized by $B(x,y)$ neighborhood at a point x, given by

$$u_x = \frac{\int_{\Omega_y} B(x,y) H(\phi(y)) I(y) dy}{\int_{\Omega_y} B(x,y) H(\phi(y)) dy} \tag{3.26}$$

$$v_x = \frac{\int_{\Omega_y} B(x,y)(1 - H(\phi(y))) I(y) dy}{\int_{\Omega_y} B(x,y)(1 - H(\phi(y))) dy} \tag{3.27}$$

Due to the localization property of the characteristic function **B**, at each point x of the contour, the energy is dominated by the intensity of points y in a neighborhood of x. This localization property plays a key role in segmenting the objects with intensity inhomogeneities, weak edges or complex background [52].

3.3.2.4 Advantages of Level Sets.

Level set formulation offers a large number of advantages that are as follows [38]:

1. **Capture Range:** The greatest advantage of this technique is that this algorithm increases the capture range of the field flow and thereby increases the robustness of the initial contour placement.

2. **Effect of Local Noise:** When the regional information is integrated into the system, then the local noise or edge will not distract the growth process. This technique is non-local and thus the local noise cannot distract the final placement of the contour or the diffusion growth process.

3. **No Need of Elasticity Coefficients:** The technique is not controlled by elasticity coefficients, unlike parametric contour methods. There is no need to fit tangents to the curves and compute normals at each vertex. In this system, the normals are embedded in the system using the divergence of the field flow. This technique has an ability to model incremental deformations in shape.

4. **Suitability for Medical Image Segmentation:** This technique is very suitable for medical organ segmentation since it can handle any of the cavities, concavities, convolutedness, splitting or merging.

5. **Finding the Global Minima:** There is no problem finding the local minima or global minima, unlike optimization techniques of parametric snakes.

6. **Normal Computation:** This technique is less prone to the normal computational error which is very easily incorporated in classical balloon force snakes for segmentation.

7. **Automaticity:** It is very easy to extend this model from semi-automatic to completely automatic because the region is determined on the basis of prior information.

8. **Integration of Regional Statistics:** This technique is based on the propagation of curves (just like the propagation of ripples in the tank or propagation of the fire flames) utilizing the region statistics.

9. **Flexible Topology:** This method adjusts to the topological changes of the given shape. Diffusion propagation methods handle a very natural framework for handling the topological changes (joining and breaking of the curves).

10. **Wide Applications:** This technique can be applied to unimodal, bimodal, and multi-modal imagery, which means it can have multiple gray level values in it. These methods have a wide range of applications in 3-D surface modeling.

11. **Speed of the System:** This technique implements the fast marching method in the narrow band for solving the Eikonal Equation for computing signed distances.

12. **Extension:** The technique is an easy extension from 2-D to 3-D.

13. **Incorporation of Regularizing Terms:** This can easily incorporate other features for controlling the speed of the curve. This is done by adding an extra term to the region, gradient and curvature speed terms.

14. **Handling Corners:** The system takes care of the corners easily unlike parametric curves, where it needs special handling at corners of the boundary.

15. **Resolution Changes:** The technique is extendable to multi-scale resolutions, which means that at lower resolutions, one can compute regional segmentations. These segmented results can then be used for higher resolutions.

16. **Multi-phase Processing:** This technique is extendable to multi-phase, which means that if there are multiple level set functions, then they automatically merge and split during the course of the segmentation process.

17. **Surface Tracking:** Tracking surfaces are implemented using level sets very smoothly.

18. **Quantification of 3-D Structures:** Computation of geometrical computations is done in a natural way, for example, one can compute the curvature of 3-D surfaces directly while performing normal computations.

19. **Integration of Regularization Terms:** Allows easy integration of vision models for shape recovery such as in fuzzy clustering, Gibbs model, Markov Random Fields and Bayesian models. This makes the system very powerful, robust and accurate for medical shape recovery.

20. **Concise Descriptions:** One can give concise descriptions of differential structures using level set methods. This is because of background mesh resolution controls.

21. **Hierarchical Representations:** Level set offers a natural scale space for hierarchical representations.

22. **Re-parameterization:** There is no need for re-parameterization for curve/surface estimation during the propagation, unlike in the classical snake model.

3.3.2.5 Disadvantages of Level Sets.

Even though level sets have dominated several fields of imaging science, these front propagation algorithms have certain drawbacks. They are as follows [38]:

1. **Initial placement of the contour:** One of the major drawbacks of parametric active contours was its initial placement. It does not have either enough capture range or enough power to grab the topology of shapes. Both of these drawbacks were removed by level sets provided the initial contour was placed symmetrically with respect to the boundaries of interest. This ensures that level sets reached object boundaries almost at the same time. On the contrary, if the initial contour is much closer to the first portion of the object boundary compared to the second portion, then the evolving contour crosses over the first portion of the object boundary. This is because the stop does not turn out to be zero. One of the controlling factors for the stop function is the gradient of the image. The relationship of the stop function to the gradient is its inverse, and also depends upon the index power in the ratio for stopping the propagation, the denominator should be large, which means image forces due to the gradient should be high. This means index should be high. In other words, if is high, then the gradient is high, which means weak boundaries are not detected well and will be easily crossed over by the evolving curve. If is low (low threshold), then the level set will stop at noisy or at isolated edges.

2. **Embedding of the object:** If some objects (say, inner objects) are embedded in another object (the outer object), then the level set will not capture all objects of interest. This is especially true if embedded objects are asymmetrically situated. Under such conditions, one needs multiple initializations of active contours. This means only one active contour can be used per object.

3. **Gaps in boundaries:** This is one of the serious drawbacks of the level set method and has been pointed out by Siddiqi and Kimia. Due to gaps in the object, the evolving contour simply leaks through gaps. As a result, objects

represented by incomplete contours are not captured correctly and fully. This is especially prominent in realistic images, such as in ultrasound and multi-class MR and CT images.

4. **Problems due to shocks:** Shocks are the most common problem in level sets. Kimia and co-workers [53] developed such a framework by representing shape as the set of singularities (called shocks) that arise in a rich space of shape deformations as classified into four types:

   a. First-order shocks are orientation discontinuities (corners) and arise from protrusions and indentations;

   b. Second-order shocks are formed when a shape breaks into two parts during a deformation;

   c. Third-order shocks represent bends

   d. Fourth-order shocks are seeds for each component of a shape. These shocks arise in level sets and can cause sometimes serious problems.

3.4 Conclusion

Active contour models are now a well-established class of segmentation methods. In this chapter, we have briefly summarized several basic concepts of image segmentation by active contour models, in particular the implementation of the level set method. In the next three chapters where we will present our contributions to this thesis; we will provide more details and explanations of the most famous and popular active contour models with the main challenges in this field.

CHAPTER IV

AN EFFICIENT LEVEL SET METHOD BASED ON GLOBAL STATISTICAL INFORMATION FOR IMAGE SEGMENTATION

"You cannot teach a man anything; you can only help him discover it in himself."

Galileo (1564 - 1642)

4.1 Introduction

Image processing is the most extensively examined problem in image processing. It has various important scientific applications, including computer vision, biomedical image, satellite images, and pattern recognition. Due to its importance, in the last few years and over the last two decades, plenty of efforts have been focusing on the segmentation process. This is the reason why, we may find in the literature a great variety of segmentation algorithms that are based on diverse theories such as statistics, differential equations, heuristics, graph theory, and algebra [56, 67, 70, 71, 72]. The choice of a particular technique or algorithm over another is based on the image type and the nature of the problem.

Since its invention by Kass et al. [26], the active contour models have been widely studied and successfully used in image processing, particularly in image segmentation. Their basic idea is to evolve a deformable curve based on an energy functional minimization, in order to provide smooth and closed contours to achieve sub-pixel accuracy of the object boundaries in a given image, which is not achievable with classical methods.

In general, there are two main approaches in active contours based on the mathematical implementation: snakes and level sets. The level set was proposed by Osher and Sethian [33]. It was widely used in solving the problems of surface evolution and in image processing (segmentation methods). The major advantage of using the level set method is that arbitrarily complex shapes can be modeled, and the topological changes, such as merging and splitting, are handled implicitly. These make computational techniques for tracking the evolution of contours and surfaces robust and accurate [71].

The existing active contour method can be roughly categorized as edge-based models [37, 59, 63] and region-based models [44, 45, 47, 49, 58, 62, 64]. Each of the

aforementioned models has its own pros and cons and the choice between both in applications depends on the different characteristics of the images.

To attract the active contour toward the object boundaries, the edge-based models use local image gradient information by involving an edge detector, which depends on the gradient of the image to stop the evolving curve at the boundary of the object.

One of the most popular edge-based models is the geodesic active contour model (GAC) proposed by Caselles et al. [54] It is based on the relationship between active contours and the computation of geodesics or minimal distance curves [54]. These types of the edge-based active contour are very sensitive to noise, and they are not effective to detect weak boundaries. Moreover, the segmentation result is highly dependent on the initial contour placement. In addition, edge-based models are prone to a local minimum and fail to detect the exterior and interior boundaries when the initial contour is far from the desired object boundary [57].

Region-based models have many advantages over edge-based ones. First, they aim to identify each region of interest by using region descriptors to guide the motion of the contours, which are less sensitive to noise and can efficiently segment images with weak edges or without edges. Second, they are robust against initial contour placements.

The well-known piecewise-constant model (PC model) proposed by Chan and Vese [45], which uses a simplified Mumford-shah function for image segmentation, has been successfully used with the assumption that image intensities are statically homogeneous. However, the PC model is less sensitive to the initial contour, but it is not efficient in the presence of intensity inhomogeneity. To overcome the limitations of the PC model and handle more general cases, both Chan and Vese [46] and Tsai et al. [47] proposed two similar models known as piecewise smooth (PS) models, based on the minimization of Mumford–Shah functional [44]. The PS model can achieve a desirable segmentation result for images with intensity inhomogeneity. However, its computational cost is expensive due to the complicated procedures involved, which limits its applications.

Recently, some effective level set methods [64, 65, 68, 67, 72] are proposed to segment images with intensity inhomogeneity. Feng et al. proposed a local inhomogeneous intensity clustering (LINC) model [64], and Wang et al. [65] utilized two different local

fitted images to construct a hybrid region intensity fitting (HRIF) energy functional. Unfortunately, some local information based models are sensitive to noise and highly dependent on the initial contours [68, 69, 72].

In this chapter, we propose a new region-based active contour model in a novel variational level set formulation for image segmentation, where we can benefit from the advantages of the CV and GAC models. For this purpose, we first define a global intensity fitting energy functional; second, we insert our function in the GAC formulation. Using the global image information, the images with weak or blurred boundaries can be effectively segmented in restricted iterations. Our model can also accurately segment images with different kinds of noise and in presence of intensity inhomogeneity. Moreover, the comparisons with well-known models such as the CV model and the DRLSE model [55] show the advantages of our method in terms of accuracy and efficiency. In addition, the initial contour can be anywhere in the image.

4.2 Backgrounds

In [33] Osher and Sethian proposed a level set theory, which provide more flexibility and convenience in the implementation of active contour models for image segmentation. As the first level set implemented active contour model for the image segmentation problem, Caselles et al. [54] proposed the geodesic active contour (GAC) model.

The corresponding level set formulation is as follows:

$$\frac{\partial \phi}{\partial t} = g(I)|\nabla \phi| \left(div \left(\frac{\nabla \phi}{|\nabla \phi|} \right) + \mu \right) + \nabla g(I) . \nabla \phi \qquad (4.1)$$

Generally, a positive decreasing and regular function $g(|\nabla I|)$ is used such that $\lim_{t \to \infty} g(t) = 0$. For instance,

$$g(|\nabla I|) = \frac{1}{1 + |\nabla G_\sigma * I|^2} \qquad (4.2)$$

where $G_\sigma * I$ denotes convolving image I with a Gaussian kernel whose standard deviation is σ.

The geodesic active contour model compares favorably to the classical snake because it does not depend on the curve parameterization. Also, due to the level set

implementation, topological changes are naturally handled, which allows detection of all the objects that appear in the image plane without knowing their exact number [63].

Based on the Munford–Shah model [44] another type of level set active contour implementation was proposed by Chan and Vese [45]. For a given image I in domain Ω, they introduced the energy functional $E_{CV}(c_1.c_2.C)$ defined by:

$$E_{CV}(c_1.c_2.C) = \mu.length(C) + v.area\big(inside(C)\big)$$

$$+\lambda_1 \int_{inside(C)} |I(x) - c_1|^2 dx + \lambda_2 \int_{outside(C)} |I(x) - c_2|^2 dx. \ x \in \Omega \qquad (4.3)$$

Where c_1 and c_2 are two constants related to the global properties of the image contents which approximate the image intensities inside and outside the contour C, respectively.

$$\begin{cases} C = \{x \in \Omega : \phi(x) = 0\}. \\ inside(C) = \{x \in \Omega : \phi(x) > 0\}. \\ outside(C) = \{x \in \Omega : \phi(x) < 0\}. \end{cases} \qquad (4.4)$$

By minimizing Eq. (4.3), it is easy to express these constants c_1 and c_2 as follows:

$$c_1(\phi) = \frac{\int_\Omega I(x).H(\phi)dx}{\int_\Omega H(\phi)dx}. \qquad (4.5)$$

$$c_2(\phi) = \frac{\int_\Omega I(x).\big(1 - H(\phi)\big)dx}{\int_\Omega \big(1 - H(\phi)\big)dx}. \qquad 4.6)$$

$H(\phi)$ is the Heaviside function and $\delta(\phi)$ is the Dirac function.

By incorporating the length and area energy terms into Eq. (4.3) and minimizing them using the steepest descent method [56], Chan and Vese obtained the corresponding variational level set formulation as follows (with $\phi(0.x.y) = \phi_0(x.y)$ defining the initial contour):

$$\frac{\partial \phi}{\partial t} = \delta(\phi) \left[\mu div\left(\frac{\nabla \phi}{|\nabla \phi|}\right) - v - \lambda_1(I - c_1)^2 + \lambda_2(I - c_2)^2 \right] \qquad (4.7)$$

Generally, the parameters are taken to be $\mu \geq 0$. $v \geq 0$. $\lambda_1 > 0$. $\lambda_2 > 0$, where μ is the scale parameter which controls the smoothness of zero level set, v increases the

propagation speed, and λ_1 and λ_2 control the image data-driven force inside and outside the contour, respectively.

4.3 The global intensity fitting Model

In this section, we will detail our active contour model for image segmentation, based on energy functional with global intensity fitting.

We note that c_1 and c_2 are the global mean intensity of the region outside and inside the zero level set respectively. So a global fitted image formulation can be expressed as follows [60]:

$$I_s = c_1 H_\varepsilon(\phi) + c_2\big(1 - H_\varepsilon(\phi)\big) \tag{4.8}$$

Our global fitting energy functional can be defined by the minimization of the difference between the global fitted image and the original image. The energy functional is given by:

$$E = \frac{1}{2}\int_\Omega |I(x) - I_s(x)|^2 dx \tag{4.9}$$

Keeping c_1 and c_2 fixed we minimize E with respect to ϕ using the standard gradient descent method [56], [61], we get the function $F_\phi(I)$ as follows:

$$F_\phi(I) = \big[I - c_1 H_\varepsilon(\phi) + c_2\big(1 - H_\varepsilon(\phi)\big)\big](c_1 - c_2)\delta_\varepsilon(\phi) \tag{4.10}$$

$$F_\phi(I) = \delta_\varepsilon(\phi)(I - I_s)(c_1 - c_2) \tag{4.11}$$

For the easy implementation of our model, we can estimate the coefficient $(c_1 - c_2)$ as a constant, which leads to simplify the Eq. (4.11). Therefore, the minimization functional can be written as (refer to Appendix A for detailed derivation):

$$F_\phi(I) = \delta_\varepsilon(\phi)(I - I_s) = \delta_\varepsilon(\phi)F(I(x)). \tag{4.12}$$

For a successful segmentation, we combined region based model and edge based model by inserting our minimized functional in the geodesic active contour formulation, so the level set formulation of our model is given by [69]:

$$\frac{\partial \phi}{\partial t} = \delta_\varepsilon(\phi)F(I(x))|\nabla\phi|\left(div\left(\frac{\nabla\phi}{|\nabla\phi|}\right) + \mu\right) + \nabla F(I(x)).\nabla\phi \tag{4.13}$$

This model enjoys the advantages of the region-based models, i.e., robustness to initialization and insensitivity to image noise, and the advantages of the edge-based models, i.e., good local characteristics and boundary capture capability.

In order to simplify the implementation, the level set formulation of the proposed model can be written as follows:

$$\frac{\partial \phi}{\partial t} = \mu . \delta_\varepsilon(\phi)\left[I - I_1 H_\varepsilon(\phi) - I_2\big(1 - H_\varepsilon(\phi)\big)\right]|\nabla\phi| \tag{4.14}$$

In order to efficiently and robustly regularize the level set function, we can replace the regularization of the level set function ϕ by using a Gaussian filtering process. The regularization term is substituted by the filtering process expressed as follows:

$$\phi^{n+1} = K_\sigma * \phi^n \tag{4.15}$$

K_σ is a Gaussian kernel:

$$K_\sigma = \frac{1}{(2\pi)^{n/2}\sigma} e^{\left(-\frac{|x|^2}{2\sigma^2}\right)} \tag{4.16}$$

The standard deviation σ of the Gaussian kernel plays an import role in practical applications.

The main steps of the algorithm can be summarized as follows [57], [60]:

Initialize the level set function ϕ to be a binary function as follows:

$$\phi(x.t = 0) = \begin{cases} -\rho. & x \in \Omega_0 - \partial\Omega_0 \\ 0. & x \in \partial\Omega_0 \\ \rho. & x \in \Omega - \Omega_0 \end{cases} \tag{4.17}$$

Where $\rho > 0$ is a constant, Ω_0 is a subset in the image domain Ω, and $\partial\Omega_0$ is the boundary of Ω_0.

Evolve the level set function ϕ according to Eq. (4.14).

Regularize the level set function by a Gaussian kernel, $\phi = K_G * \phi$.

Check whether the evolution is stationary. If not, return to step 2.

In step 3, the standard deviation σ of the Gaussian kernel K_G is a critical parameter, which should be chosen properly.

4.4 Results and discussion

In this section, we present the experimental results of our proposed method for both synthetic and real images of different modalities and compare the segmentation results with those from the well-known active contours model. The main parameters of our model are σ, μ, and ε. μ (also ε in some cases) need to be tuned for different images, whereas σ can be fixed (σ = 1 or σ = 3) for most of the applications. Except for specified cases, where σ can tack different values in this chapter.

We first demonstrate the effectiveness of the proposed method for tree synthetic images in Figure 4.1.
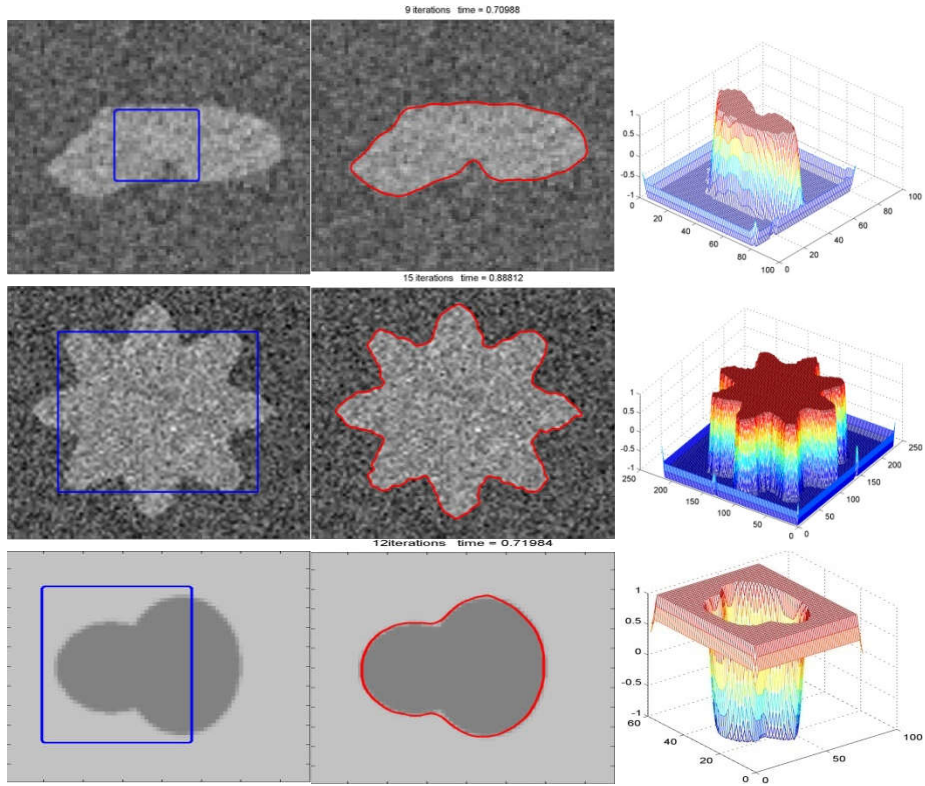
Figure 4.1: Applications of our method to three synthetics images: the first column shows initial contour; the second shows segmentation results and the third column shows the corresponding final level set function

Figure 4.1 demonstrates the segmentation results for our level set formulation regularized by Gaussian filter for tree synthetic images.

The first column shows initial contour, the second shows segmentation results and the third column shows the corresponding final level set function. For the image in the first row (82 × 82 pixels), we used the parameters μ = 17, σ = 3.0, ε = 3.0, the image in the

second row (233 × 216 pixels), we used the parameters μ = 7, σ = 3.0, ε = 3.0, and for the image in the third row (77 × 59 pixels), we used the parameters μ = 15, σ = 3.0, ε = 3.0.

It can be seen that the final level set function is very smooth. This demonstrates clearly the effect of the Gaussian filtering process in keeping the level set function smooth and regular during the evolution of the segmentation process, which leads the evolution to be stable.
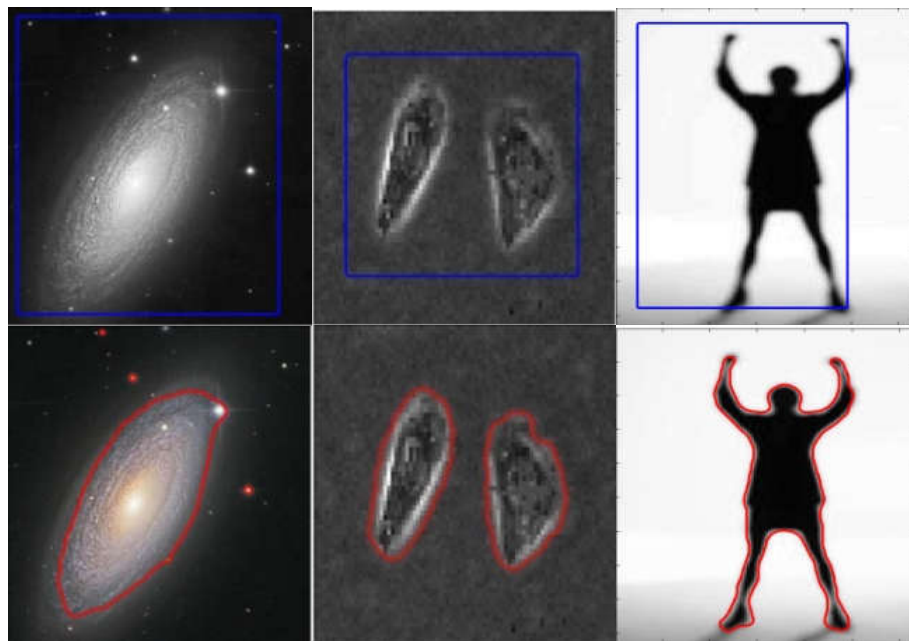
Figure 4.2: Segmentation results of tree images with weak and blurred edges. The first row shows the initial contours which are around the objects. The second row shows the corresponding segmentation results.

The first column of Figure 4.2 shows the segmentation results of a galaxy image of 272 × 297 pixels. For this image, we set μ = 3.5, σ = 3.0, ε = 1.1, the contour of the galaxy is accurately detected in 110 iterations and 5.75 s. The second column of Figure2 shows the result for a real microscope cell image of 83 × 65 pixels. For this image, we used the parameters μ = 15, σ = 1.0, ε = 1.0, the curve evolution converges in 33 iterations and takes only 0.90 s. The third column of Figure 4.2 shows the result of a synthetic image of a man of 128 × 185 pixels. For this image, we used the parameters μ = 30, σ = 1.0, ε = 1.0, the curve evolution converges in 28 iterations and takes only 0.89 s.

We can see that some parts of the boundaries of the two images are quite blurry, which demonstrates the robustness of our model in the presence of weak and blurred edges.
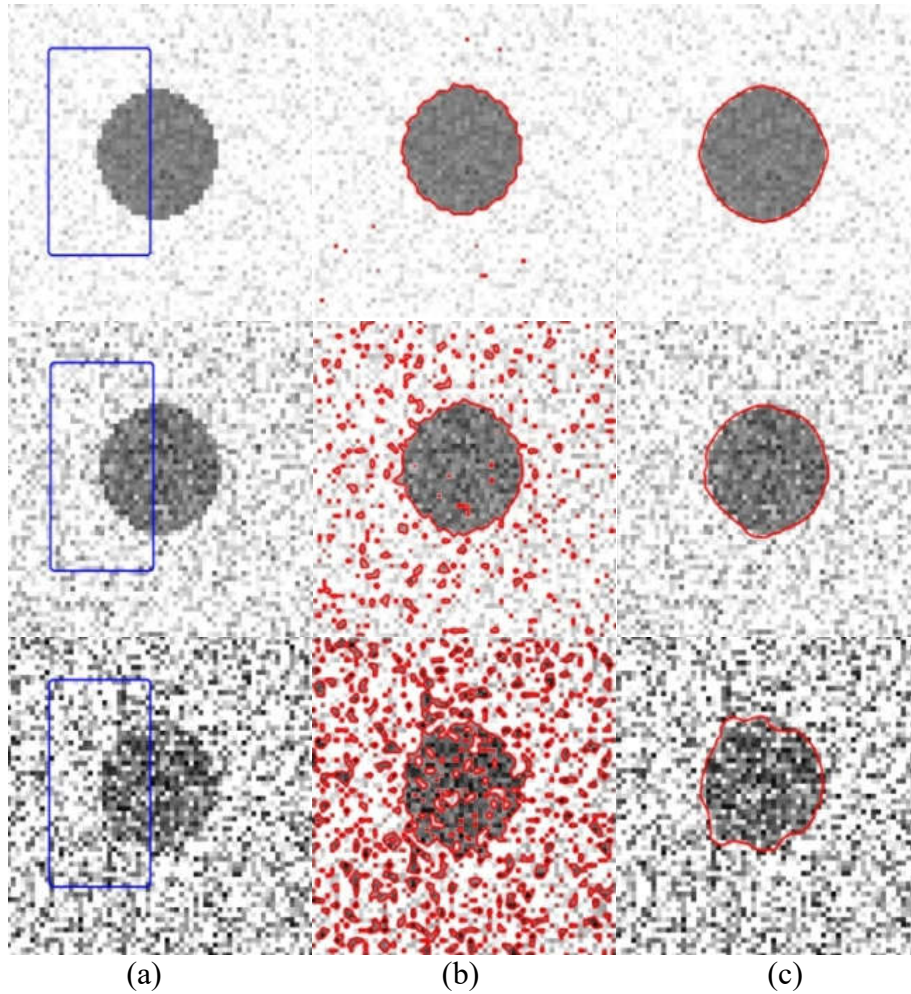
Figure 4.3: Comparison of our model with CV model on three synthetic images in presence of noise: (a) initial contours; (b) the results by the CV model; and (c) the results by our model. Top row: Images with Gaussian noise; middle row: Images with Nakagamy noise; bottom row: Images with Rayleigh noise.

Figure 4.3: shows segmentation results on three synthetic images (1668 × 1400 pixels) in the presence of noise. These images have the same object but different kinds of noise (Gaussian, Nakagamy, and Rayleigh).

The results showed how the object in the presence of noise was successfully segmented and demonstrated the performance of our model over the CV model. For the first row (images with Gaussian noise) we obtained almost the same results (we can see that our model is a little bit better and much faster than the CV model). But for the two other kinds of noise (bottom row and middle row), the results showed that using our model the contour surrounds only the desired objects, which is not the case with the CV model. This illustrates that our model is more efficient than the CV model, which does not succeed in the presence of those kinds of noise (Nakagamy and Rayleigh).
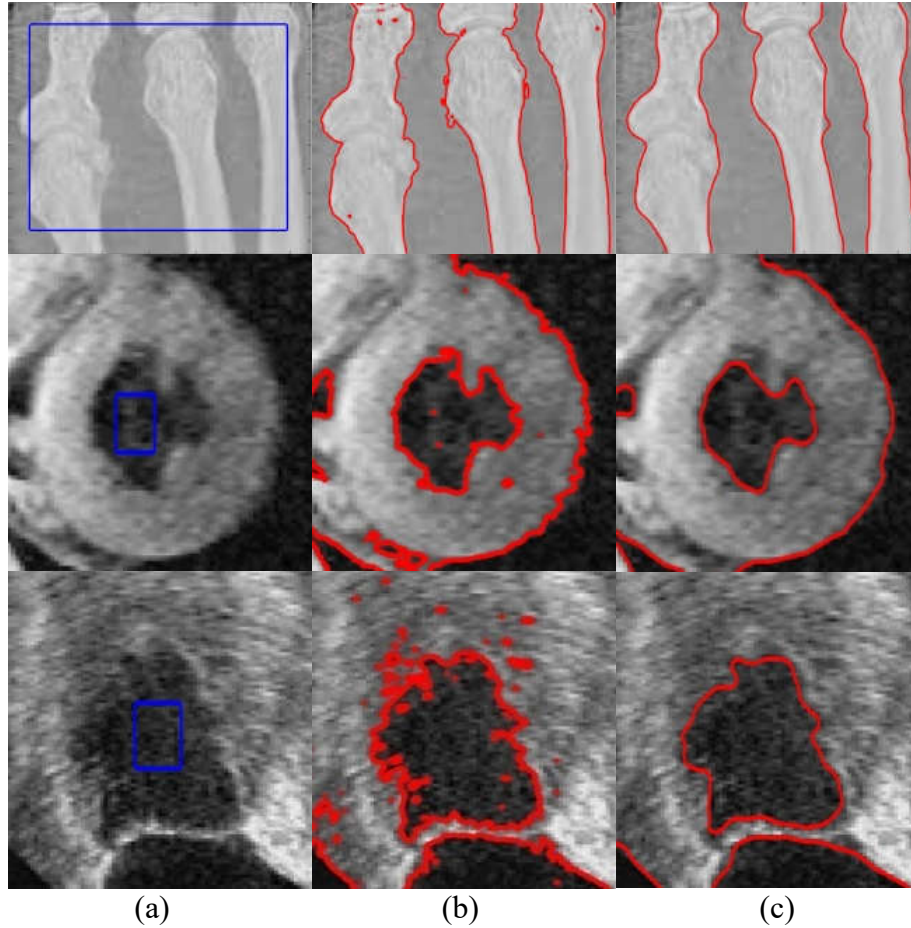
Figure 4.4: Comparison of our model with CV model on medical images in the presence of weak and blurred edges: (a) initial contours; (b) the results by the CV model; and (c) the results by our model.

Figure 4.4 shows segmentation results on medical images with weak and blurred edges and in the presence of noise. The first row shows the segmentation results of an x-ray image of bones of 128×105 pixels. For this image, we used the parameters $\mu = 7$, $\sigma = 3.0$, $\varepsilon = 3.0$, the curve evolution converges in 37 iterations and takes only 0.98 s, while for the CV model, the evolution converges in 849 iterations and takes for 13.00 s. The second row shows the segmentation results of a magnetic resonance image of the left ventricle of a human heart of 136×132 pixels. For this image, we used the parameters $\mu = 11$, $\sigma = 5$, $\varepsilon = 1.0$, the curve evolution converges in 70 iterations and takes only 1.7988 s, instead of 1600 iterations takes for 33.271 s using the CV model. The third row shows the segmentation results of a noisy ultrasound image of the left ventricle of a human heart of 81×92 pixels. For this image, we used the parameters $\mu = 25$, $\sigma = 3$, $\varepsilon = 1.0$, the curve evolution converges in 25 iterations and takes only 1.273 s, instead of 600 iterations takes for 9.928 s using the CV model.

67

We focus on comparing our model with the CV model in terms of computational efficiency and accuracy. The segmentation results of both the CV model and our method (shown in Figure 4.3 and Figure 4.4) demonstrated the advantage of our model in the presence of noise and on images with or without edge. Even after more than 1500 iterations, the CV model presents an unsatisfactory segmentation which is illustrated in Figure 4.3 (b) and Figure 4.4 (b).

Figure 4.3 (c) and Figure 4.4 (c) shows the segmentation result of the proposed model which can successfully stop on the boundary of the object after few iterations (between 15 and 70 iterations), therefore, it is obvious that our model is more efficient in terms of accuracy.

The CPU times, the number of iteration and the sizes of the tested images are listed in Table 4.1, it can be observed that our method is much faster than the CV model. This demonstrates the significant advantage of our model in terms of robustness and computational efficiency.

Table 4.1 The CPU times and the number of iteration for our model and CV.

	Figure3						Figure4					
	Row 1 64 × 64		Row 2 64 × 64		Row 3 64 × 64		Row 1 128 × 105		Row 2 136 × 132		Row 3 81 × 92	
	Iterations	Time (s)	Iterations	Time (s)	Iterations	Time (s)	Iterations	Time (s)	Iterations	Time (s)	Iterations	Time (s)
Our model	17	0.771	15	0.769	19	0.858	37	0.98	70	1.798	25	1.273
CV model	600	4.945	437	6.841	600	12.361	849	13.00	1600	33.271	600	9.928

To evaluate the accuracy of a segmentation result, we use a simple but effective metric based on the image similarity measure.

The Jaccard index is calculated between the segmentation result A and its grand truth image B as shown in equation 25:

$$JS(A.B) = \frac{|A \cap B|}{|A \cup B|} \tag{4.25}$$

The segmentation accuracy was also evaluated using the Dice similarity coefficient (DSC) defined as follows:

$$DSC(A.B) = 2\frac{|A \cap B|}{|A| + |B|} \tag{4.26}$$

The closer the JS and DSC values to 1, the higher the segmentation accuracy.

We applied our method to three images (real and synthetic images) in Figure 4.5. We used the same initial contour for the two models and all the three images. In this experiment: $\mu = 15$, $\sigma = 1.0$, $\varepsilon = 1.0$ were being used as parameters.

Table 4.2 Segmentation accuracy and computational efficiency.

	Our model				CV model			
	JS	DSC	Iterations	Time (s)	JS	DSC	Iterations	Time (s)
128 × 128 pixels.	0.9391	0.9685	19	0.8537	0.1469	0.2561	700	20.9512
83 × 65 pixels.	0.8574	0.9232	33	0.9673	0.1778	0.3556	470	05.1440
128 × 128 pixels.	0.9615	0.9803	17	0.7718	0.3205	0.4854	123	02.7854

The Jaccard indexes of the corresponding results of both models for the three images are shown in Figure 4.5

(a) (b)

(c) (d) (e)
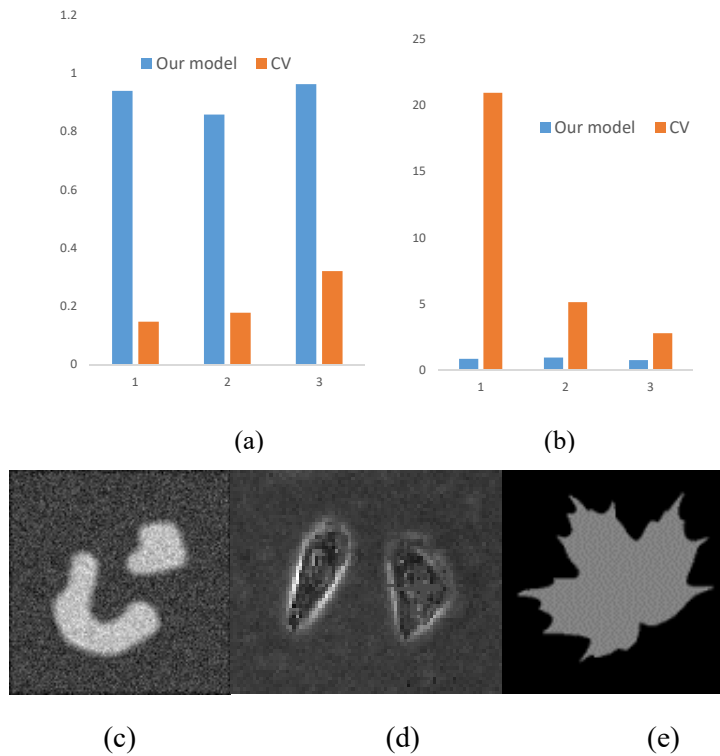
Figure 4.5: Comparison of our model and the CV model in terms of accuracy and CPU time. (a) Jaccard index. (b) CPU times. (c), (d), and (e) test images.

By comparing the Jaccard index and the computation time in our model and in the CV, it is obvious that our method is much simpler, more efficient, and produces more accurate segmentation results.

Figure 4.5 shows that:

- The Jaccard indexes of our model are notably higher than those of the CV model.
- Our model is more efficient and much faster than the CV model.
- The number of iterations by our method is fewer than that by the CV model.
- This is validated and confirmed by the experimental results using the same images and the same initial contours, which demonstrate the important advantage of our model in terms of computational efficiency and accuracy.
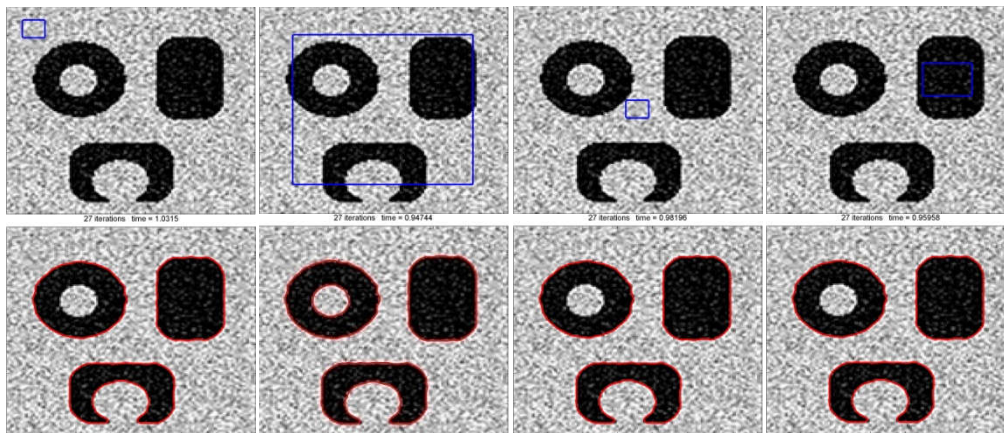
Figure 4.6: Performance of the proposed model with different contour initializations. Top row: The initial contours; Bottom row: Segmentation results

In order to demonstrate the performance of the proposed model with different contour initializations. We applied our method to a synthetic noisy image with three objects of 142×141 pixels with different initializations of the contour and the same settings of parameters: $\mu = 17. \sigma = 3.0. \varepsilon = 3.0$. We test the proposed model with different initial contour and in different positions; the initial contour encloses all the objects of interest, in the left corner of the image or in the center of the image, and totally inside of one object as shown in the examples in Figure 4.6 even though the great difference of these initial contours, the corresponding results are almost the same as shown in the bottom row of Figure 4.6, all accurately capturing the object boundaries. For the different contour initializations, the curve evolution converges in the same number of iterations (27 iterations) with a little difference of consuming time: 1.03s, 0.94s, 0.98s,

and 0.95s respectively. The experimental results demonstrate the accuracy and the robustness of our model to contour initializations.
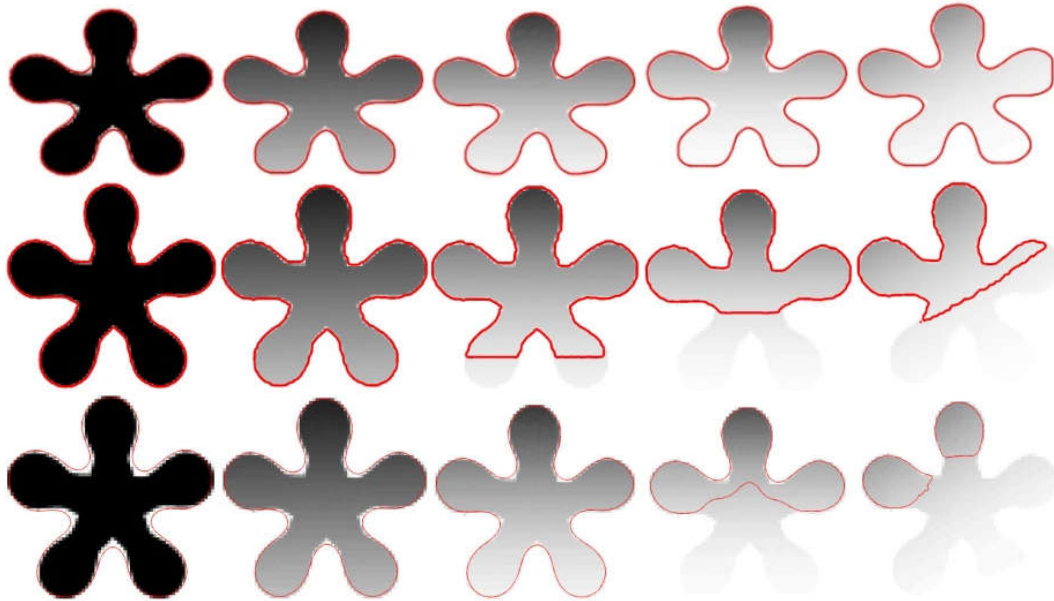
Figure 4.7: Robustness of our model to intensity inhomogeneity Segmentation results: Top row: Our model; Middle row: CV model; Bottom row: DRLSE

To demonstrate the performance of our model, we are now focusing on the comparison of our model with the two well-known models, the CV model and the DRLSE model using the same initial contours. Figure 4.7 shows the segmentation results of our model, CV model and DRLSE model for five synthetic images of the same object with increased intensity inhomogeneity.

The corresponding results of our model are shown in the upper row of Figure7. It can be seen that our method achieves satisfactory results for increasing levels of intensity inhomogeneity, which proves the robustness of our model in dealing with different levels of intensity inhomogeneity.

Both CV and DRLSE models can obtain good results when images are contaminated with a slight intensity inhomogeneity (see image 1, 2). However, for images with more severe inhomogeneity of intensity (see images 3-5 in the middle row), the CV model fails to segment the object accurately. Also, the DRLSE fails totally when the strength of intensity inhomogeneity is strong (see images 4 and 5 in the lower row), the performance of this method also degenerates severely.

This experiment shows that our model is more efficient and more robust to intensity inhomogeneity than the CV and DRLSE models.

We compare the computation speeds of our model, the CV model and, the DRLSE model, by applying them to the same medical images. The first row of Figure8 shows an MR image of the left ventricle of a human heart of 152×128 pixels, and the second row shows an MR image of a human bladder of 107×180 pixels. The third column shows the corresponding segmentation results.

Our method achieves almost the same results as the DRLSE model, but the CV model fails (Figure 4.8). For our model, the evolution of the level set function converges in 90 iterations and takes only 2.905 s. While for the DRLSE model, the evolution converges in 940 iterations and takes 51.360 s and for the CV model, and with the second image the evolution of the level set function converges in 15 iterations and takes only 1.019 s, while for the DRLSE model, the evolution converges in 210 iterations and takes 6.474s. Obviously, our model is significantly faster than the DRLSE model.
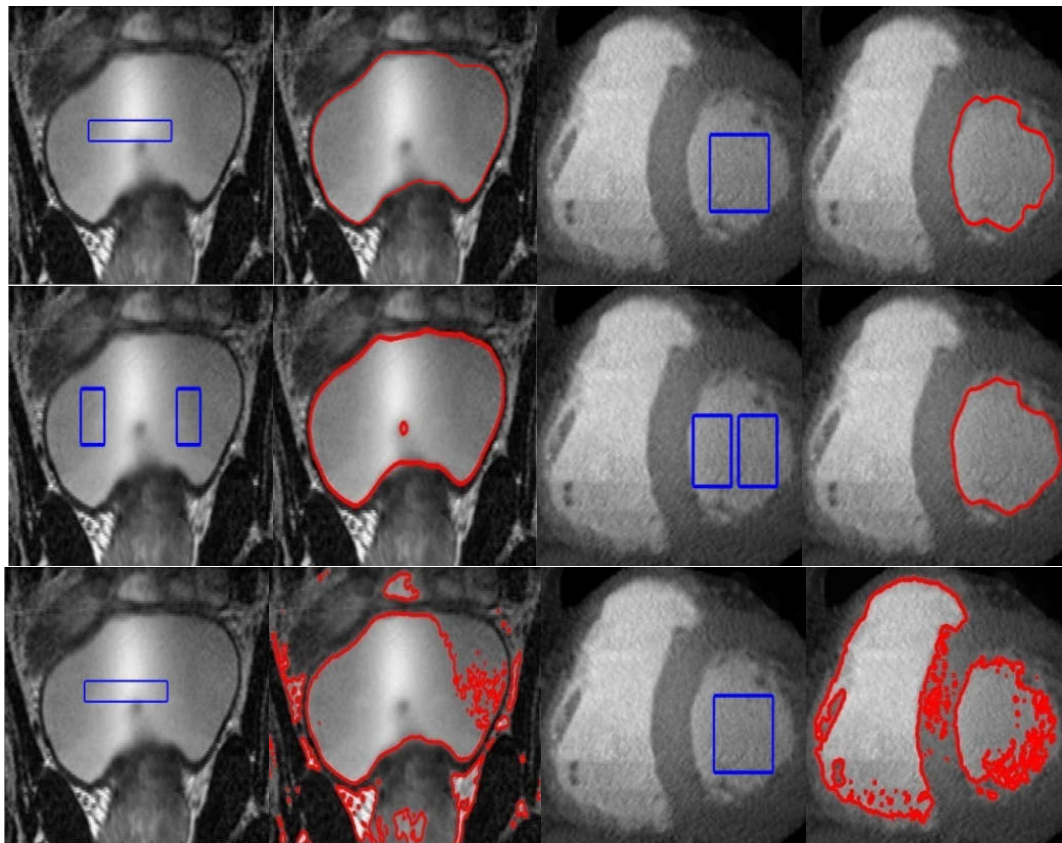
Figure 4.8: Comparison of our model with the DRLSE model and the CV model on two medical images: Top row: the results by our model, middle row: the results by the DRLSE model, bottom row: the results by the CV model, the blue solid lines represent the initial contours.

4.5. Conclusions

In this chapter, we proposed a novel region-based active contour model in a variational level set formulation. We define a global intensity fitting energy functional, which was implemented in a new level set method with the adoption of the Geodesic algorithm, which can improve the robustness of the proposed method. Our model enjoys the advantages of the region-based models, i.e., robustness to initialization and insensitivity to image noise, and the advantages of the edge-based models, i.e., good local characteristics and boundary capture capability. Experimental results demonstrate the desirable performance of our method for different kinds of images with weak or blurred edges and in the presence of intensity inhomogeneities and various types' noises. Moreover, our model is significantly faster than classical active contours methods such as GAC model, CV model, and DRLSE model, in terms of computational efficiency and more effective in terms of accuracy, and that has a good impact in different areas especially in medical diagnosis and computer vision.

CHAPTER V

A ROBUST REGION-BASED ACTIVE CONTOUR MODEL BASED ON LOCAL
AVERAGE INTENSITY FOR IMAGE SEGMENTATION

"We cannot solve problems with the same thinking we used to create them."

Albert Einstein (1879 - 1955)

5.1 Introduction

During the last decades, the use of the level set method [73, 56] knew an enormous
diffusion in the field of image processing and computer vision especially in the
segmentation of the images. The most used techniques [73, 74] based on level set
method can be regrouped in some categories like: region-based segmentation, edge-
based segmentation, and classification-based segmentation. Commonly, region based
segmentation methods are able to deal with images with or without edges. However,
most of these methods [45-79] assume that image intensity is homogeneous, leading to
the failure in segmenting images containing heterogeneity of intensity. In [45], Chan
and Vese developed the CV model, one of the most popular active contour models for
image segmentation, relying on the optimal approximation by piecewise smooth
functions proposed by Mumford and Shah in [44]. The CV model has been successfully
applied on different kinds of images with the assumption that the intensities in each
region are homogeneous. However, the CV model and their homologues region based
models often fail to segment images with intensity inhomogeneity.

In fact, during the process of acquiring medical images and even in other imaging
systems, they frequently appear intensity inhomogeneities in the captured images,
which is often caused by the characteristics of the imaging devices or the techniques
adopted in these devices or illumination variations [81]. In order to overcome this
functionality and get good results in the presence of inhomogeneity of intensity in
images, a lot of research has been done to suggest new and improved models that can
deal effectively with this problem such as the piecewise smooth (PS) model proposed
by Vese and Chan [45] and their analogue proposed by Tsai et al.[47] Although the two

models dealt with the problem of intensity inhomogeneities significantly, they cost a long computational time, which is a reason to limit their practical applications. In order to overcome the difficulty caused by the presence of the inhomogeneity of the intensity, many models have been proposed during the last two decades, the best known are: the local binary fitting (LBF) model [58] the region-scalable fitting (RSF) model [76] local intensity clustering (LIC) method [79] LRB method [50] local region model (LRM) [83] patch driven level set method [84] and edge driven level set method [85] etc.

In this chapter, we propose a novel local region-based method for image segmentation in presence of intensity inhomogenities. The main idea behind the proposed model is to create an energy functional-driven by the difference between the local average intensity inside and outside the contour. The energy functional is incorporated into a level set functional to achieve its minimization. As an important application our method can be used for segmentation of synthetic medical and other kinds of real images with or without intensity inhomogenities in limited iterations. Furthermore, we greatly reduce the computational time using the Gaussian filtering to regularize our level set function which keeps the level set function smooth and reduce the effect of the noise to a certain degree [57, 82]. Moreover, the comparison of our model with the will-known models like CV model. LBF and Local Gaussian distribution (LGD) model [75] show the superiority of our model over them in term of robustness efficiency and time consuming.

5.2 Region-based active contour models

One of the first implementations of the Mumford–Shah model [44] piecewise-constant case is the curve evolution of the Chan-Vese model. Firstly, we give the general equation of the Mumford–Shah energy functional by:

$$E_{MS}(u.C) = \int_{\Omega} |u_0(x.y) - u(x.y)|^2 dxdy$$

$$+ \mu \int_{\Omega \backslash C} |\nabla u(x.y)|^2 dxdy + v.lengh(C). \tag{5.1}$$

where μ and v are positive constants. Ω denotes the image domain. the segmenting curve $C \subset \Omega$.

The Chan–Vese (CV) model solves the minimization of (5.1) by minimizing the following energy functional:

$$E_{CV}(c_1.c_2.C) = \mu.length(C) + v.area(inside(C))$$

$$+\lambda_1 \int_{inside(C)} |I(x) - c_1|^2 dx + \lambda_2 \int_{outside(C)} |I(x) - c_2|^2 dx . \ x \in \Omega \qquad (5.2)$$

they used certain global features of the content of the image designated by two constants c_1 and c_2 to estimate the intensities inside and outside the contour C.

$$\begin{cases} C = \{x \in \Omega : \phi(x) = 0\}. \\ inside(C) = \{x \in \Omega : \phi(x) > 0\}. \\ outside(C) = \{x \in \Omega : \phi(x) < 0\}. \end{cases}$$

By minimizing Eq. (2). it is easy to express these constants c_1 and c_2 as follows:

$$c_1(\phi) = \frac{\int_\Omega I(x).H(\phi)dx}{\int_\Omega H(\phi)dx}. \qquad (5.3)$$

$$c_2(\phi) = \frac{\int_\Omega I(x).(1 - H(\phi))dx}{\int_\Omega (1 - H(\phi))dx}. \qquad (5.4)$$

$H(\phi)$ is the Heaviside function and $\delta(\phi)$ is the Dirac function.

using the gradient descent method to update the level set function $\phi(x,y)$ and benefiting of the Euler-Lagrange equations, we solve the minimization problem:

$$\frac{\partial \phi}{\partial t} = \delta(\phi) \left[\mu div \left(\frac{\nabla \phi}{|\nabla \phi|} \right) - v - \lambda_1 (I - c_1)^2 + \lambda_2 (I - c_2)^2 \right] \qquad (5.5)$$

where λ_1 and λ_2 are used to control the force driven by the image data inside and outside the contour, they have zero as value for both, μ is the positive parameter used to control the regularity of zero level set, and v a positive parameter which raises the speed of propagation.

The main advantages of CV model are it can detect objects with or without boundaries and can efficiently segment noisy images. However, the CV model was often unable to segment images characterized by the presence of heterogeneity. To overcome the limitations of CV model in dealing with the images with intensity inhomogeneity some methods of local region based have been proposed to deal with images with intensity inhomogeneity Li et al. [58] and [76] proposed the local binary fitting (LBF) model by incorporating the local intensity information into region-based level set method. The energy functional of LBF model in terms of the level set function ϕ is as follows:

$$E_{LBF} = \lambda_1 \int \left[\int k_\sigma(x-y)|I(y)-f_1(x)|^2 H(\phi)dy \right] dx$$

$$+\lambda_2 \int \left[\int k_\sigma(x-y)|I(y)-f_1(x)|^2 (1-H(\phi))dy \right] dx + \mu P(\phi) + \nu L(\phi). \qquad x.y \in$$

$$\Omega \qquad (5.6)$$

where λ_1. λ_2. μ and ν are fixed parameters k_σ is a Gaussian kernel with standard deviation σ:

$$k_\sigma(x) = \frac{1}{(2\pi)^{n/2}\sigma} e^{\left(-\frac{|x|^2}{2\sigma^2}\right)} \qquad (5.7)$$

to approximate the local image intensities inside and outside the contour they adopt the two smooth functions f_1 and f_2 given by:

$$\begin{cases} f_1(x) = \frac{K_\sigma * [I(x)H_\varepsilon(\phi)]}{K_\sigma * H_\varepsilon(\phi)}. \\ f_2(x) = \frac{K_\sigma * [I(x)(1-H_\varepsilon(\phi))]}{K_\sigma * (1-H_\varepsilon(\phi))}. \end{cases} \qquad (5.8)$$

Generally, the regularized versions of Heaviside function H and Dirac function δ are used as follows:

$$\begin{cases} H_\varepsilon(z) = \frac{1}{2}\left(1 + \frac{2}{\pi}arctan\left(\frac{z}{\varepsilon}\right)\right) \\ \delta_\varepsilon(z) = \frac{1}{\pi} \cdot \frac{\varepsilon}{\varepsilon^2 + z^2}. \qquad z \in R \end{cases} \qquad (5.9)$$

Despite the fact that the LBF model has segmented images with intensity inhomogeneity in an efficient way but it still has the disadvantage of very high computation time.

5.3 The local average intensity model

We briefly explain in this section the local region-based active contour model that we propose based on the differences between the local average intensity in the local regions. First we replace the two constants C_1 and C_2 of the CV model by the two smooth functions f_1 and f_2 introduced by Li et al. [58] which makes it possible to approximate the local image intensities inside and outside the contour C, we can, therefore, obtain the functional energy of our proposed model by substituting Eq. (5.8) into Eq. (5.2) our energy functional is written as follows:

$$E_{CV}(c_1.c_2.C) = \lambda_1 \int_{inside(C)} |I(x) - f_1|^2 dx + \lambda_2 \int_{outside(C)} |I(x) - f_2|^2 dx \,.\, x$$

$$\in \Omega \tag{5.10}$$

Since we use another method to regularize the level set function § 4. the regularized term was omitted from Eq. (5.2).

In this chapter the level set function ϕ can take positive and negative values outside and inside the contour C. we define the energy functional by:

$$E(c_1.c_2.\phi) = \lambda_1 \int_{inside(C)} (I(x) - f_1(x))^2 H_\varepsilon(\phi) dx$$

$$+ \lambda_2 \int_{outside(C)} (I(x) - f_2(x))^2 (1 - H_\varepsilon(\phi)) dx \,.\, x$$

$$\in \Omega \tag{5.11}$$

For fixed f_1 and f_2 we minimize the energy functional $E(c_1.c_2.\phi)$ with respect to ϕ to obtain the gradient descent flow as:

$$\frac{\partial \phi}{\partial t} = \delta(\phi)[-\lambda_1(I(x) - f_1(x))^2 + \lambda_2(I(x) - f_2(x))^2] \tag{5.12}$$

In our model we use $\lambda_1 = \lambda_2 = \lambda$. and then we rewrite the Eq. (5.12) to become as follows [56]:

$$\frac{\partial \phi}{\partial t} = 2\delta(\phi)\left[\lambda(f_1(x) - f_2(x))\left[I(x) - \frac{f_1(x) - f_2(x)}{2}\right]\right] \tag{5.13}$$

During the level set evolution. the coefficient $2\lambda(f_1(x) - f_2(x))$ can be approximated as a constant. Therefore. we can omit the coefficient. and Eq. (5.13) can be simplified as follows [73, 79]:

$$\frac{\partial \phi}{\partial t} = \delta(\phi)\left[I(x) - \frac{f_1(x) + f_2(x)}{2}\right] \tag{5.14}$$

5.4 Implementation

In order to efficiently and robustly regularize the level set function. The regularization term is substituted by the filtering process expressed as follows [82]:

$$\phi^{n+1} = K_\sigma * \phi^n \tag{5.15}$$

where K_σ is a Gaussian kernel with variance σ.

The main steps of the algorithm can be summarized as [57, 79]:

Step 1: Initialize the level set function f to be a binary function as following:

$$\phi(x.t = 0) = \begin{cases} -\rho. & x \in \Omega_0 - \partial\Omega_0 \\ 0. & x \in \partial\Omega_0 \\ \rho. & x \in \Omega - \Omega_0 \end{cases} \tag{5.16}$$

Where $\rho > 0$ is a constant. Ω_0 is a subset in the image domain Ω. and $\partial\Omega_0$ is the boundary of Ω_0.

Step 2: Compute f_1 and f_2 from Eq. (5.8).

Step 3: Update the level set function ϕ according to Eq. (5.14).

Step 4: Convolve the level set function with the Gaussian kernel as in Eq. (5.15).

Step 5: Check if the evolution is stationary. If not. return to step 2.

5.5 Experimental results

In this Section, we validate our proposed model by various experiments on several challenging images (synthetic real and medical images) which demonstrate the effectiveness and robustness of our model compared to some of the well-known models.
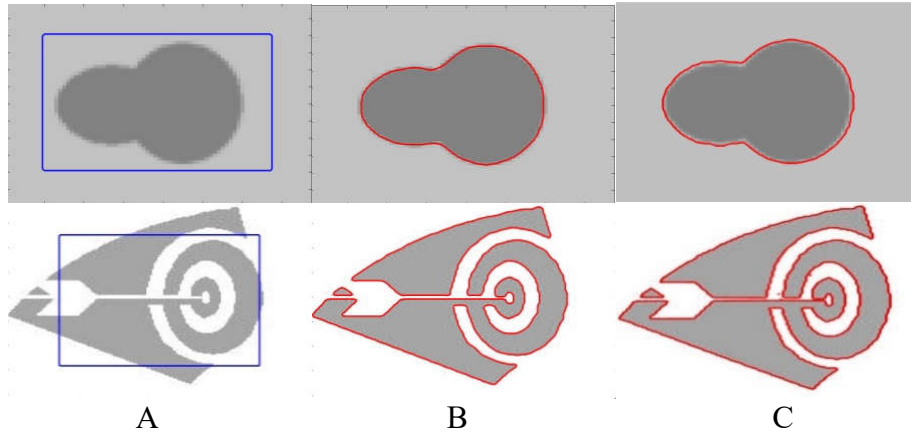
Figure 5.1: Segmentation of synthetic images using the proposed model

A: the initial contour. B: our model C: The DRLSE model

Firstly, we test our proposed model on images with the intensity homogeneity which is the simplest case in image segmentation. Figure 5.1 shows the segmentation process of two synthetic images using the proposed model (with $\sigma = 25$ and $\varepsilon = 1$ for the first image and $\sigma = 47$ and $\varepsilon = 5$ for the second image). The sizes of two images are 77×59 pixels and 167×166 pixels from top to bottom. The first column is the initial contour.

For our model and in both the two images the evolving curves stop on the true boundary of each shape after only one iteration and takes only 0.80 s for the image in the top row and takes only 2.48 s for the image in the bottom row while for the first image for example the DRLSE model [55] converge in 85 iterations and take 1.87 s.

in the second experiment, we compare our model with the traditional CV model using noisy synthetic images. It can be seen from Figure 5.2 that there are three separated shapes within the top image (142×141 pixels). one shape within the middle image (64×64 pixels) and two shapes within the bottom image (128×128 pixels). The first column is the initial contours. We note that the segmentation results corresponding to our model shown in the second column are more precise and faster than that of the CV model which are presented in the third column.

Table 5,1 shows the number of iterations and the time consumed for the results shown in Figure 5.2 which demonstrates the performance of the proposed model compared to the CV model in terms of precision and time-consuming

(A)   (B)   (C)
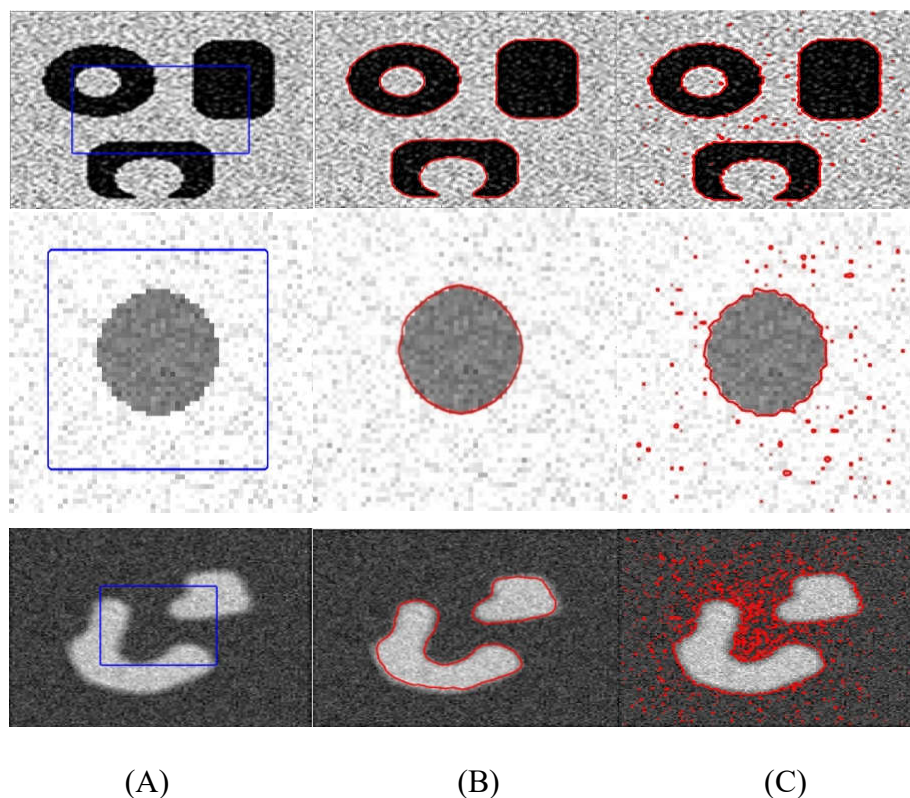
Figure 5.2: Comparison of our model with the CV model using noisy synthetic images. The parameters: $\sigma = 27$ and $\varepsilon = 1$ for the top image. $\sigma = 29$ and $\varepsilon = 1$ for the top image and $\sigma = 17$ and $\varepsilon = 1$ for the bottom image.

Table 5.1 Iterations and CPU time.

		Our model		CV model	
		Iterations	Time (s)	Iterations	Time (s)
Figure 5.1	Row 1	1	0.80	39	1.129
	Row 2	1	2.483	255	6.528
Figure 5.2	Row 1	5	2.688	443	11.086
	Row 2	1	0.72	300	4.523
	Row 3	1	0.998	700	25.741
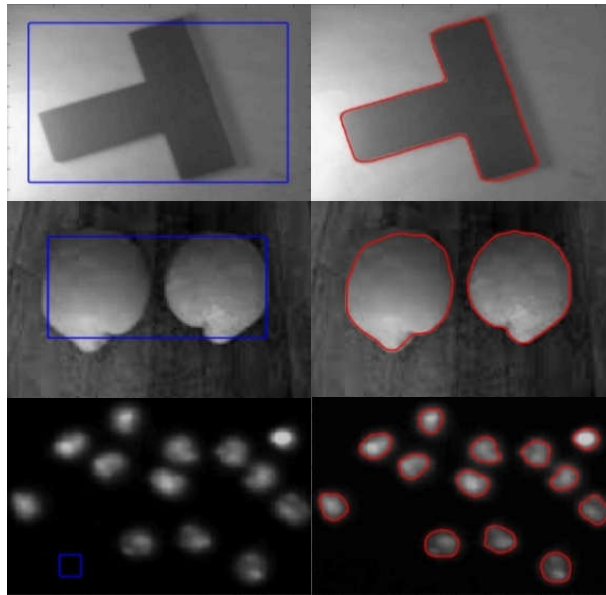
Figure 5.3: Real images with intensity inhomogeneity.

Figure 5.3 presents the results for real images. The images in the first two rows (a T-shaped object and image of Limon) are characterized by intensity inhomogeneity due to non-uniform illumination. which is often occurring in camera images. Our method successfully extracts the object boundaries for these two images. The third row shows the result of a real image of DNA channel. Even some nuclei are very close to each other. and traditional thresholding methods may fail to segment them our method segment successfully all the nuclei in just one iteration taking only 1.42s (here $\sigma = 21$ and $\varepsilon = 1$) whereas the LCV (local Chan–Vese model) method segment them at the 25th iteration and take 5.2s [80]. We obviously note that our model has segmented these images with great precision.
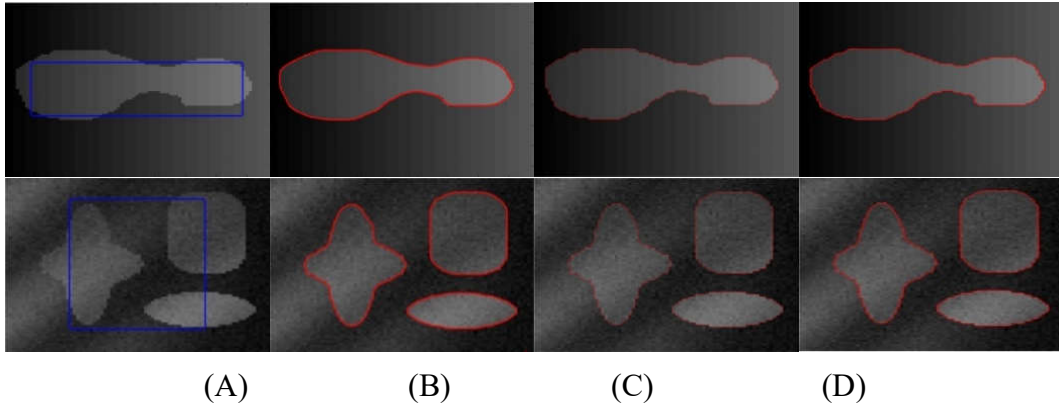
Figure 5.4: Comparison of our model with LBF model and LGD model for synthetic images.
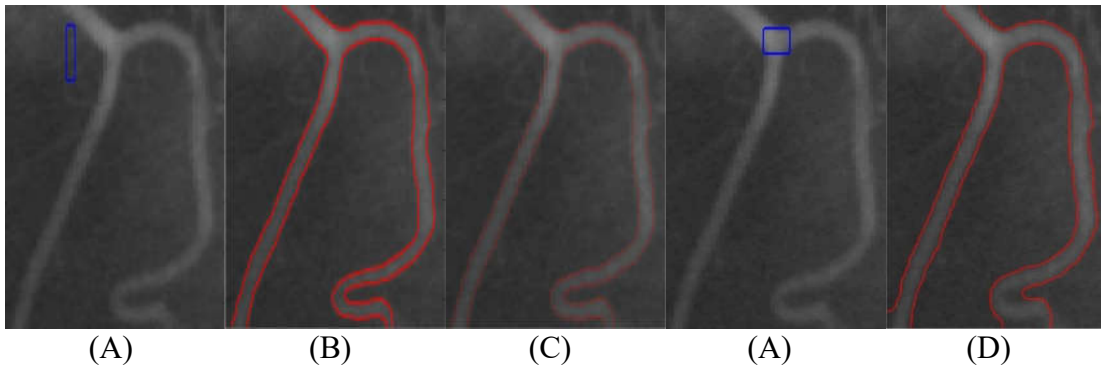
Figure 5.5: Comparison of our model with LBF model and LGD model for a medical image. (A) initial contours. (B) results of our model. (C) results of the LBF model. (D) results of the LGD model.
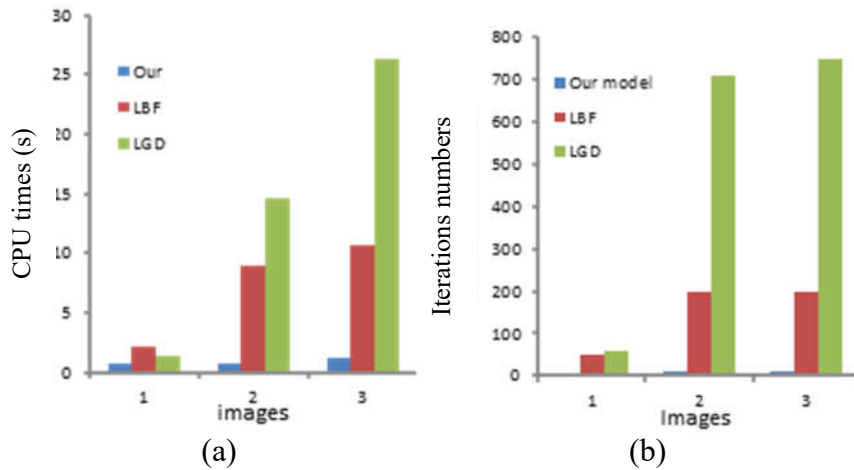
Figure 5.6: Comparison of our model with LBF model and the LGD model.

(a) CPU times. (b) Iterations numbers.

Figure 5.4 and Figure 5.5 show the segmentation results for three images with intensity inhomogeneity. The two synthetic images in the first and second row of Figure 5.4 are

generated with intensity inhomogeneity where the first one is a clean image and the second one was contaminated by a high level noise. The image in Figure5 is an X-ray image of a blood vessel. In this image. parts of the vessel boundaries are quite weak. which renders the blood vessel segmentation a reel challenge. Both model shave succeeded in the segmentation task with the same initial contours. except for the LGD model that has failed for the third image so we used another initial contour. but the result was not satisfactory. Their iterations numbers and CPU time for segmenting images in Figure 5.4 and Figure 5.5 are presented in Figure 5.6 It can be seen from Figure6 that the iteration number and CPU time for our model are both less than that of the LBF model and the LGD model for all three image segmentation. The proposed model is proved to be more efficient in segmenting the images with the intensity inhomogeneity in term of accuracy and computational time.
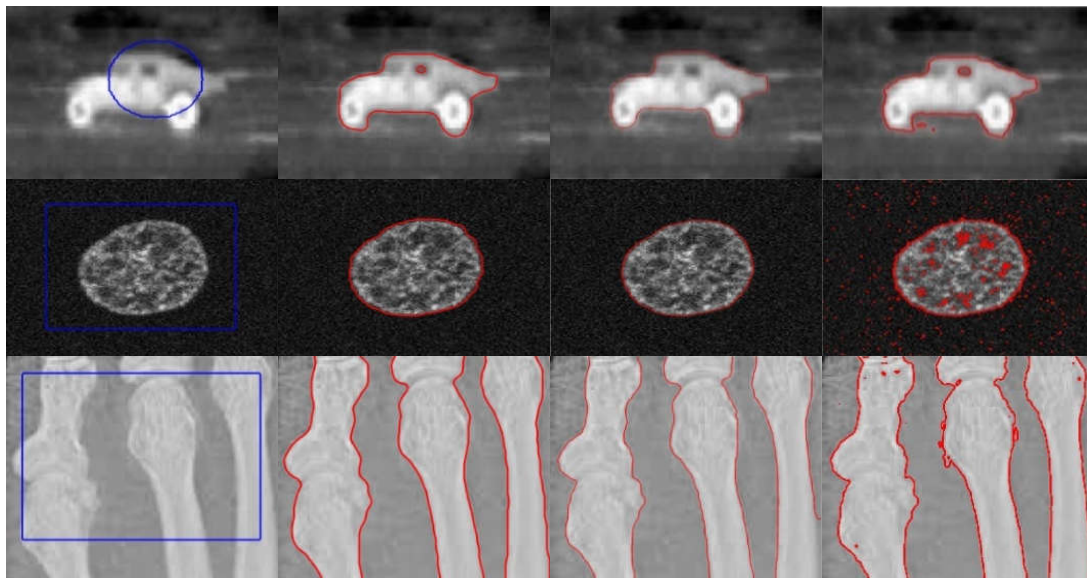
Figure 5.7: Comparison of our model with LGD model and CV model for infrared and medical images.

In this experiment Figure 5.7, we compare our model with two famous models, the CV model and the LGD model using images featured by intensity inhomogeneities. An infrared image with object having weak edges and interior holes in the first row nucleus fluorescence micrograph image in the second row and an X ray image of bones in the third row. The size of the test images is 118×93 pixels. 128×128 pixels and 128×105 pixels respectively. we show in figure 5.7 the initial contours then the results of the three models: our model, LGD and CV model respectively, it is easy to observe that for the first image our model detect with precision the contours inside and outside the

object while the LGD model did not succeed in this case. Both the LGD model and our mode have the same results for the second image where the CV model failed. We have the same observation for the third image where we can note that our model is once again more accurate than the two models LGD and CV model. This experiment shows rates the performance of the proposed model over the LGD model and the CV model in terms of accuracy computational time and number of iterations as shown in table 2.

Table 5.2 CPU time (s) for the images in Figure 5.7.

	Image 2 118×93 pixels		Image 2 128×128 pixels		Image 3 128×105 pixels	
	Iterations	Time (s)	Iterations	Time (s)	Iterations	Time (s)
Our model	2	1.42	1	1.15	2	1.58
LGD model	275	6.29	570	16.42	670	22.84
CV model	228	3.58	2700	138.59	849	13.00
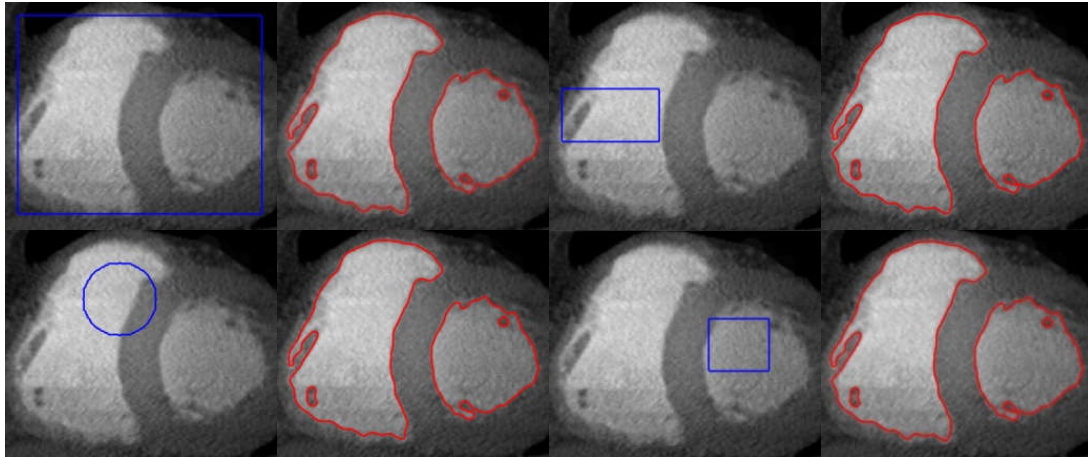
Figure 5.8: Effectiveness of our model toward the initialization problem.

Figure 5.8 demonstrates the robustness of the proposed method in medical image segmentation with different contour initializations. We applied our method to a magnetic resonance image of the left ventricle of a human heart in Figure8 with different initializations of the contour and the same settings of parameters ($\sigma = 23$ and $\varepsilon = 3$). We test the proposed model with different initial contour shapes (rectangular, circular) and in different positions; the initial contour encloses all the objects of interest crosses the left objects or the right objects and totally inside of one object as shown in the examples in Figure 5.8 even though the great difference of these initial contours we have the same results, the contours of the objects have been captured

with great precision, moreover, we can say that our model succeeded in overcoming the initialization problem which clearly shows its efficiency and robustness.
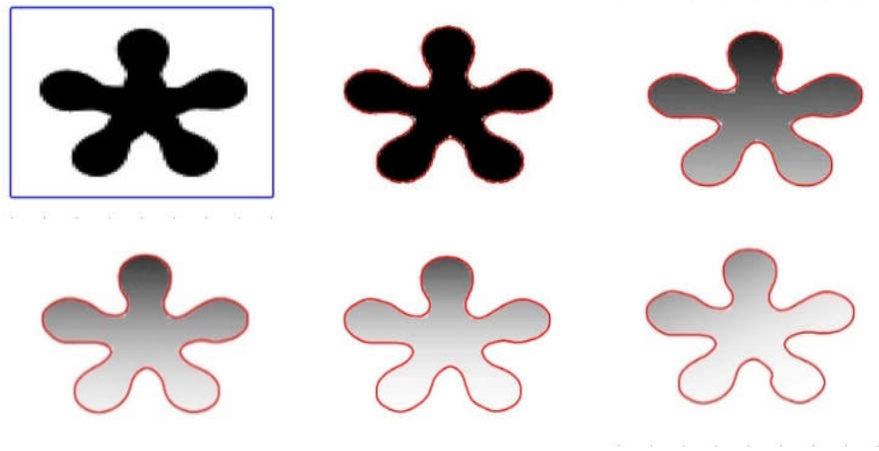
Figure 5.9: Results for several degrees of intensity homogeneity

In order to further demonstrate the capability of our method in dealing with intensity inhomogeneity we test our method for five synthetic images of the same object with increased intensity inhomogeneity (Figure 5.9). The upper row of Figure 5.9 shows the initial contour. the segmentation result of: a homogeneous intensity image and an image with a slight intensity inhomogeneity. The lower row presents images with more severe intensity inhomogeneity, despite this, we can see that our method obtains satisfactory results for these images. Witch proves that our model can handle images with different levels of intensity inhomogeneity very well. This experiment shows the efficiency and the robustness of our method to intensity inhomogeneity.
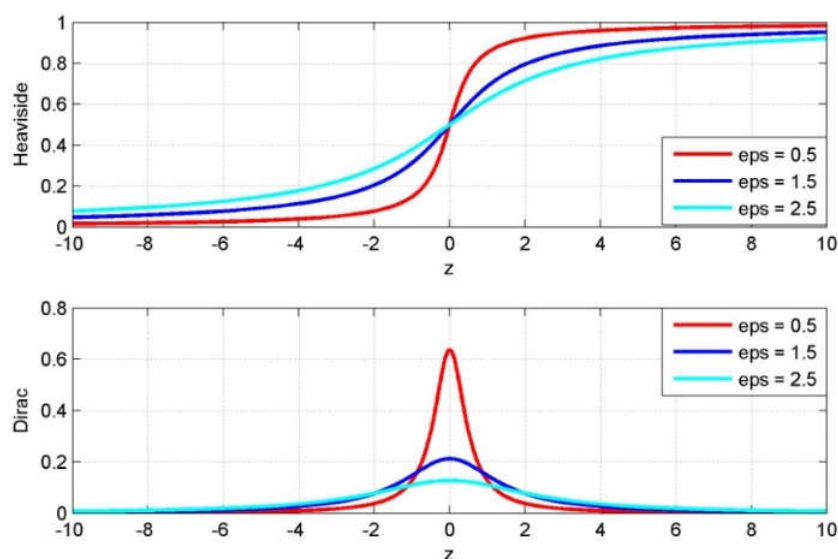
Figure 5.10: Representation of the Heaviside function and the Dirac function.
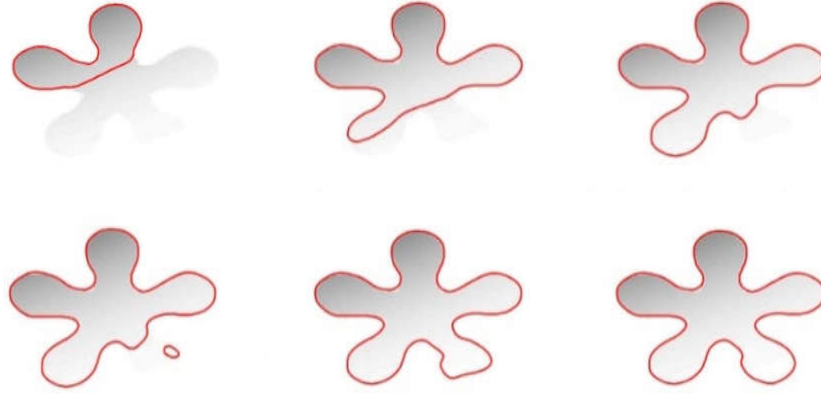
Figure 5.11: The ε parameter effect on the segmentation results

Our model converges in 22 iterations for all images and takes 1.93s. 1.84s. 1.87s. 1.88s. 1.86s. 1.85s respectively , for our model we have two main parameters: The standard deviation (σ)of the Gaussian kernel. and the parameter ε. The parameter ε affects the profile of $\delta_\varepsilon(z)$ and $H_\varepsilon(z)$. which means that the parameter ε is related to the the local image intensities inside and outside the contour C. As shown in Figure 5.10. if ε is too small. the energy function tends to its local minimum when the values of $\delta_\varepsilon(z)$ approach zero, which means that the effective range of $\delta_\varepsilon(z)$ is small. but a larger ε will lead to a broader profile. which will enlarge the capture range and increase the accuracy in the final contour location [57]. Thus. we test our model for different values of the parameter ε (5. 17. 95. 129. 155. 175) and $\sigma = 10.9$ on a synthetic image with severe intensity inhomogeneity. Figure 11 demonstrates the effect of the parameter ε on the segmentation results obtained. The experiment illustrates that to accurately segment the parts with increasing intensity inhomogeneity. we should enlarge the capture range by increasing the value of the parameter ε.

5.6. Conclusion

In this chapter we proposed a new robust region-based active contour model based on local average intensity for image segmentation in presence of intensity inhomogeneity and noise. Profiting local average intensity our model effectively completed the segmentation of the images characterized by high-intensity inhomogeneity. From the experimental results on a set of real and synthetic images, we can say that our model is really very robust and effective. Compared with famous models like LBF model LGD model and the CV model our model is not only much more computationally efficient and but also much more efficient.

CHAPTER VI

A FAST LEVEL SET IMAGE SEGMENTATION DRIVEN BY A NEW REGION
DESCRIPTOR.

"Whether you think that you can, or that you can't, you are usually right."

Henry Ford (1863-1947)

6.1 Introduction

In recent decades, the level set technique has become widespread and widely used in the field of image processing, especially in image segmentation. in fact, and from different points of view we can classify the use of the level set method in image segmentation into two main categories: region-based models [85], [88], [45], [47], [49], [57], [93], [95], [96], [97] and [98] and edge-based models [54], [84], [37], [89], and [94].

Inasmuch as the edge-based models do not assume intensity homogeneities, it can therefore be applied effectively to segment images with intensity inhomogeneities. However, with these methods, we cannot achieve effective segmentation for noisy images or when there are weak boundaries in the image. Most region-based models [45] and [47] are based on region descriptors to guide the curve evolution assuming the homogeneity of the intensity. However, defining a region descriptor for images with intensity inhomogeneities is one of the major challenges for these types of methods.

Since the Mumford and Shah model has appeared [44], in the last decades, many region-based active contour methods have been proposed for image segmentation. Amongst them: Li et al. in [58] developed a local binary fitting method (LBF) and after that, using local intensity, Zhang et al. developed a new local image adjustment method [60], next they proposed the SBGFRLS model [57] for selective and global image segmentation. Wang et al. [75] proposed a local Gaussian distribution fitting (LGD) method for modelling images by Gaussian distributions with local variances which lead to improve the LBF model. In another paper [90] Li et al. proposed a new local intensity clustering model for image segmentation and bias correction based on the local intensity clustering criterion. in [81] Zhang et al. developed a new local statistical active contour to improve the local intensity

clustering model. Although these methods can deal with intensity inhomogeneities, they are not designed to deal with different types of noise. Furthermore, they are very sensitive to initialization, their algorithm consumes more time and some of them cannot handle images with blurred contours. Therefore, their utilities are very limited [57].

To contribute to the improvement of image segmentation techniques, a new active contour model based on the region was proposed in this chapter. This model can handle noisy images and images with the presence of inhomogeneity of intensity. The major contributions are as follows:

- We formulate our model based on the modified and simplified version of the CV [45] model and the Legendre polynomials.
- To ensure the segmentation accuracy, we define a local region descriptor for image intensities using a linear combination of Legendre functions instead of the average intensity of the region adopted in the SBGFRLS model.
- We avoid the regularizing terms, like the length of C and the area inside C used in the CV model which reduces the calculation time.

That leads to ameliorate the important points cited below:

- Elimination of the re-initialization and all the drawbacks that come with it.
- Our method is less sensitive to the initial contour.
- Our method is more computationally efficient with lower computational cost and fewer number of iterations.
- The images with weak or blurred boundaries can be effectively segmented in restricted iterations.
- Our model can also accurately segment images with different kinds of noise and in the presence of intensity inhomogeneity.

In addition, we use a Gaussian filter to keep the level set function regularized and smooth during the evolution process, and at the same time avoid re-initialization. Quantitative evaluations using difficult images (real and synthetic) is carried out, as well as comparisons with previous work such as CV [45], SBGFRLS [57], LGD [75], L0MOS [95] and L0RDLSM [93] models.

6.2 Region intensity approximation using Legendre polynomials

Using the Mumford-Shah model [44], Chan-Vese [45] implements a piecewise-constant model for image segmentation. The general form of the energy function of the Mumford - Shah model has been defined by:

$$E_{MS}(u.C) = \int_{\Omega} |u_0(x.y) - u(x.y)|^2 dxdy$$

$$+ \mu \int_{\Omega \backslash C} |\nabla u(x.y)|^2 dxdy + v.lengh(C). \tag{6.1}$$

where Ω represent the image domain, the segmenting contour $C \subset \Omega$, μ and v are positive constants.

The Chan–Vese (CV) model minimizes the functional energy (2) to solve the minimization of the Mumford-Shah equation (1):

$$E_{CV}(c_1.c_2.C) = \mu.length(C) + v.area\big(inside(C)\big) + \lambda_1 \int_{inside(C)} |I(x) - c_1|^2 dx$$

$$+ \lambda_2 \int_{outside(C)} |I(x) - c_2|^2 dx . x \in \Omega \tag{6.2}$$

With c_1 the average of the image intensities inside the contour C, and c_2 the average of the image intensities outside the contour C. The values of c_1 and c_2 are re-estimated during the propagation of the curve.

$$\begin{cases} C = \{x \in \Omega : \phi(x) = 0\}. \\ inside(C) = \{x \in \Omega : \phi(x) > 0\}. \\ outside(C) = \{x \in \Omega : \phi(x) < 0\}. \end{cases} \tag{6.3}$$

Where ϕ represents the level set function, λ_1 and λ_2 are positive constants that control the force driven by the image data, generally, they are taken to be $\lambda_1 > 0$ $\lambda_2 > 0$.

In [57] Zhang et al. proposed a new active contour model based on selective local or global image segmentation SBGFRLS, where they used a novel signed pressure function (spf) defined as:

$$spf(I(x.y)) = \frac{I(x.y) - \frac{c_1 - c_2}{2}}{max\left(I(x.y) - \frac{c_1 - c_2}{2}\right)} \tag{6.4}$$

The spf function modulates the signs of the pressure force inside and outside the region of interest so that the contour expands when inside the object, or shrinks when outside the object. Then they regularized the level set function with a Gaussian filter process after each iteration. The level set function of the SBGFRLS model was formulated as follows:

$$\frac{\partial \phi}{\partial t} = spf(I(x)). \alpha. |\nabla \phi| \tag{6.5}$$

α is a scale parameter tuned according to the image, its role is to control the speed of level set update.

For the SBGFRLS model, the energy functional was formulated using the difference between each pixel and the average intensity of the region.

In our model, we have reformulated and generalized the Chan-Vese functional (6.2) by substituting the constants c_1 and c_2 by two smooth functions $c_1^m(x)$ and $c_2^m(x)$ presented in [92] as follow:

$$\begin{cases} c_1^m(x) = \sum_k \alpha_k p_k(x) \\ and \\ C_2^m(x) = \sum_k \beta_k p_k(x) \end{cases} \tag{6.6}$$

p_k is a multidimensional Legendre polynomial, to calculate the 2-D polynomial we use the following equation:

$p_k(x.y) = p_k(x)p_k(y). \quad x = (x.y) \in \Omega \subset [-1.1]^2$

The one dimensional Legendre polynomial p_k was given by:

$$p_k(x) = \frac{1}{2^k} \sum_{i=0}^{k} \binom{k}{i} (x-1)^{k-i}(x+1)^i \tag{6.7}$$

where k is the Legendre polynomial degree.

A linear combination of $(m+1)^2$ basic functions of Legendre 2D will represent the regions of the image.

Given the vector of Legendre polynomials by $\mathbb{P}(x) = (\mathfrak{p}_0(x)\ldots\mathfrak{p}_N(x))^T$. The coefficient vectors for the two regions are: $A = (\alpha_0\ldots\alpha_N)^T$ and $B = (\beta_0\ldots\beta_N)^T$. And the basic functions global number is $N = (m+1)^2$. We can now rewrite the modified and simplified version of (2) in matrix form as:

$$E_{CV}(A, B, \phi) = \int_{inside(C)} |I(x) - A^T\mathbb{P}(x)|^2 H_\varepsilon(x)dx + \lambda_1\|A\|^2$$

$$+ \int_{outside(C)} |I(x) - B^T\mathbb{P}(x)|^2(1 - H_\varepsilon(x))dx + \lambda_2\|B\|^2, \quad x \in \Omega \quad (6.8)$$

$H_\varepsilon(x)$ denotes the regularized version of the Heaviside function [57].

We minimize the energy functional $E_{CV}(A, B, \phi)$ with respect to ϕ to obtain the gradient descent flow as:

$$\frac{\partial\phi}{\partial t} = \delta_\varepsilon(\phi)\left[\left|I(x) - \widehat{A}^T\mathbb{P}(x)\right|^2 + \left|I(x) - \widehat{B}^T\mathbb{P}(x)\right|^2\right] \quad (6.9)$$

The optimal A and B ($\widehat{A}$ and $\widehat{B}$) are calculated by[92]:

$$\begin{cases} \widehat{A} = [K + \lambda_1\mathbb{I}]^{-1}P \\ \widehat{B} = [L + \lambda_2\mathbb{I}]^{-1}Q \end{cases} \quad (6.10)$$

where

$$P = \int_\Omega \mathbb{P}(x)I(x)m_1(x)dx$$

$$(6.11)$$

$$Q = \int_\Omega \mathbb{P}(x)I(x)m_2(x)dx$$

$$m_1(x) = H_\varepsilon(x) \text{ and } m_2(x) = (1 - H_\varepsilon(x))$$

And the Gramian matrices [K] and [L] are obtained as [91]:

$$[K]_{i,j} = \langle\sqrt{m_1(x)}\mathfrak{p}_i(x).\sqrt{m_1(x)}\mathfrak{p}_j(x)\rangle$$

$$(6.12)$$

$$[L]_{i,j} = \langle\sqrt{m_2(x)}\mathfrak{p}_i(x).\sqrt{m_2(x)}\mathfrak{p}_j(x)\rangle$$

$0 \leq$ i. j $\leq$ N. $\langle . \rangle$: the inner product operator

We rewrite the Eq. (12) to become as follows [56]:

$$\frac{\partial \phi}{\partial t} = 2\delta_\varepsilon(\phi)\left[\left(\widehat{A}^T\mathbb{P}(x) - \widehat{B}^T\mathbb{P}(x)\right)\left[I(x) - \frac{\widehat{A}^T\mathbb{P}(x) - \widehat{B}^T\mathbb{P}(x)}{2}\right]\right] \tag{6.13}$$

During the level set evolution. the coefficient $2\left(\widehat{A}^T\mathbb{P}(x) - \widehat{B}^T\mathbb{P}(x)\right)$ can be approximated as a constant. Therefore, we can omit the coefficient and Eq. (13) can be simplified as follows:

$$\frac{\partial \phi}{\partial t} = \delta_\varepsilon(\phi)\left[I(x) - \frac{\widehat{A}^T\mathbb{P}(x) - \widehat{B}^T\mathbb{P}(x)}{2}\right] \tag{6.14}$$

6.3 Implementation and results

In this section, the proposed model has been validated by several experiments on various difficult images such as noisy images and images with intensity inhomogeneities which illustrate the robustness and the efficiency of our model compared to some of the well-known models. The use of the Gaussian filtering process leads to regularize the level set function and to make it smooth and its evolution more stable [57]:

$$\phi^{n+1} = K_\sigma * \phi^n \tag{6.15}$$

The standard deviation σ of the Gaussian filter is a critical parameter that must be carefully tuned for each image. If σ is too small, the evolution of the level set function will be unstable. On the other hand, if σ is too large, an edge leak may occur and the detected contour may be inaccurate.

In, the experiments the parameters are set as follows: The Legendre polynomial degree $m = 1$, the regularizing constants $\lambda_1 = \lambda_2 = 1$, time step $\Delta t = 1$, $\varepsilon = 3$, and $\sigma = 3$. In specified cases some parameters are tuned according the image.

We summarize the proposed method algorithm in the few next steps:

Step 1: Normalize the input image.

Step 2: Adjust the parameters and Initialize the level set function.

Step 3: Calculate the optimal A and B using Eq. (9).

Step 4: Evolve the level set function according to Eq. (8).

Step 5: Convolve the level set function with a Gaussian filter as in Eq. (12).

Step 6: Verify if the evolution of the level set function has converged. Otherwise, go back to step 3.

A. Segmentation of real and synthetic images

a   b   c
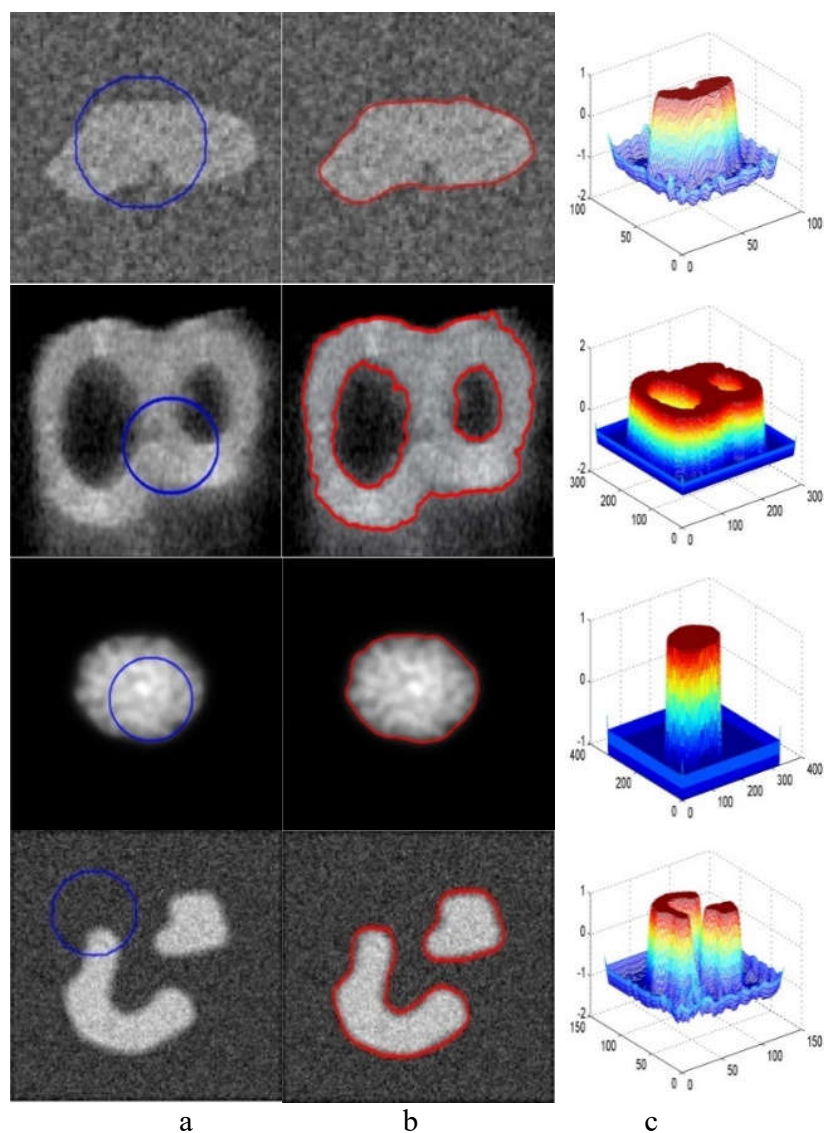
Figure 6.1: Segmentation of noisy images
(a) the initial contour, **(b)** our model, **(c)** the level set function.

We begin the test of the proposed model by a set of noisy images Figure 6.1 presents the segmentation process of two real images and two synthetic images using our model. In both the two real images the true boundaries of the objects are well extracted after only 2 iterations, and takes only 0.064 s for the first image and 0.07 s for the second image. For the two synthetic images, our model achieves satisfying results after only 5 iterations, and takes only 0.013 s for the image in the top row and 3 iterations, in only 0.019 s for the image in the bottom row. Afterward, we have tested our model on real images, Figure 6.2 shows two images among them. These results show that our model can provide a satisfying segmentation result for these kinds of images which prove its general efficiency.
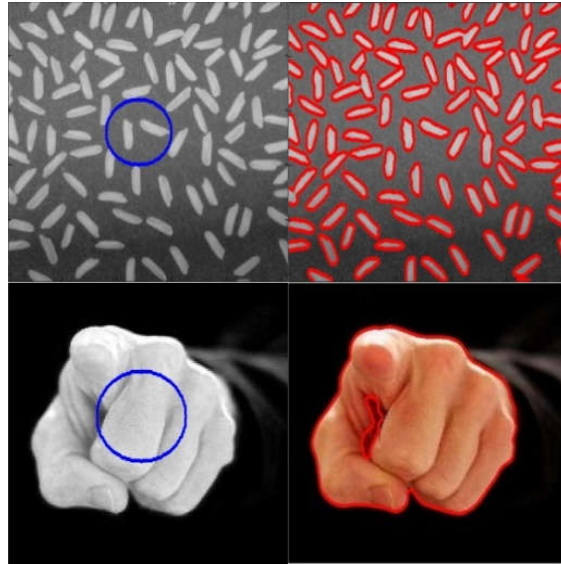
Figure 6.2: Segmentation results for real images.

(m = 1, ε = 3, and σ = 1) and (m = 1, ε = 3, and σ = 3) respectively.

B. Performance for different types of noises

In this section, we quantitatively evaluate the efficiency of our model for images with different types of noise using Jaccard similarity (JS). The JS index is given by:

$$JS = \frac{I_1 \cap I_2}{I_1 \cup I_2} \tag{6.16}$$

where I_1 represent the ground-truth, and I_2 represent the segmentation results.

We can also evaluate the segmentation accuracy using Dice similarity coefficient (DSC) defined as follows:

$$DSC = 2 \frac{|I_1 \cap I_2|}{|I_1| + |I_2|} \tag{6.17}$$

It is evident if I_1 is very similar to I_2, JS and DSC are closer to 1 and the higher the segmentation.

We test our model on five artificial images having the same object and in the presence of different types of noise. We illustrate the results of the segmentation in Figure 6.3, where we have used a clear image for which we add different types of noise; Gaussian, Nakagami, Raghleit and rice respectively. From these results, we can say that our model has succeeded in obtaining efficient results in the presence of different types of noise.
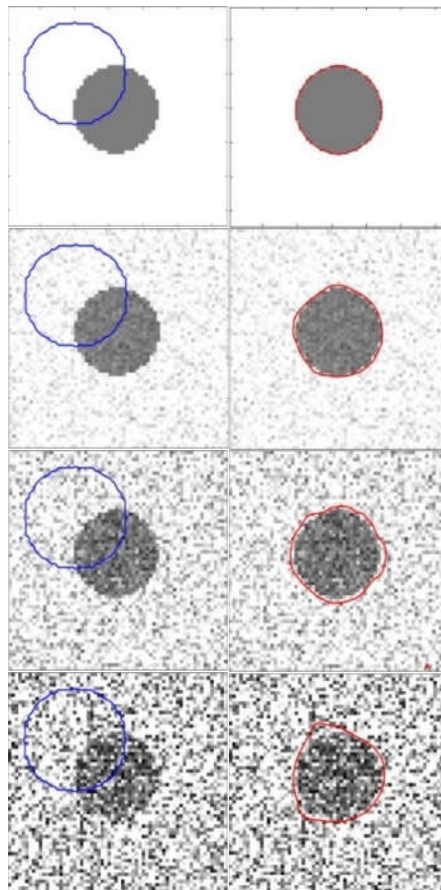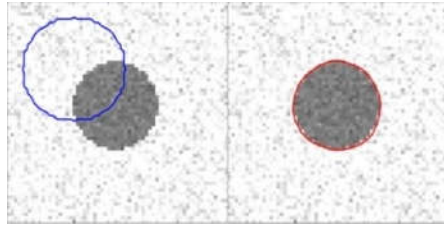
Figure 6.3: Segmentation accuracy in the presence of different types of noises: Gaussian, Nakagami, Raghleit, and rice respectively.
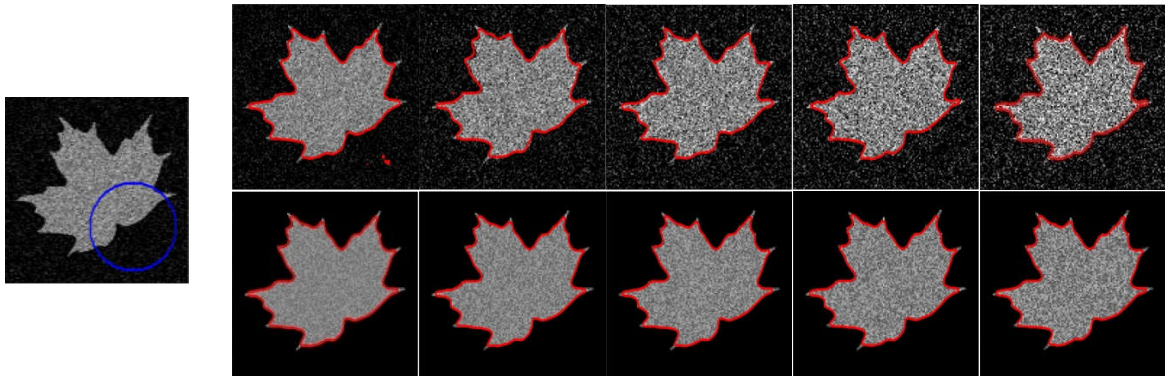
Figure 6.4: Results of Segmentation for noisy images with $\mu = 0$ and different values of σ.

First row: Gaussian noise second row: speckle noises.
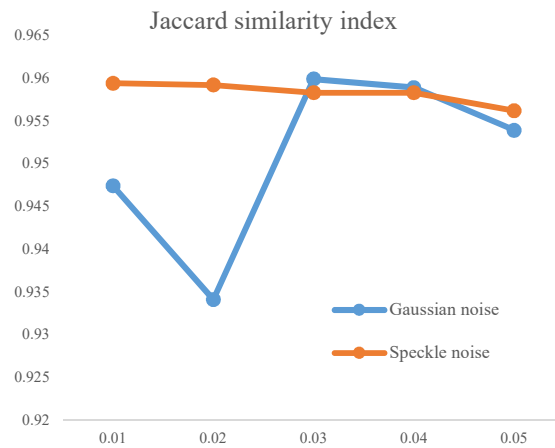
Figure 6.5: Illustration of the JS values for segmentation results shown in Figure 6.4.

In order to prove the effectiveness and robustness of our model in the case of attendance of different types of noises, we apply our model to a set of images where we increase

gradually the variances of the noise. Figure 6.4 presents in the first line the results on the images with different values of variances of the Gaussian noises, while the second line shows the results on the images with different values of variances of the speckled noises. The segmentation results validate the performance and efficiency of our model against different kinds of noises and even in cases of strong noises. In Figure 6.5, we present the quantitative evaluation of the performance of our model using JS index, for the images with speckle noises we have a high JS value changes from 0.955 to 0.960 and from 093 to 0.96 for those with Gaussian white noises, which demonstrate the robustness and efficiency of our model.

C. Robustness to level set initializations
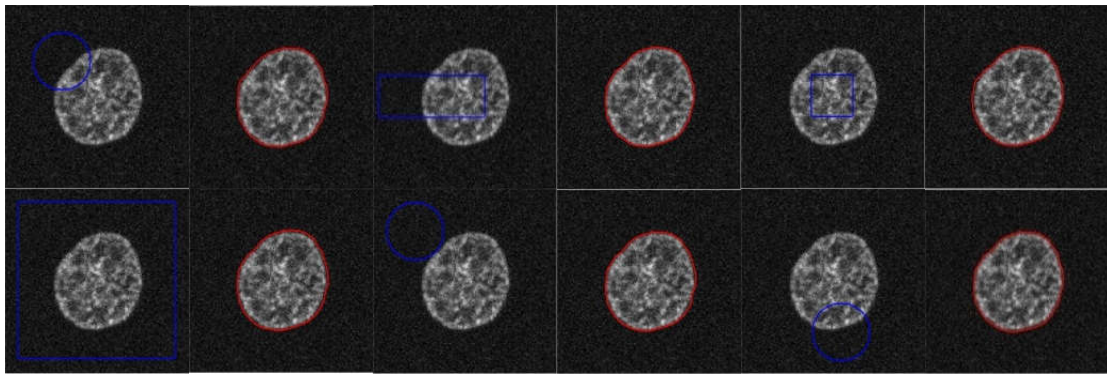
Figure 6.6: Segmentation results using different initializations.

Using the same metric (JS), we can assess the precision of the segmentation and quantitatively evaluate the performance of our model using different initial contours. Figure 6.6 shows the results of applying our model to a nucleus fluorescence micrograph image using various initial contours, where we initialize our function according to the four possible cases: the first case the initial contour completely surrounds the objects, the second case the initial contour is found in the objects, the third case the initial contour crosses the objects and background and the last case the initial contour is in the background, which is far from the object. We can see obviously that the object boundaries are accurately segmented and the results for all contours are almost the same despite the different initializations, these results are clearly verified by the quantitative evaluation presented in Figure 6.7 which proves the robustness of our model to different level set initialization in fewer iterations number and high computational speed (see Table 6.1).

Jaccard similarity index
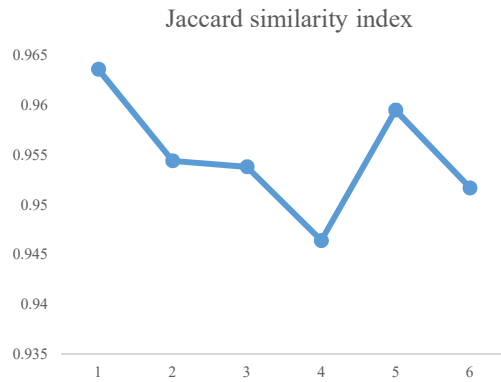
Figure 6.7: Robustness to level set initializations.

Table 6.1 The segmentation accuracy of our model using different level set initialization.

Initial contour	1	2	3	4	5	6
Jaccard index	0.9636	0.9517	0.9595	0.9464	0.9538	0.9544
Time (s)	0.0212	0.0128	0.0130	0.0226	0.0406	0.0375
Iterations number	3	1	1	2	5	3

D. Image segmentation in the presence of intensity inhomogeneity
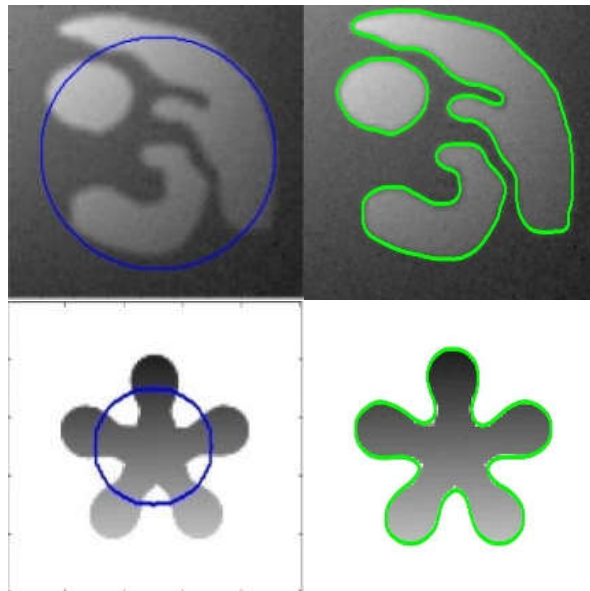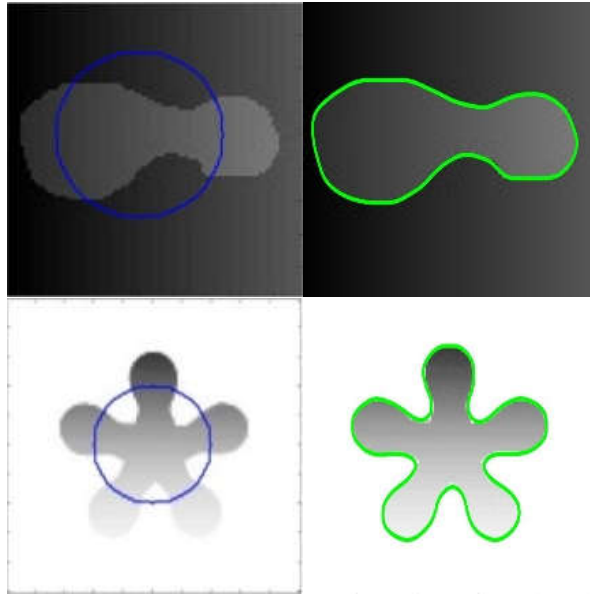
Figure 6.8: Results of our method for images with intensity inhomogeneity. (m = 1, ε = 3, and σ = 5) for the first image and (m = 1, ε = 3, and σ = 3) for the others.

We present in Figure 6.8 the segmentation results of our model for synthetic images corrupted by intensity inhomogeneity where we set the parameters as follows: m=1, ε=1, and σ=5 for the image in the first row, m=1, ε=3, and σ=3 for the image in the second row, m=1, ε=1, and σ=3 for the image in the third row, m=1, ε=3, and σ=3 for the image in the last row. Our model accurately extracts the object boundaries for these images: in just 7 iterations taking only 0.073 s for the first image and takes 0.020 s in 5 iterations for the second image, and in just 9 iterations taking only 0.037 s for the third image and 11 iterations and takes 0.029 s for the fourth image. These results demonstrate the robustness and the high speed of our model in the presence of intensity inhomogeneities.

E. Comparison of our model with L0MOS and L0RDLSM model
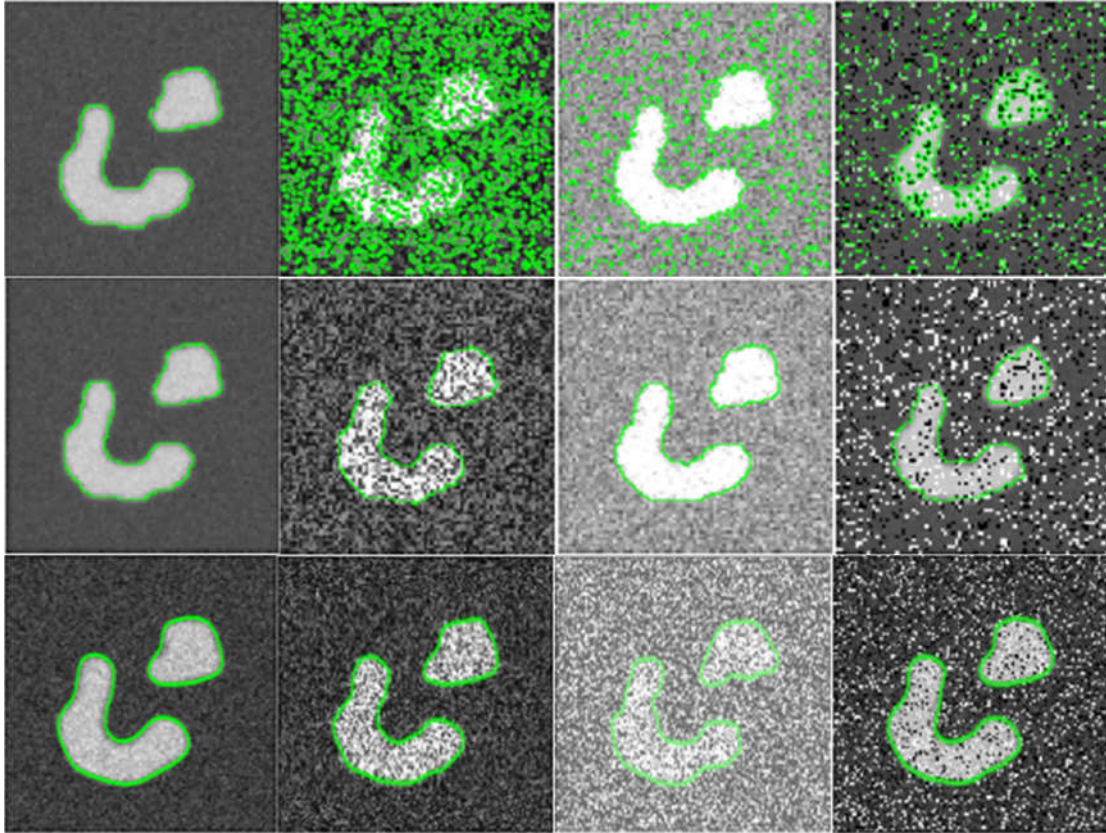
Figure 6.9: Segmentation results using four images (left to right: noise-free; zero mean, variance 0.2 for speckle; zero mean, variance 0.3 for Gaussian; 0.2 for salt & pepper). Upper row: L0MS model (α = 0.005, 0.1, 0.01 and 0.015). Second row: L0-RDLSM (α = 0.5, 6, 2 and 7). Bottom row: our method (m = 1, ε = 3, and σ = 3).

In Figure 6.9, we show the segmentation results of our model compared to the results of L0MOS [95] and L0RDLSM [93]. For this purpose, we used four synthetic images, the original image in the first column with three noisy images created from the first image by adding a different noise (speckle: means zero, contrast 0.2; Gaussian: means zero, contrast 0.3; salt and pepper: 0.2), successively. As Figure 6.9 shows, we can see that the L0MOS model only succeeded in dividing the first image, while it failed with the other images. In contrast, our model and the L0RDLSM model had almost the same effective results. However, we can clearly see that the results of our model are smoother than the results of

the L0RDLSM model, in addition, our model is much faster. This shows the performance and the advantages of our model.

F. Comparison of the segmentation results for our model with, SBGFRLS, LGD, and CV model
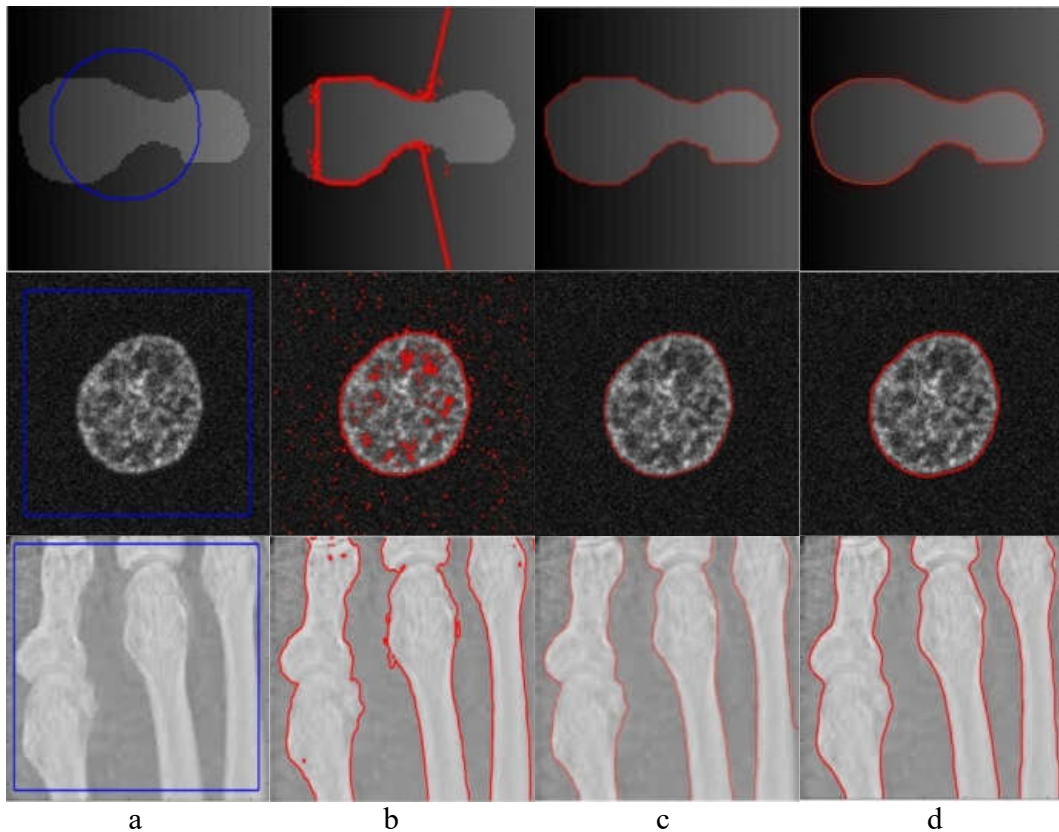
Figure 6.10: Comparison of segmentation results of our model with LGD model and CV model. **(a)** Initial contours, **(b)** CV model, **(c)** LGD model, **(d)** Our model.

For the comparison, we use in this experiment, the CV, and LGD models. Figure 6.10 shows the segmentation results of the following images: a synthetic image corrupted by inhomogeneity of intensity, an image under a fluorescence microscope of the nucleus, and an X-ray image of the bones. Figure 6.10 presents the initial contours in blue, then in red the segmentation results using the CV model, LGD model, and our model respectively. our model accurately extracts the boundary the object for the first image, whereas the CV model has missed the object boundaries extraction. In the case of the second image, we note that the CV model did not succeed in obtaining good results while the proposed model

and the LGD mode give precise results. The third image results show the great effectiveness of our model against the CV and LGD models.

Then again, our model performs very well than the other models in terms of time-consuming and number of iterations for each image. Table 6.2 clearly shows the high speed of our model compared to the CV and LGD models, noting an enormous speed factor, which can reach 3745.67 between the proposed model and the traditional CV model especially for the second image.

Table 6.2 CPU time of the three models.

	Image 1 88×88 pixels		Image 2 128×128 pixels		Image 3 128×128 pixels	
	Time (s)	Iterations	Time (s)	Iterations	Time (s)	Iterations
The proposed model	0.037	9	0.037	3	0.013	1
LGD model	1.420	60	16.420	570	22.84	670
CV model	17.86	600	138.59	2700	13.00	849

As presented in Figure 6.11, this experience, therefore, shows the great performance of our model over the CV and LGD models in terms of accuracy, computational time and the iterations number.
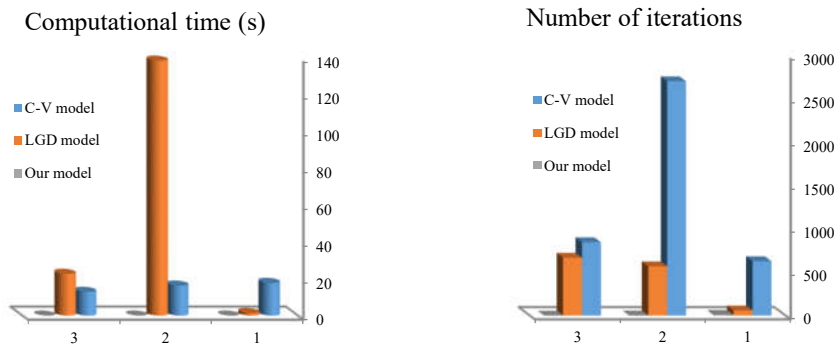
Figure 6.11: Computational time and number of iterations.

To quantitatively evaluate segmentation accuracy, our model is compared with LGD, and SBGFRLS models in segmenting several noisy images. Figure 6.11 shows two images among them. for all the images, it can be seen that the proposed model and the other models have obtained satisfactory segmentation results.
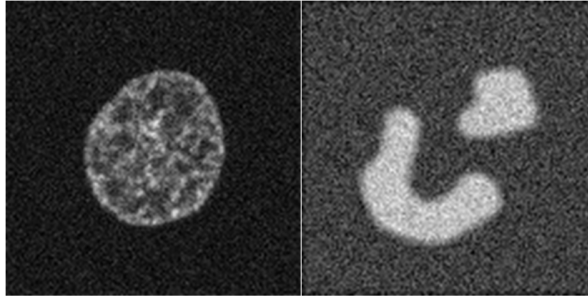
Figure 6.12: Noisy images.

Table 6.3 Quantitative evaluation of segmentation accuracy for the images in Figure 6.13.

		Time (s)	JS	DSC	MSE
Image 1 128×128 pixels	Our model	00.014	0.9683	0.9838	0.0048
	SBGFRLS	00.859	0.9602	0.9796	0.0060
	LGD	11.627	0.9438	0.9710	0.0087
Image 2 128×128 pixels	Our model	00.021	0.9627	0.9809	0.0076
	SBGFRLS	00.792	0.9558	0.9774	0.0090
	LGD	22.537	0.9617	0.9804	0.0078

The segmentation results are evaluated by JS, DSC (the Dice metric) and MSE (Mean square error) which are presented in table 6.3, with the time consumed for each method. Figure 6.12 shows the bar plot of the JS values for the three models: our model, LGD, and SBGFRLS models. We can conclude from the bar chart of the Jaccard index Figure 6.12 and table 6.2 that our model achieves the highest average value of JS and DSC with the lowest mean square error value in the shorter time among all the three methods. This clearly illustrates that our model is very fast and robust to noise, and it achieves efficient and precise segmentation results.

Jaccard similarity index
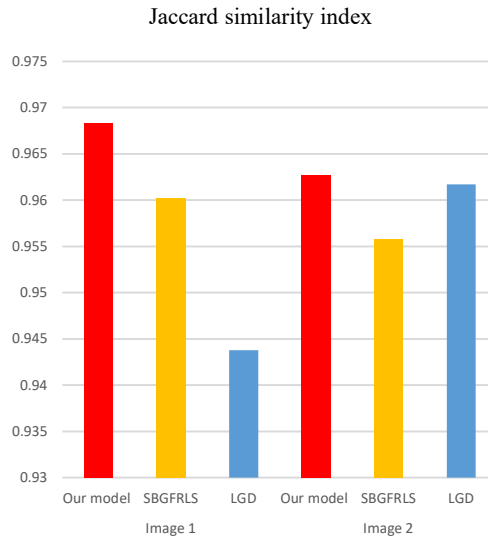
Figure 6.13: Quantitative evaluation of our model and the SBGFRLS and LGD model using Jaccard similarity index.

6.4 Conclusion

Using Legendre polynomials for region intensity approximation, we formulate a robust image segmentation method in level set active contour model framework which demonstrates excellent robustness and accuracy in image segmentation, especially images that have an inhomogeneous distribution of intensity and images with the presence of a lot of noise. In the numerical implementation, to overcome the traditional problem of re-initialization the level set function has been regularized by convolving it with a Gaussian filter, which greatly minimizes the time consuming during the evolution process. The performance of our model has been demonstrated by quantitative evaluations using real and synthetic images, as well as comparisons with previous work such as CV, SBGFRLS, LGD, L0MOS, and L0RDLSM models. Experimental results on different kinds of images (i.e., real images and medical images) show that our proposed model is very fast, precise and more robust than other popular models, all in very few iterations.

CHAPTER VII

CONCLUDING REMARKS

"Of all things, I liked books best."
Nikola Tesla (1856-1943)

Image segmentation plays a crucial role in the extraction of useful information and attributes from images for all imaging applications. It is one of the important steps leading to medical image understanding, analysis, and interpretation. Image segmentation is not only important for feature extraction and visualization but also for image measurements, 3D visualization, registration, computer-aided diagnosis, and compression, to name just a few. In this study, we focused on the analysis of the image segmentation using active contour methods. We aimed at developing new region-based active contour models for image segmentation that may for instance help a clinician in better understanding, diagnosing, and treating patients.

While existing methods can be effective, they have a number of limitations like the presence of intensity inhomogeneities, noise, and the high computational cost... etc. Therefore, this work is motivated by these limitations. Those limitations led us to consider the following challenges to achieve accurate segmentation for medical images:

- Overcome the problem of the presence of intensity inhomogeneities in medical images to achieve efficient segmentation results.
- Segment accurately blurred images, or in the presence of different kinds of noises.
- Develop segmentation techniques less sensitivity to the initialization.
- Reduce the high computational cost and segment images in a few iterations.

we have provided a brief introduction to the fundamental concepts of segmentation, Major applications of image segmentation, and future trends. In addition to an overview of the main evaluation metrics for objective evaluation and quantitative testing procedures and the famous dataset used in image processing studies. Then we have briefly summarized several basic concepts of image segmentation by the active contour models, where we have provided a brief classification of the main active contours. Next, we present the two

categories of active contours: the parametric/explicit active contour and the geometric/implicit active contour known as the level set method. we focus more on the level sets method, presenting its different categories of applications: edge-based models, region-based models, and local-region-based models, then some implementation techniques of the level sets method, and its drawbacks and its advantages.

In this thesis, three major contributions are presented that fall into the field of region-based active contour for image segmentation:

An Efficient Level Set Method Based on Global Statistical Information for Image Segmentation: In the first contribution, we propose a new region-based active contour model in a novel variational level set formulation for image segmentation, where we can benefit from the advantages of the C–V and GAC models. For this purpose, we first define a global intensity fitting energy functional; second, we insert our function in the GAC formulation. Our model enjoys the advantages of the region-based models, i.e., robustness to initialization and insensitivity to image noise, and the advantages of the edge-based models, i.e., good local characteristics and boundary capture capability. Using the global image information, the images with weak or blurred boundaries can be effectively segmented in restricted iterations. this model can also accurately segment images with different kinds of noise and in the presence of intensity inhomogeneity. Moreover, this model is significantly faster than classical active contours methods such as the GAC model, CV model, and DRLSE model, in terms of computational efficiency and more effective in terms of accuracy, and that has a good impact in different areas especially in medical diagnosis and computer vision.

A Robust Region-Based Active Contour Model Based On Local Average Intensity for Image Segmentation: In the second contribution, we propose a novel local region-based method for image segmentation in the presence of intensity inhomogeneities. The main idea behind this model is to create an energy functional-driven by the difference between the local average intensity inside and outside the contour. The energy functional is incorporated into a level set function to achieve its minimization. As an important application, our method can be used for the segmentation of synthetic medical and other kinds of real images with or without intensity inhomogeneities in limited iterations.

106

Furthermore, we greatly reduce the computational time using the Gaussian filtering to regularize our level set function which keeps the level set function smooth and reduces the effect of the noise to a certain degree. Moreover, the comparison of our model with well-known models like the CV model, LBF, and Local Gaussian distribution (LGD) model show the superiority of this model over them in term of robustness efficiency and time-consuming.

A Fast level set Image Segmentation driven by a new region descriptor: In the third contribution, to ensure the segmentation accuracy, we define a local region descriptor for image intensities using a linear combination of Legendre functions. involving this descriptor, we formulating a robust image segmentation method in level set active contour model framework, which demonstrates excellent robustness and accuracy in image segmentation, especially images that have an inhomogeneous distribution of intensity and images with the presence of a lot of noise. The performance of this model has been demonstrated by quantitative evaluations using real and synthetic images, as well as comparisons with previous work such as CV, SBGFRLS, LGD, L0MOS, and L0RDLSM models.

We can summaries the main advantages of the three contributions as follows:

- Avoid the regularizing terms, like the length of C and the area inside C used in the CV model which reduces the calculation time.
- Elimination of the re-initialization and all the drawbacks that come with it.
- less sensitivity to the initial contour.
- Computational efficiency with lower computational cost and fewer number of iterations.
- The images with weak or blurred boundaries can be effectively segmented in restricted iterations.
- Accurate segmentation of images with different kinds of noise and in the presence of intensity inhomogeneity.

In addition, we use a Gaussian filter to keep the level set function regularized and smooth during the evolution process, and at the same time avoid re-initialization.

Quantitative evaluations using difficult images (real and synthetic) are carried out, as well as comparisons with previous works which demonstrate that the three proposed models are much more computationally efficient and much more efficient.

APPENDIX

Derivation of the gradient descent flow

To obtain ϕ minimizing $E(\phi)$ we will use the steepest descent method, which is the simplest of the gradient methods. It is simple, easy to implement for any functional for which we can compute the Euler-Lagrange equation, and each iteration is fast. It is also very stable, if the minimum points exist, the steepest descent method is guaranteed to locate them. It amounts to calculating the derivative of $E(\phi)$, and at each iteration taking a step in the direction in which $E(\phi)$ decreases fastest [66].

In Eq. (4.17), we add the variation η to the level set function ϕ such that $\tilde{\phi} = \phi + \varepsilon\eta$ as in [60]. Keeping c_1 and c_2 fixed, differentiating with respect to ϕ, and letting $\varepsilon \to 0$, we have

$$\frac{\delta E(\phi)}{\delta \phi} = \lim_{\varepsilon \to 0} \frac{d}{d\varepsilon}\left(\frac{1}{2}\int_{\Omega} \left|I - c_1 H_\varepsilon(\tilde{\phi}) - c_2\left(1 - H_\varepsilon(\tilde{\phi})\right)\right|^2 dx\right)$$

$$= \lim_{\varepsilon \to 0}\left(-\int_{\Omega}\left[I - c_1 H_\varepsilon(\tilde{\phi}) - c_2\left(1 - H_\varepsilon(\tilde{\phi})\right)\right](c_1 - c_2)\delta_\varepsilon(\tilde{\phi})\eta dx\right)$$

$$= -\int_{\Omega}\left[I - c_1 H_\varepsilon(\phi) - c_2\left(1 - H_\varepsilon(\phi)\right)\right](c_1 - c_2)\delta_\varepsilon(\phi)\eta dx$$

So we obtain the Euler–Lagrange equation

$$-\left[I - c_1 H_\varepsilon(\phi) - c_2\left(1 - H_\varepsilon(\phi)\right)\right](c_1 - c_2)\delta_\varepsilon(\phi) = 0$$

Using the steepest gradient descent method [61], we can simply get the gradient descent flow as follows:

$$\frac{\partial \phi}{\partial t} = -\left[I - c_1 H_\varepsilon(\phi) - c_2\left(1 - H_\varepsilon(\phi)\right)\right](c_1 - c_2)\delta_\varepsilon(\phi)$$

This can be written as follows:

$$\frac{\partial \phi}{\partial t} = \delta_\varepsilon(\phi)(I - I_s)(c_1 - c_2)$$

Where $I_s = c_1 H_\varepsilon(\phi) - c_2\left(1 - H_\varepsilon(\phi)\right)$

REFERENCES

[1] I. N. Bankman, Handbook of Medical Image Processing and Analysis, 2nd Edition. Elsevier, 2009.

[2] Geoff Dougherty - Digital image processing for medical applications - Cambridge University Press (2009).

[3] Hui Li, Jianfei Cai, Thi Nhat Anh Nguyen, Jianmin Zheng. A Benchmark for Semantic Image Segmentation. IEEE ICME 2013.

[4] King, Paul. Digital Image Processing and Analysis: Human and Computer Applications with CVIPtools, 2nd Edition (2012).

[5] R. Kramme et al., Springer Handbook of Medical Technology Springer-Verlag Berlin Heidelberg 2011.

[6] T.M. Deserno, Biomedical Image Processing, Biological and Medical Physics, Biomedical Engineering, Springer-Verlag Berlin Heidelberg 2011.

[7] Zhu, Hongyuan & Meng, Fanman & Cai, Jianfei & Lu, Shijian. Beyond Pixels: A Comprehensive Survey from Bottom-up to Semantic Image Segmentation and Cosegmentation. J. Vis. Commun. Image R. 34 (2016) 12–27.

[8] Lankton, Shawn. "Localized statistical models in computer vision." (2009).

[9] S. Horowitz and T. Pavlidis, "Picture segmentation by a tree traversal algorithm," J. the Association for Comput. Machinery, vol. 23, no. 2, pp. 368-388, 1976.

[10] Pavlidis, Theodosios. "The Use of Algorithms of Piecewise Approximations for Picture Processing Applications." ACM Trans. Math. Softw. 2 (1976): 305-321.

[11] Y. J. Zhang. Half century for image segmentation (2015).

[12] Jahne, B.. "Digital image processing (5. ed.)." (2002).

[13] Lee, C.P. Robust Image Segmentation using Active Contours: Level Set Approaches. (2005).

[14] R. Gonzales and R. Woods, Digital Image Processing. Addison-Wesley Publishing, 1st ed.,1993

[15] Marr D, Hildreth E. Theory of edge detection. Proc Roy Soc London. 1980; 27 :187–217.

[16] L. Zhang. "A unified probabilistic graphical model and its application to image segmentation." (2009).

[17] D.R. Martin, C. Fowlkes, D. Tal, J. Malik, A database of human segmented natural images and its application to evaluating segmentation algorithms and measuring ecological statistics, in: ICCV, 2001.

[18] P. Arbelaez, M. Maire, C. Fowlkes, and J. Malik. Contour detection and hierarchical image segmentation. IEEE Trans. Pattern Anal. Mach. Intell., 33(5):898–916, May 2011.

[19] Xiaofang Wang. Graph based approaches for image segmentation and object tracking. Other. Ecole Centrale de Lyon, 2015.

[20] J. Shotton, J. M. Winn, C. Rother, and A. Criminisi. TextonBoost: Joint appearance, shape and context modeling for multi-class object recognition and segmentation. In Computer Vision-ECCV 2006, pages 1–15, 2006.

[21] Hui Zhang, Jason E Fritts, and Sally A Goldman. Image segmentation evaluation: A survey of unsupervised methods. computer vision and image understanding, 110(2):260–280, 2008a.

[22] Suri, J.S., Wilson, D., Laxminarayan, S.: Handbook of Biomedical Image Analysis, vol. 2. Springer Science & Business Media, Berlin, Germany (2005)

[23] Kumar, S N & Haridhas, Ajay Kumar & Varghese, P. Performance Metric Evaluation of Segmentation Algorithms for Gold Standard Medical Images: Proceedings of the 5th ICACNI 2017, Volume 3. (2018).

[24] Mitiche, Amar & Ben Ayed, Ismail. Variational and Level Set Methods in Image Segmentation. Springer-Verlag Berlin Heidelberg (2011).

[25] Zhang, Yu-Jin. An Overview of Image and Video Segmentation in the Last 40 Years. Advances in Image and Video Segmentation, pp.1-16 (2006).

[26] M. Kass, A. Witkin, D. Terzopoulos, "Snakes: active contour models", International Journal of Computer Vision, vol. 1, no. 4, pp. 321-331, 1988.

[27] D. Cremers, "Statistical shape knowledge in variational image segmentation," Ph.D. dissertation, University of Mannheim, Germany, 2002.

[28] L. Cohen, "On active contour models and balloons," in CVGIP Image Understanding, vol. 53, no. 2, 1991, pp. 211-218.

[29] Qing Yang. Ultrasound image segmentation using local statistics with an adaptative scale selection. Computer Science [cs]. Université de Technologie de Compiègne, 2013.

[30] C. Xu, J.L. Prince, Snakes, shapes, and gradient vector flow, IEEE Trans. Image Process. 7 (3) (1998) 359–369.

[31] C. Xu, J.L. Prince, Generalized gradient vector flow external forces for active contours, Signal Process. 71 (2) (1998) 131–139.

[32] S. Zhu, R. Gao "A novel generalized gradient vector flow snake model using minimal surface and component-normalized method for medical image segmentation" Biomedical Signal Processing and Control 26 (2016) 1–10.

[33] S. Osher and J. A. Sethian. Fronts propagating with curvature dependent speed: Algorithms based on Hamilton-Jacobi formulations. Journal of Computational Physics, 79(l):12–49, November 1988.

[34] Caselles, V., Catte, F., Coll, T. and Dibos, F., A geometric model for active contours, Numerische Mathematik, Vol. 66, No. 1, pp. 1-31, 1993.

[35] Chopp, D. L., Computing Minimal Surfaces via Level Set Curvature Flow, J. Computational Physics, Vol. 106, No. 1, pp. 77-91, 1993.

[36] Rouy, E. and Tourin, A., A viscosity solutions approach to shape-fromshading, SIAM J. of Numerical Analysis, Vol. 23, No. 3, pp. 867-884, 1992.

[37] R. Malladi, J. A. Sethian, and B. C.Vemuri, "Shape modeling with front propagation: A level set approach," IEEE Trans. Pattern Anal. Mach. Intell., vol. 17, no. 2, pp. 158–175, Feb. 1995.

[38] Suri, Jasjit S. and Swamy Laxminarayan., PDE and Level Sets: Algorithmic Approaches to Static and Motion Imagery., Kluwer Academic Publishers (2004)

[39] Malladi, R. and Sethian, J. A., An O(N log N) algorithm for shape modeling, Applied Mathematics, Proc. Natl. Acad. Sci. (PNAS), Vol. 93, No. 18, pp. 9389-9392, Sept. 1996.

[40] Kichenassamy, S., Kumar, A., Olver, P., Tannenbaum, A. and Yezzi, A., Conformal curvatures flows: from phase transitions to active vision, Arch. Rational Mech. Anal., Vol. 134, No. 3, pp. 275-301, 1996.

[41] Yezzi, A., Kichenassamy, S., Kumar, A., Olver, P. and Tannenbaum, A., A geometric snake model for segmentation of medical imagery, IEEE Trans. on Med. Imag., Vol. 16, No. 2, pp. 199-209, 1997

[42] Siddiqi, K., Lauriere, Y. B., Tannenbaum, A. and Zucker, S. W., Area and Length Minimizing Flows for Shape Segmentation, IEEE Trans. on Img. Proc., Vol. 7, No. 3, pp. 433-443, 1998.

[43] Siddiqi, K., Tannenbaum, A. and Zucker, S. W., Hyperbolic Smoothing of Shapes, Sixth International Conference on Computer Vision (ICCV), Mumbai, India, Vol. 1, pp. 215-221, 1998

[44] D. Mumford, J. Shah, Optimal approximation by piecewise smooth function and associated variational problems, Communication on Pure and Applied Mathematics 42, pp.577–685, 1989.

[45] T. F. Chan and L. A. Vese, "Active contours without edges," IEEE Transactions on Image Processing, vol.10, no. 2, pp. 266–277, 2001.

[46] T. Chan and L. Vese. Image segmentation using level sets and the piecewise-constant Mumford-Shah model. Technical Report 00-14, UCLA CAM Report, 2000.

[47] A. Tsai, A. Yezzi, A.S. Willsky, "Curve evolution implementation of the Mumford–Shah functional for image segmentation, denoising, interpolation, and magnification", IEEE Transaction on Image Processing vol.10, pp.1169–1186, 2001.

[48] Thomas Dietenbeck. Segmentation of 2D-echocardiographic sequences using level-set constrained with shape and motion priors. Other. INSA de Lyon, 2012.

[49] L. A. Vese and T. F. Chan, "A multiphase level set framework for image segmentation using the Mumford and Shah model," International Journal of Computer Vision, vol. 50, no. 3, pp. 271–293, 2002.

[50] S. Lankton, A. Tannenbaum, Localizing region-based active contours, IEEE Trans. Image Process. 17 (11) (2008) 2029–2039.

[51] T.F. Chan, S. Esedoglu, M. Nikolova, Algorithms for finding global minimizers of image segmentation and denoising models, SIAM J. Appl. Math. 66 (5) (2006) 1632–1648

[52] Zhou, Yan & Shi, Wei-Ren & Chen, Wei & Chen, Yong-lin & Li, Ying & Tan, Li-Wen & Chen, Daiqiang. "Active contours driven by localizing region and edge-based intensity fitting energy with application to segmentation of the left ventricle in cardiac CT images." Neurocomputing. (2015).

[53] Kimia, B. B., Tannenbaum, A. R. and Zucker, S. W., Shapes, shocks and deformations, I: The components of shape and the reaction-diffusion space, Int. Journal of Computer Vision (IJCV), Vol. 15, No. 3, pp. 189-224, 1995

[54] V. Caselles, R. Kimmel, and G. Sapiro, Geodesic active contours, International Journal of Computer Vision vol.22, no.1, pp. 61–79, 1997.

[55] C. M. Li, C. Xu, C. Gui, and M. D. Fox, "Distance Regularized Level Set Evolution and Its Application to Image Segmentation", IEEE Transactions on Image Processing, vol. 19, no. 12, pp.3243–3254, 2010.

[56] G. Aubert, P. Kornprobst, "Mathematical Problems in Image Processing: Partial Differential Equations and the Calculus of Variations", Springer, New York, 2002.

[57] K. Zhang, L. Zhang, H. Song, W. Zhou, "Active contours with selective local or global segmentation: A new formulation and level set method", Image and Vision Computing, vol. 28, pp. 668–676, 2010.

[58] C. M. Li, C. Kao, J. Gore, Z. Ding, "Implicit active contours driven by local binary fitting energy", in: IEEE Conference on Computer Vision and Pattern Recognition, pp. 1-7, 2007.

[59] C. Li, C. Xu, C. Gui, and M. D. Fox, "Level set evolution without re-initialization: a new variational formulation", Proceedings of IEEE Conference on Computer Vision and Pattern Recognition, vol. 1, pp. 430–436, 2005.

[60] K. Zhang, L. Zhang, H. Song, "Active contours driven by local image fitting energy", Pattern Recognition, V43, pp. 1199-1206, 2010.

[61] N. Paragios, R. Deriche, Geodesic active regions and level set methods for supervised texture segmentation, International Journal of Computer Vision vol.46, pp. 223–247, 2002

[62] C. Li, C. Kao, J. Gore, Z. Ding, "Minimization of region-scalable fitting energy for image segmentation", IEEE Transactions on Image Processing, vol. 17, no. 10, pp.1940–1949, 2008.

[63] N. Paragios, R. Deriche, "Geodesic active contours and level sets for detection and tracking of moving objects", IEEE Transaction on Pattern Analysis and Machine Intelligence vol.22, pp.1–15, 2000.

[64] Feng, C., Zhao, D., Huang, M.: "Image segmentation and bias correction using local inhomogeneous iNtensity clustering (LINC): a region-based level set method", Neurocomputing, 219, pp. 107–129, 2017.

[65] Wang, L., Zhu, J., Sheng, M., et al.: "Simultaneous segmentation and bias field estimation using local fitted images", Pattern Recognit., 74, pp. 145–155, 2018.

[66] O. Alexandrov, F. Santosa, "A topology-preserving level set method for shape optimization", Journal of Computational Physics, pp 121-130, 2005.

[67] Wei Xiaoqiong & Yin E. Zhang, "Image segmentation algorithm based on dynamic particle swarm optimization and K-means clustering", International Journal of Computers and Applications, 2018.

[68] Chen, Y., Yue, X., Da, X., et al.: "Region scalable active contour model with global constraint", Knowl. Based Syst., 2017, 120, pp. 57–73

[69] Mondal, A., Ghosh, S., Ghosh, A.: "Robust global and local fuzzy energy based active contour for image segmentation", Appl. Soft Comput., 47, pp. 191–215, 2016.

115

[70] Mohammed Debakla, Mohammed Salem, Rochdi Bachir Bouiadjra & Mohammed Rebbah, "CMA-ES based fuzzy clustering approach for MRI images segmentation", International Journal of Computers and Applications, 2019.

[71] C. yufei, Z. weidong, W. zhicheng, "Level Set Segmentation Algorithm Based on Image Entropy and Simulated Annealing", Proceedings of 1st International Conference on Bioinformatics and Biomedical Engineering (ICBBE 2007), p.999-1003, China, 2007.

[72] Lv, H., Wang, Z., Fu, S., et al.: "A robust active contour segmentation based on fractional-order differentiation and fuzzy energy", IEEE. Access, 5, pp. 7753–7761, 2017.

[73] S. Osher. R. Fedkiw. "Level Set Methods and Dynamic Implicit Surfaces". Springer. New York. 2002.

[74] D.L. Pham. C.Y. Xu. J.L. Prince "A survey of current methods in medical image segmentation" Ann. Rev. Biomed. Eng. 2 pp. 315–337. (2000).

[75] L. Wang. L. He. A. Mishar. C. Li. "Active contours driven by local Gaussian distribution fitting energy". Signal Processing (2009).

[76] C. Li. C. Kao. J. Gore. Z. Ding. "Minimization of region-scalable fitting energy for image segmentation". IEEE Transactions on Image Processing. vol. 17. no. 10. pp.1940–1949. 2008.

[77] K. Zhang. Q. Liu. H. Song. and X. Li. "A variational approach to simultaneous image segmentation and bias correction." IEEE Trans. Cybern.. Oct. 2014.

[78] C. Li. C. Xu. C. Gui. and M. D. Fox. "Level set evolution without re-initialization: a new variational formulation". Proceedings of IEEE Conference on Computer Vision and Pattern Recognition. vol. 1. pp. 430–436. 2005.

[79] C. Li. R. Huang. Z. Ding. C. Gatenby. D. N. Metaxas. and J. C. Gore. "A level set method for image segmentation in the presence of intensity inhomogeneities with application to MRI." IEEE Trans. Image Process. vol. 20. no. 7. pp. 2007–2016. Jul. 2011.

[80] X. Wang. D. Huang. H. Xu. An efficient local Chan–Vese model for image segmentation. Pattern Recognition 43 (3) 603–618 (2010).

[81] K Zhang. L Zhang. KM Lam. D Zhang. "A Level Set Approach to Image Segmentation with Intensity Inhomogeneity". IEEE Transactions on Cybernetics. 46 (2) 546-557. 2016.

[82] X. Xie. C. Wang. A. Zhang. X. Meng. "A robust level set method based on local statistical information for noisy image segmentation". Optik 125 (2014) 2199–2204

[83] T. Brox and D. Cremers. "On local region models and a statistical interpretation of the piecewise smooth Mumford–Shah functional". Int. J. Comput. Vis. vol. 84. pp. 184–193. 2009.

[84] L. Wang et al. "Patch-driven neonatal brain MRI segmentation with sparse representation and level sets." in Proc. IEEE 10th Int. Symp. Biomed. Imag. (ISBI). San Francisco. CA. USA. 2013. pp. 1090–1093.

[85] H. Song. "Active contours driven by regularized gradient flux flows for image segmentation". Electron. Lett. vol. 50. no. 14. pp. 992–994. 2014.

[86] S. Kichenassamy, A. Kumar, P. Olver, A. Tannenbaum, and A. Yezzi, "Gradient flows and geometric active contour models," in Proc. 5th Int. Conf. Comput. Vis. (1995) pp. 810–815.

[87] R. Kimmel, A. Amir, and A. Bruckstein, "Finding shortest paths on surfaces using level set propagation," IEEE Trans. Pattern Anal. Mach. Intell. (1995) vol. 17, no. 6, pp. 635–640.

[88] A. Vasilevskiy and K. Siddiqi, "Flux-maximizing geometric flows," IEEE Trans. Pattern Anal. Mach. Intell. (2002) vol. 24, no. 12, pp. 1565–1578.

[89] R. Ronfard, "Region-based strategies for active contour models," Int. J. Comput. Vis. (1994) vol. 13, no. 2, pp. 229–251.

[90] C. Li, R. Huang, Z. Ding, C. Gatenby, D. N. Metaxas, and J. C. Gore, "A level set method for image segmentation in the presence of intensity inhomogeneities with application to MRI," IEEE Trans. Image Process. (2011) vol. 20, no. 7, pp. 2007–2016.

[91] N. Barth, "The gramian and k-volume in n-space: some classical results in linear algebra," J Young Investig, (1999) vol. 2.

[92] Mukherjee, Suvadip & T. Acton, Scott. "Region Based Segmentation in Presence of Intensity Inhomogeneity Using Legendre Polynomials". Signal Processing Letters, IEEE. (2015). 22. 298-302.

[93] Y. Liu, C. He, Y. Wu, Z. Ren, "The L0-regularized discrete variational level set method for image segmentation", Image and Vision Computing 75 (2018) 32–43.

[94] Guopeng Huang, Hongbing Ji, Wenbo Zhang, Zhigang Zhu, "Adaptive multilayer level set method for segmenting images with intensity inhomogeneity", IET Image Process., Vol. 13 (2019), pp. 1714-1724.

[95] Y. Duan, H. Chang, W. Huang, J. Zhou, Z. Lu, C. Wu, "The L0 regularized Mumford-Shah model for bias correction and segmentation of medical images", IEEE Trans. Image Process. 24 (11) (2015) 3927–3938.

[96] Y. Wu, M. Li, Q. Zhang, Y. Liu, "A retinex modulated piecewise constant variational model for image segmentation and bias correction", Appl. Math. Model., 54 (2018), pp. 697-709.

[97] L. Wang, G. Chen, D. Shi, Y. Chang, S. Chan, J. Pu, X. Yang, "Active contours driven by edge entropy fitting energy for image segmentation", Signal Process., 149 (2018), pp. 27-35.

[98] Y. Yang, D. Tian, W. Jia, X. Shu, B. Wu, "Split Bregman method based level set formulations for segmentation and correction with application to MR images and color images", Magn. Reson. Imaging, 148 (2019), pp. 50-67.

[99] Fan, A., J. Fisher, Jonathan Kane and A. Willsky. "MCMC curve sampling and geometric conditional simulation." Electronic Imaging (2008).

[100] Ott, Patrick. "Segmentation features, visibility modeling and shared parts for object detection." (2012).

[101] Birane Abdelkader, Hamami Latifa, "A Fast level set Image Segmentation driven by a new region descriptor." IET Image Processing, Accepted date: 10-08-2020.

[102] Birane Abdelkader, Hamami Latifa, "An efficient level set method based on global statistical information for image segmentation", International Journal of Computers and Applications, (2019), DOI: 10.1080/1206212X.2019.1690797.

[103] Birane Abdelkader, Hamami Latifa, "A Robust Region-Based Active Contour Model Based On Local Average Intensity for Image Segmentation", Not yet published.

[104] Birane Abdelkader, Hamami Latifa, "Legendre polynomials Active contour method for image segmentation", International Journal of Systems Applications, Engineering & Development, Volume 12, (2018).

[105] Abdelkader, Birane and Hamami Latifa. "Efficient Region Active Contours for Images Segmentation.", Recent Advances in Circuits, Systems, Signal Processing and Communications, (2013) Proceedings of the 8th WSEAS International Conference on Circuits, Systems, Signal and Telecommunications (CSST '14), Tenerife, Spain.